TÉCNICO LISBOA

# Hypersonics: Laying the Road Ahead

**Pedro Miguel Rodrigues da Costa Simões Gonçalves**

Thesis to obtain the Master of Science Degree in

## Aerospace Engineering

Supervisor(s): Prof. Mário António Prazeres Lino da Silva
Prof. José Carlos Fernandes Pereira

### Examination Committee

Chairperson: Prof. Full Name
Supervisor: Prof. Full Name 1 (or 2)
Member of the Committee: Prof. Full Name 3

**May 2018**

# Acknowledgments

# Resumo

O desafio hipersónico começou há quase um século atrás; não obstante, apesar dos recentes progressos tecnológicos, continua a não ser uma realidade nos dias de hoje. Desta forma, o objectivo deste trabalho prendeu-se em identificar as razões por detrás disto e apresentar possíveis soluções. Para isso, foi realizada uma pesquisa sobre actuais barreiras tecnológicas, identificando os requisitos críticos. Seguidamente, elaborou-se uma lista de potenciais tecnologias com capacidade de preencher esses requisitos, reunindo informação do seu estado atual de maturação e tempo estimado até implementação. Algumas destas tecnologias foram recomendadas para as diferentes aplicações hipersónicas. Desta lista, modelaram-se três motores no SUAVE, uma ferramenta desenvolvida pela Embraer e pela Universidade de Stanford, para correr uma análise de baixa-fidelidade de um veículo genérico hipersónico. Como o SUAVE não estava dotado de capacidades hipersónicas, adicionou-se um modelo aerotermodinâmico e outro de distribuição de peso. Os novos modelos foram comparados com códigos numéricos ou dados experimentais para serem validados. Finalmente, foram introduzidos em dois casos de estudo diferentes (uma aeronave de voo cruzeiro e uma SSTO), que avaliaram o desempenho dos mesmos e os requisitos básicos da missão. Com este trabalho, o SUAVE é agora capaz de correr simulações hipersónicas de baixa-fidelidade, o que permite a realização de estudos paramétricos para avaliar a influência de sistemas específicos no desempenho da aeronave; além do mais, também estima a ordem de grandeza dos fluxos de calor em pontos de estagnação. Esta ferramenta tornou-se mais abrangente e está aberto a modificações para oferecer uma análise mais robusta.

**Palavras-chave:** hipersónico, roadmap, tecnologia, baixa-fidelidade

## Abstract

Hypersonics is a very challenging concept that dates back almost a century ago but, despite recent relevant progress, there are still no fully-capable hypersonic products. Therefore, the scope of this work was to identify the reason(s) behind this fact and provide possible solutions. To do so, a survey on barriers preventing hypersonic flight was conducted, which helped identify critical requirements. Next, a list of potential technologies to address them was put together, compiling information on readiness level and expected timeline for implementation. From here, some technologies were recommended for the different applications identified prior. From this filtered list, three supersonic/hypersonic engines (ramjet, scramjet and rocket) were numerically modeled in SUAVE, a framework tool developed by Embraer and Stanford University, to run low-fidelity hypersonic vehicle analysis. Since the tool lacked a solid hypersonic background, a simple aerothermodynamic and weight distribution model were also added. These new features were compared with numerical codes and/or experimental data for validation before being implemented in SSTO and atmospheric cruise mission scenarios that assessed the usefulness of new technologies and the performance of its subcomponents. With this work, SUAVE is now able to run basic hypersonic simulations; parametrization studies on engine subcomponents can be conducted to identify critical subsystems; it also provides an order of magnitude for the heat fluxes at the vehicle nose. The tool has become more comprehensive and is now open to further modifications and enhancements to provide a more robust analysis.



**Keywords:** hypersonic, roadmap, technology, low-fidelity

# Contents

# List of Tables

# List of Figures

# Nomenclature

### Greek symbols

| | |
|---|---|
| $\beta$ | Ballistic coefficient. |
| $\epsilon$ | Emissivity |
| $\eta$ | Adiabatic efficiency. |
| $\Gamma$ | Vandenkerckhove function. |
| $\gamma$ | Specific heat ratio. |
| $\kappa$ | Nozzle xpansion ratio |
| $\pi$ | Pressure ratio. |
| $\psi$ | Cycle static temperature ratio. |
| $\rho$ | Density. |
| $\zeta$ | Throttle. |

### Roman symbols

| | |
|---|---|
| $\frac{u_{f_x}}{u_3}$ | Fuel injection axial velocity ratio |
| $\frac{u_f}{u_3}$ | Fuel injection velocity ratio |
| $C_L$ | Coefficient of lift. |
| $L/D$ | Lift-to-drag ratio. |
| $q$ | Dynamic pressure. |
| $\dot{m}$ | Mass flow rate. |
| $A$ | Area. |
| $C_D$ | Drag coefficient. |
| $C_F$ | Thrust coefficient. |
| $C_p$ | Specific heat at constant pressure. |

$D$ Drag.

$F$ Thrust.

$f$ Fuel-to-air ratio.

$g$ Acceleration of gravity.

$h$ Altitude.

$I$ Impulse.

$L$ Lift.

$M$ Mach number.

$M_w$ Gas molecular weight.

$n$ Load factor.

$O/F$ Oxidizer-fuel ratio.

$P$ Static pressure.

$P_t$ Stagnation pressure.

$Q$ Heat of combustion.

$Q_w$ Heat load

$q_w$ Heat rate

$R$ Gas constant.

$r_{crv}$ Curvature radius.

$R_{Earth}$ Radius of Earth.

$Sa$ Air stream thrust

$T$ Static temperature.

$t$ Time.

$T_R$ Maximum stagnation temperature dictated by Rayleigh flow.

$T_t$ Stagnation temperature.

$T_{mtl}$ Maximum stagnation temperature dictated by material properties.

$U$ Utility function.

$u$ Velocity.

$EW$ Empty weight.

$q$ Dynamic pressure.

$W$ Weight.

$a$ Acceleration.

$h$ Altitude.

$h_s$ Earth scale height.

$M$ Mass.

$t$ Time.

$X$ Range.

$x$ Horizontal position.

**Subscripts**

$0$ Initial estimate.

$max$ Maximum.

$min$ Minimum.

$prop$ Propellant.

$re$ Reentry.

$b$ Burner.

$c$ Chamber.

$d$ Diffuser.

$n$ Nozzle.

$bd$ Fuselage body.

$eng$ Engine.

$lgr$ Landing gear.

$sys$ Systems.

$thr$ Thrust support structure.

$tl$ Tail.

$tps$ Thermal Protection System.

$wg$ Wing.

$a$ Air

$f$ Fuel.

$prop$ Propellant.

$sp$ Specific.

$1 - 10$ Station numbering

$\infty$ Free-stream.

$e$ Exit

$t$ Throat.

$i$ Shockwave upstream.

$ii$ Shockwave downstream.

ref Reference condition.

$SL$ Sea level.

$vac$ Vacuum.

**Superscripts**

$cor$ Corrected.

# Glossary

| | |
|---|---|
| **AFRL** | United States Air Force Research Laboratory |
| **AOTV** | Aero-assisted Orbital Transfer Vehicle |
| **ARV** | Ascent and Re-entry Vehicle |
| **BNNT** | Boron Nitride NanoTube |
| **CAV** | Cruise and Acceleration Vehicle |
| **CFD** | Computational Fluid Dynamics |
| **CMC** | Ceramic Matrix Composites |
| **CNES** | National Centre for Space Studies |
| **CNR-ISTEC** | Institute of Science and Technology for Ceramics of the National Research Council of Italy |
| **CNT** | Carbon NanoTubes |
| **CRDE** | Continuous Rotating Detonation Engine |
| **DMR** | Dual-Mode Ramjet |
| **EASA** | European Aviation Safety Agency |
| **ESA** | European Space Agency |
| **EU** | European Union |
| **EW** | Empty Weight |
| **FAA** | Federal Aviation Administration |
| **FW** | Fuel Weight |
| **GNC** | Guidance, Navigation and Control |
| **GTOW** | Gross Take-Off Weight |
| **HASA** | Hypersonic Aerospace Sizing Analysis |
| **HGV** | Hypersonic Glide Vehicle |
| **HIAC** | Hypersonic I-shaped Aerodynamic Configuration |
| **HMV** | Hypersonic Multi-purpose Vehicle |
| **ICAO** | International Civil Aviation Organization |
| **IMI** | Internal Multi-screen Insulation |
| **IXV** | Intermediate eXperimental Vehicle |
| **JAXA** | Japan Aerospace Exploration Agency |

| | |
|---|---|
| **LAPCAT** | Long-Term Advanced Propulsion Concepts and Technologies |
| **LEO** | Low Earth Orbit |
| **LH2** | Liquid Hydrogen |
| **LOX** | Liquid Oxygen |
| **MDO** | Multi-Disciplinary Optimization |
| **MHD** | Magneto-Hydrodynamic Drive |
| **MMC** | Metal Matrix Composite |
| **MTOW** | Maximum Take-Off Weight |
| **NASA** | National Aeronautics and Space Administration |
| **OFI** | Opacified Fibrous Insulation |
| **OpenVSP** | Open Vehicle Sketch Pad |
| **PAX** | Number of passengers |
| **PCTJ** | PreCooled TurboJet |
| **PMC** | Polymer Matrix Composite |
| **PW** | Payload Weight |
| **RBCC** | Rocket Based Combined Cycle |
| **RCC** | Reinforced Carbon–Carbon |
| **RV** | Reentry Vehicle |
| **R&D** | Research and Development |
| **SABRE** | Synergetic Air-Breathing Reaction Engine |
| **SITPS** | Structurally Integrated Thermal Protection System |
| **SSTO** | Single Stage To Orbits |
| **SUAVE** | Stanford University Aerospace Vehicle Environment |
| **TBCC** | Turbine-Based Combined Cycle |
| **TPS** | Thermal Protection System |
| **TRBCC** | Turbine Rocket Based Combined Cycle |
| **TRL** | Technology Readiness Level |
| **TUFROC** | Toughened Uni-Piece Fibrous Reinforced Oxidation-Resistant Composite |
| **UHTC** | Ultra-High Temperature Ceramics |
| **USAF** | United States Air Force |
| **USA** | United States of America |
| **WAATS** | Weight Analysis for Advanced Transportation Systems |
| **ZEHST** | Zero Emission Hyper Sonic Transport |

# Chapter 1

# Introduction

## 1.1 Motivation

Imagine traveling from the United Kingdom to Australia in less than four hours. Imagine a regular round-trip flight aboard a commercial spaceplane to a space hotel in Low Earth Orbit (LEO) for an affordable price. More than half a century after the technological marvels that put Mankind on the Moon, these two concepts still seem somewhat eccentric and share a common notion of uncertainty. As of March 2018, a flight from London to Perth doesn't take less than 17 hours, an all-time record [1]; on the other hand, the only handful of space tourists who have visited and stayed at the International Space Station (ISS) since the turn of the century have paid no less than $20,000,000 (2018) for their journey [2], far from affordable. However, all of these projects may become a reality if sustainable hypersonic capabilities are provided.

Hypersonic flight may be the next major leap forward in aerospace and despite not being an entirely new concept, it has been gathering more attention from the scientific community in recent years. The ability to significantly cut travel times and bring cities, nations and people even closer will revolutionize and strengthen interpersonal and economical ties, as well as redefine the notion of distance: traveling to the opposite side of the world by plane could take almost the same time as road trip across the entire extent of continental Portugal. Rightfully so, this justifies the research and development of new technologies to enable sustainable and affordable hypersonic transport. The implications of a successful hypersonic program are tremendous, not only for terrestrial applications but also for routine space access, a goal that dates back almost 60 years and is yet to be accomplished. Not only hypersonics can connect people all over the planet, it can act as the bridge towards space exploration and colonization by lowering costs associated with Space endeavors.

However, this domain requires mastering the severe and complex challenges of hypervelocity, including the harsh aerothermodynamic coupling effects. The extreme heat and stress loads require global system integration to maximize performance and minimize penalties from highly viscous flows. Hypersonic theory and its effects must be studied to their full extent and technology must evolve and achieve higher readiness levels to allow all this to happen in an affordable, reusable, green manner.

## 1.2 Overview

To better grasp the challenges associated with hypersonic flow, a brief overview of main challenges and proposed concepts follows.

### 1.2.1 Hypersonic conditions

To understand hypersonics, subsonic and supersonic conditions are briefly explained.

Subsonic flight refers to speeds below the speed of sound and it is used by the overwhelming majority of aerial vehicles; particularly in the field of commercial aviation, it is the only reality today. This flight regime is characterized aerodynamically by compressible flow from Mach 0.3 [3] onwards and lower mechanical loads, further simplifying the requirements for aircraft design in terms of aerodynamics, structures and propulsion.

As the vehicle moves faster and transposes the sonic limit, it becomes supersonic and the flow is no longer isentropic. From the transonic regime onwards, attached (e.g., on the wing upper surface) and detached (e.g., front of the vehicle nose) shockwaves are formed and the drag increases. These shockwaves are a consequence of the aircraft traveling faster than flow perturbations can be acoustically transmitted upstream, at the characteristic speed of sound. As such, for aircraft flying faster than that (Mach $> 1$), additional complications must be taken into consideration in aircraft design: as drag increases, more powerful engines and consequently larger amounts of fuel are required, adding to the overall aircraft weight. This makes it more expensive and inefficient, undermining its performance and preventing the deployment in the commercial sector where efficiency is of utmost importance.

This partly explains why, since the dawn of commercial aviation, aircraft design speeds have increased towards Mach 1 but have not generally surpassed it even though current propulsion methods enable it so; instead the effort has been shifted towards increasing Maximum Take-Off Weight (MTOW) while maintaining an optimum, subsonic flight speed and improving engine performance.

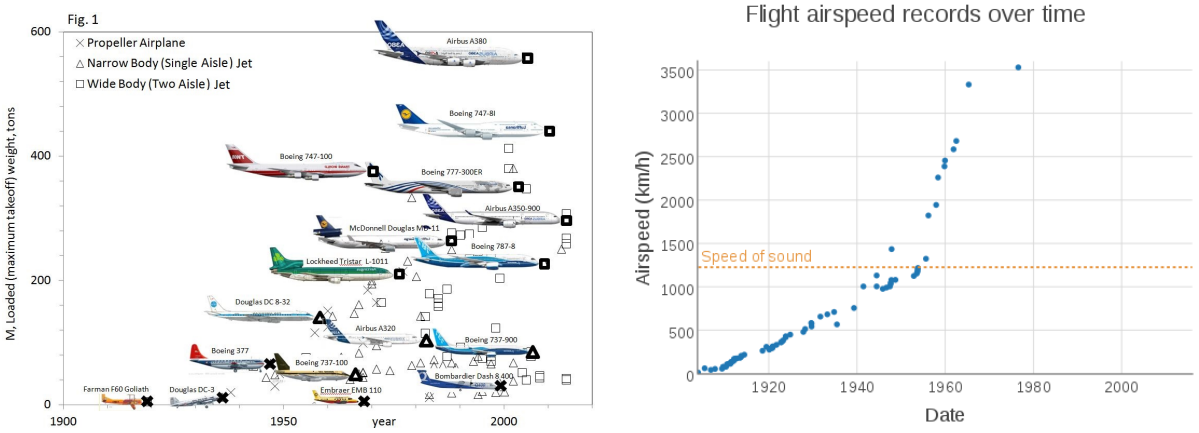


(a) MTOW evolution

(b) Flight airspeed records time

Figure 1.1: Trends and records in the aviation industry [4]

Hypersonics is a regime of hypervelocity flow characterized by extremely high dynamic pressure

and temperature, with thin shock layers, large pressure and temperature gradients and viscous interactions. Moreover, at even higher speeds, physical-chemical processes such as ionization, dissociation and other molecular phenomena also take place [5]. Contrary to the subsonic and supersonic flight, there is no clear transition to hypersonic flight. Mach 1 is a punctual phenomena that results in a physical discontinuity in the flow regime and therefore constitutes a clear abrupt change in flow conditions; this delimits the transition to supersonic flight. On the other hand, hypersonics takes over when aerodynamic and thermodynamic effects can no longer be decoupled and, for this reason, Mach 5 is the most widely accepted start of hypersonic flight [6]; however, this can vary according to surrounding conditions. There are several stages of hypersonic flight depending on the dominating phenomena, all of which are dependent on the flow temperature. Because sound speed and flow temperature are directly connected, variations in temperature induce changes in the local sound speed which can distort the perception of airspeed when using Mach as a speed indicator. In this fashion, some authors prefer to use true air speed as a more clear guideline for hypersonic operation.

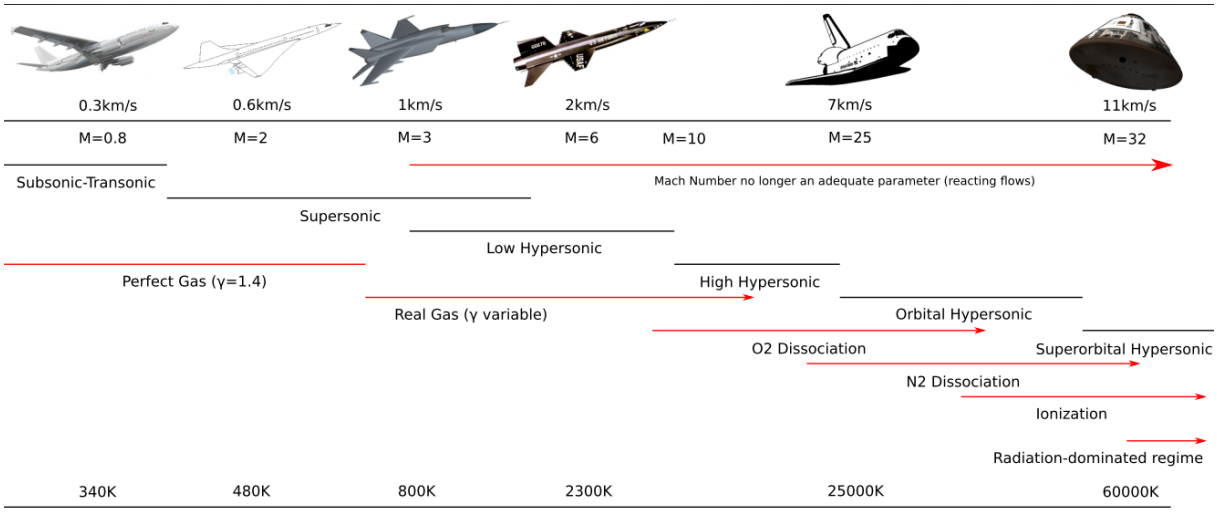


Figure 1.2: Overview of different hypersonic flight regimes [7]

Hypersonics is therefore a very complex flow regime, where compressibility issues are intertwined with extreme thermal and mechanical loads, resulting in very harsh conditions for aerospace structures to thrive. Propulsion methods, thermal protection systems, sonic signatures, structural integrity and aerodynamic performance are issues to be tackled simultaneously and interdependently in order to obtain an efficient hypersonic aircraft. The study of hypersonics is therefore fundamental to understand what the current gaps and obstacles are and how they may be overcome.

### 1.2.2 Vehicle categories

Prior to listing the different hypersonic concepts, it is important to notice how flight trajectory strongly dictates the hypersonic conditions a vehicle is bound to face. Therefore, before progressing any further, it is important to establish different classes of hypersonic flight vehicles in view of their specific design and technology features. According to the North Atlantic Treaty Organization (NATO) [8], there are four

different major classes of hypersonic flight vehicles: winged re-entry, cruise and acceleration, ascent and re-entry and aero-assisted orbital transfer. These are just broad categories and all shades in between are possible. Table 1.1 displays the basic characteristics of each vehicle.

| Vehicle Category | Mach range | Configuration | Dominant flow field effects | Aerodynamic lift/drag ratio | Thermal loads |
|---|---|---|---|---|---|
| Winged re-entry (RV) | 28-0 | Blunt | Compressibility | Small | Large |
| Airbreathing cruise and acceleration (CAV) | 0-7 | Slender | Viscosity | Large | Medium |
| Air-breathing ascent and re-entry (ARV) | 0-28 | Mixed | Compressibility and viscosity | Large/small | Medium/large |
| Aero-assisted orbital transfer (AOTV) | 20-35 | Very blunt | Compressibility | Small | Large |

Table 1.1: Hypersonic vehicle categories and main profile characteristics (adapted) [8]

### 1.2.3 Applications

Hypersonic technologies applied in the aerospace industry may represent a societal change as drastic as that of the full establishment of commercial aviation in the aftermath of World War II. Upon examining and cross-checking existing literature on hypersonic applications, these have been divided in three separate sectors: military, civil and Space. Despite overlapping with both military and civilian branches, the Space sector represents a heavily unexplored area, large enough to be categorized separately.

#### Military

There is currently a race between world superpowers to develop hypersonic capabilities. Over the last decades, China, Russia and the United States of America (USA) have dedicated large resources towards research and development of hypersonic technologies under the pretext of national security as it becomes not only a matter of delivering said capabilities but to be the first one to do so. These new aerial systems are game-changers: they provide enhanced battlefield effectiveness and carry with them the possibility to reshape warfare doctrine. These may be take form as new weapons, conceived to perform a wide variety of tasks.

The most active research topic is focused on the development of advanced, un-powered glide vehicles launched by ballistic missiles, which could be used for nuclear weapon delivery but also perform precision-strike conventional missions. Compared to ordinary RV, an hypersonic glide vehicle (HGV) can execute a pull-up maneuver after entering the atmosphere and flatten its glide, therefore delaying its detection and reducing the time available to counter it. Moreover, its added aerodynamic maneuverability requires a much more complex defensive system, which must be able to outmaneuver the HGV. RV's, on the other hand, fly on predictable ballistic trajectories upon re-entry, making them easier targets [9].

Progress has also taken place in powered hypersonic cruise missiles for long range tactical strikes. A missile flying at Mach 4-6+ would be difficult to intercept during high altitude cruise and terminal dive.

However, it requires hypersonic air-breathing capabilities in the order of several minutes, far beyond today's state-of-the-art performance. Additionally, there are still several unresolved issues related to structural integrity, propulsion efficiency and flight control before upgrading to a higher readiness level [6].

Lastly, hypersonic aircraft design could be applied to reconnaissance or weapon delivery by re-usable powered hypersonic vehicles. Entire systems and subsystems would now be un-expendable depending on the desired degree of re-usability, increasing their complexity when compared to traditional missiles. Studies on reusable hypersonic aircraft will pave the way for future civilian applications.

**Commercial Aviation**

The potential for the air cargo market is enormous. However, in the civil sector, aircraft requirements are more thorough, interposed by airliner demands (e.g., range, capacity and speed) and federal or environmental regulations (e.g, safety, noise and pollution). One of the immediate complications that arise for Mach $> 1$ is the ground overpressure produced by supersonic flight (commonly known as "sonic boom"). It is an inevitability that must be accounted for when plotting commercial routes, which are only possible over regions of very low population density (i.e., oceans and the North/South Poles), given current regulations. Nonetheless, there have been several international projects aimed at evaluating and developing new technologies for commercial hypersonic flight. Funded by the European Union (EU), the LAPCAT and LAPCAT II projects have provided concepts for hypersonic cruise passenger vehicles such as the MR2, which could fly from Brussels to Sydney in less than 4 hours [10, 11]. Further economic viability of hypersonic flight has been debated in HIKARI project, which came to the conclusion that a carefully designed aircraft is capable of guaranteeing high competitive ticket price and market capture, a crucial requirement for hypersonic business models. With it, the share of premium traffic (business and first class passengers) could exceed 15% and allow sustainable operations for worldwide fleets as large as 200 aircraft by 2040-2050 [12].

Smaller aircraft may also represent a significant share of commercial applications. These could be drones designed to transport perishable goods (e.g., human organs for transplant, vaccines and other high-value cargo) and deliver them when time is of utmost importance. Slightly larger designs may be used for emergency response, deployment of security forces, or time-sensitive diplomatic meetings.

**Space access**

Hypersonic air-breathing propulsion is likely to be a the game changer for affordable Space access, much like turbojets revolutionized the airline business. Rocket-powered vehicles have limits in terms of mission flexibility and robustness even as we witness the innovative cost-effective introduction of partial and near full re-usability, with SpaceX's Falcon 9. Regardless, air-breathing launch systems bring increased safety and accessibility while at the same time having the potential to marginally cut down on costs [13].

Current ascent trajectories are set in motion through vertical takeoff. Since an object on the Earth

surface moves with a speed equivalent to the tangential velocity of that latitude due to the Earth's rotation, launch locations are placed near the equator so that rockets require significant less energy to reach certain orbits. This limitation narrows the potential for spaceport expansion. However, horizontal takeoff is much less reliant on this effect, allowing spacecraft to reach different latitudes before the orbital boost phase: this leads to increased flexibility in terms of possible achievable orbits from a specific spaceport and also enables launch sites to be placed further away from the equator [14]. Furthermore, by using the aircraft airframe to generate lift, there is an increase in lift/drag coefficient and consequently an impact on energy consumption. Further reports also refer these characteristics to indicate safety increases by several orders of magnitude [15].

If reaching and returning from space in a single stage could be performed, it would reduce the heavy costs and penalties associated with production and integration of any external and expendable (or partially reusable) structures. This single-stage-to-orbit (SSTO) capability has long been envisioned by aerospace engineers but it hasn't been achieved yet due to technology limitations.

Routine access to space would increase payload deployment for civilian and military purposes, as well as allowing for immediate emergency response for unforeseen situations aboard other spacecraft such as the ISS. The recent rise of the nanosat industry may also act as a driver for affordable space access [16]. Moreover, it could lead to the creation and establishment of the Space tourism sector. Market studies have been produced with optimistic forecasts of suborbital touristic flights, with the main setback being the high costs involved [17]. The creation of other Space destinations can be accelerated and made cheaper, broadening the range of Space tourist destinations, a vital condition for the expansion of the sector beyond suborbital flight.

### 1.2.4 Hypersonic vehicle concepts

#### Military drones

Hypersonic unmanned aerial vehicles could soon be deployed on the battlefield as progress in hypersonic defense continues. The latest concept is the Lockheed Martin SR-72, a successor to the retired SR-71 "Blackbird", a manned spy plane built in the 1960s and capable of reaching Mach 3. The SR-72 is going to be an air-breathing cruise and acceleration aircraft for intelligence, surveillance and reconnaissance, capable of reaching Mach 6. It is the culmination of several hypersonic programs led by the USA over the past 40 years in different aerospace fields. The aircraft is powered by a combined-cycle propulsion system that merges turbojets with dual-mode supersonic ram compression engines. Since it is a classified project, there isn't much information available and a service date has not yet been announced [18, 19].

On the other hand, AYAKS is another project for a CAV-like vehicle under development since the 1980s. Initiated by the former Soviet Union and now under Russian administration, this hydrogen-fueled concept would provide military reconnaissance high above the stratosphere, at an altitude of at least 50 km, far beyond any current military aircraft service ceiling. This would be possible given a serious of innovative technologies in the field of propulsion and aerothermodynamics, by using magneto-

hydrodynamic concepts to accelerate the flow and create non-equilibrium cold plasma to reduce shock strength and, therefore, drag and heat. To date, there is no schedule for a demonstration flight [20].

(a) Lockheed Martin SR-72 concept art

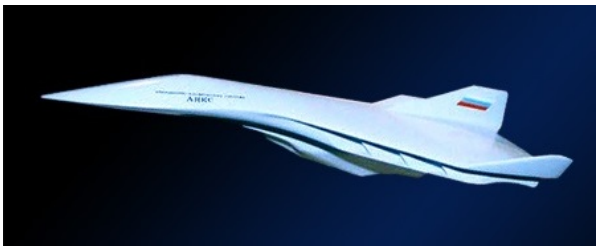

(b) AYAKS concept art

Figure 1.3: Hypersonic military aircraft concepts [21, 22]

**Spaceplanes**

Spaceplanes are designed to operate as spacecraft in Space and aircraft in Earth's atmosphere, combining features from both designs. These vehicles are generally equipped with wings and use rocket, air-breathing or mixed propulsion systems to reach Space. There are five spaceplaces who have successfully flown to date [1]: they completed atmospheric reentry, maneuvered in Earth's atmosphere and landed. However, all aircrafts were essentially a second or third stage of a broader, globally expendable launch system.

Currently, the major SSTO-capable concept is Skylon, a hydrogen-fueled spaceplane designed by British company Reaction Engines Limited. Its mission profile incorporates a horizontal take-off followed by an acceleration to Mach 5.4 at an altitude of 26 kilometers, on full air-breathing mode. For the final boost to orbit, the engine would switch to an internal liquid oxygen (LOX) supply. The vehicle would finally re-enter the atmosphere and land on a runway. While on the ground, it would undergo inspection and necessary maintenance, with a turnaround of one day.

By saving on oxidizer for the initial acceleration, the vehicle would allow for much higher payload capacity. It could carry up to 11 tonnes of cargo to the ISS, roughly 20% more than the reusable Falcon 9 rocket [23, 24]. In addition, Skylon is designed to complete 200 orbital flights whereas Falcon 9 should not fly more than 10 times, which means that, overtime, Skylon could potentially lower the cost of launching payload to LEO. Using interchangeable payload containers, Skylon could be fitted to carry satellites, propellants or even passengers. The mix of passengers and logistics is very flexible, but if optimized for passenger flight it may carry up to 24 people [23].

Currently, Reaction Engines Limited is funded by the United Kingdom government and the European Space Agency (ESA). The firm hopes to have a ground-based test engine working by the end of this decade and begin unmanned test flights by 2025 [25].

[1] North American X-15, Space Shuttle orbiter, Buran, SpaceShipOne, Boeing X-37

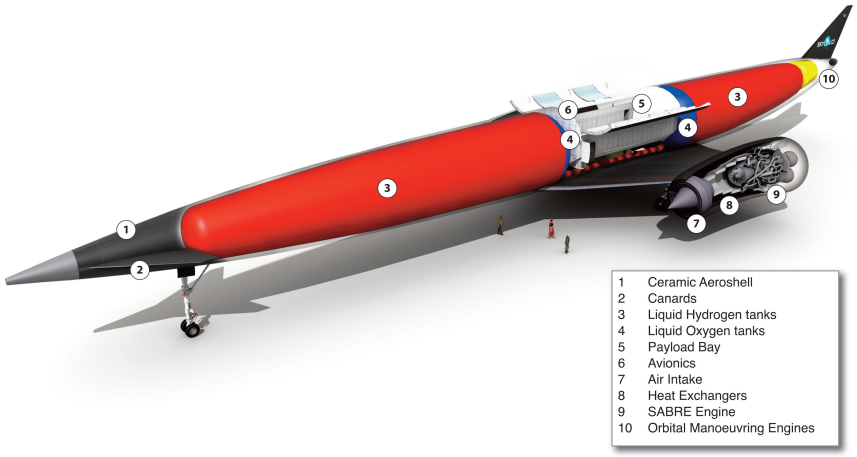


Figure 1.4: Skylon concept art [26]

**Commercial jet airliner**

There are several concepts for commercial hypersonic aircraft. Drag and aerodynamic heating are strongly dependent of cross-section area and therefore different concepts are used for smaller and larger jet airliners.

Collaboration between Europe and Japan resulted in the The Zero Emission Hyper Sonic Transport (ZEHST) concept. This passenger jet airliner is projected to transport 50 to 100 people at a cruise altitude of 32 km, flying at Mach 4. The propulsion system is comprised of three sets of engines, each one operating at different speeds. This is, in fact, a turbine rocket based combined cycle engine, a concept explained in detail in Chapter 4. For ZEHST designed cruising altitude, carbon emissions are predicted to have an high impact on the ozone layer and therefore the engines should be emission free. This may be accomplished by using seaweed based biofuel for the subsonic acceleration and liquid hydrogen for supersonic portion. The time-frame for the ZEHST is “around 2050, but a small scale demonstrator could be a reality by 2020” [27].

For larger commercial airplanes, two designs resulted from the European LAPCAT II program among many other proposed studies: A2 and MR2.

The Reaction Engines Limited LAPCAT Configuration A2 (LAPCAT A2) is a design study for a 300-passenger, hydrogen-fueled hypersonic jet aircraft, with an estimated MTOW of 400,000 kg, powered by four combined-cycle engines. Its design mission is a flight from Brussels to Sydney via North Pole to avoid supersonic land overflight. The aircraft would climb to an altitude of 30km and cruise at Mach 5.2, equivalent to 6,400km/h or 1.8 km/s. At such speeds, LAPCAT A2 could cover a distance of 18,700 km in 4.6 hours, accounting for air traffic control conditions. Prices for a one-way ticket would be similar to that of current business class tickets [28].

The LAPCAT MR2 is a different design for a 300-passenger aircraft. This design would be capable of cruising at Mach 8, allowing an antipodal distance (range between two diametrically opposite points on the globe) to be completed within 3 hours. Initial analysis has shown the feasibility of the concept

provided liquid hydrogen is used as fuel, as it has a much higher specific impulse than ordinary kerosene. The same initial study has proven that a combined high aerodynamic and propulsion efficiency could be guaranteed even at Mach 8. Its radical airframe is necessary to sustain the extreme heat fluxes that are generated at Mach 8. The MR2 is an evolution from the MR1, from the first LAPCAT program [11].

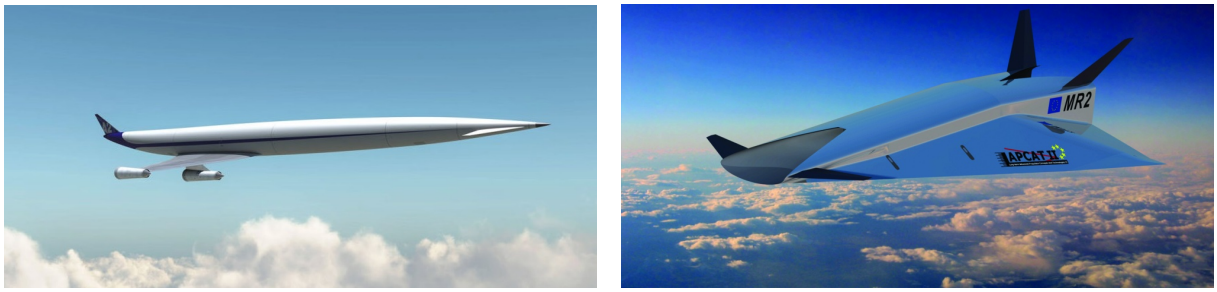


(a) LAPCAT A2 concept art

(b) MR2 concept art

Figure 1.5: Large hypersonic commercial jet aircraft concepts [29]

## 1.3 Objectives

There are two main objectives for this dissertation:

1. Propose a technology roadmap for hypersonic product development;
2. Create the capability of studying hypersonic vehicle configurations in the preliminary design tool SUAVE.

To achieve these goals, a state-of-art survey of current technology and developments for hypersonic flight will be carried out, coupled with an evaluation of civil and defense applications enabled by this flight regime. Such will feed into the creation of a technology roadmap for hypersonic product development across identified applications. To showcase how a further evaluation of the application viability may be pursued, a hypersonic test case will be created and demonstrated using the open source tool SUAVE.

## 1.4 Thesis Outline

The structure of this dissertation is organized as follows:

Chapter 2 describes state-of-art models as well as current hypersonic technologies and their limitations..

Chapter 3 describes the preliminary phase of the technology roadmap, citing the needs, requirements and stating its scope and boundaries.

Chapter 4 is part of the development phase of the technology roadmap and provides detailed insight into research and development of different technologies for hypersonic flight.

Chapter 5 recommends which technologies to pursue, provides a visual representation of the expected timeline for product delivery and concludes the roadmap process.

Chapter 6 introduces the test case that benchmarks new hypersonic technologies and capabilities as well as the framework that is used for this study.

Chapter 7 describes the new numerical models that were implemented to provide the design tool with hypersonic capabilities necessary to conduct the analysis on the case study from the previous chapter.

Chapter 8 details the results yielded by the framework tool.

Chapter 9 provides the final remarks.

# Chapter 2

# State of the art

This chapter is used to discuss the current state-of-art of hypersonic technology. Section 2.1 explains in more detail some of the requirements of hypersonic vehicles, current technological capabilities and obstacles preventing extended application, in different areas. Finally Section 2.2 lists flight-proven vehicles which have already demonstrated, to some extent, robust hypersonic capabilities.

## 2.1 Technology

### 2.1.1 Aerodynamics

Aerodynamics plays a vital role in aircraft performance and, particularly in faster-than-sound flight, its importance cannot be overstated. Aerodynamics-wise, the main objectives to strive for are high lift to drag ratio ($L/D$), high lift coefficient ($C_L$) and high volumetric efficiency. While the latter is important to provide sufficient space to carry cargo, passengers, systems and other equipments, the others are of utmost importance for mission design: $L/D$ is directly proportional to range according to Breguet's equation and a larger $C_L$ can raise the vehicle to higher altitudes, where low atmospheric density results in an overall more desirable aerothermal environment. However, high $L/D$ are very difficult to obtain in hypersonics for a generic configuration because of the strong viscosity effects and intense shock-wave drag. This is further accentuated by the divergent requirements posed by these three variable, intertwined with the rigorous thermal demands of high-speed flight.

One of the most promising concepts in hypersonic aerodynamics is the waverider configuration which makes use of the shock waves being generated by the airframe to act as lifting surface, in a phenomenon known as compression lift: because of their sharp noses and leading edges, the underside shock-surface remains attached and the air flowing in through the shock surface is trapped between the shock and fuselage, forcing itself to escape at the rear. The Boeing X-51, properly nicknamed "WaveRider", is the latest known vehicle to have demonstrated such capacity, in 2013. Waveriders have generally sharp noses and leading edges. Extreme heat fluxes on the sharp leading edges are countered by air rarefaction effects in high-altitude flight.

However, despite its success, there are major technological issues preventing a wider application.

First, scaling this concept to the size of commercial airliners or spacecraft is currently unfeasible as a result of the very low volumetric efficiency of the waverider concept. Another problem is that this design only works for a particular Mach number, resulting in a significant reduced lift capacity when operating in off-design conditions.

### 2.1.2 Sonic signature mitigation

Flow perturbations propagate in the air at the speed of sound; the Mach number then acts as a measure of information propagation in a specific medium. When an object moves faster than this speed, the fluid is not capable of reacting properly to deviate from said object before it is reached. Flow properties change abruptly and almost instantaneously in a phenomena commonly known as a shockwave. Shock waves are formed when a pressure disturbance moves at supersonic speeds and pushes the surrounding air. In the region where this occurs, sound waves traveling against the flow direction reach a point where they cannot travel any further upstream and the pressure progressively builds in that region: the waves are bound together, or compressed, since they cannot get out of the way of each other. Eventually they merge into a single wave traveling at the speed of sound and create a sonic boom.

Various sonic boom tests were conducted to assess their impact on civilian life; in particular, the United States Air Force (USAF) and the Federal Aviation Agency (FAA) conducted a six-month study over Oklahoma City in 1964, where eight sonic booms were generated per day. The study was useful to gather data from the experiment but ultimately resulted in over 15,000 complaints; windows would rattle and dislodge as a consequence of the vibrations and common health effects of noise would apply [30].

Currently there are no industry standards for the acceptability of a sonic boom. The National Aeronautics and Space Administration (NASA) is currently experiencing with design innovations such as boom shaping for the Quiet Supersonic Technology demonstrator with the goal of reassessing current regulations and providing a quiet(er) alternative for supersonic transport [31].

### 2.1.3 Propulsion

Aerospace propulsion mechanisms are categorized separately according to their means of producing thrust. Two main categories are considered for the scope of this work: air-breathing and non-air-breathing engines.

Air-breathing engines, as the name indicates, use the freestream air to act as oxidizer in the combustion process, generating thrust. There is, therefore, no need to carry oxidizer on board, resulting in significant weight savings. An overwhelming majority of engines used in commercial and military aviation are of air-breathing type, such as turbojets, turbofans and turboprops. Ramjet and scramjet engines are mode adequate for supersonic and hypersonic regimes but the technological challenges related with their development have limited their application; they will described more detailedly in Chapter 4.

Non air-breathing engines use oxidizer in the combustion process, which needs to be carried on board. The advantage in using this propulsion system comes from the fact that it works independently of the surrounding conditions. Rocket and nuclear propulsion are the most widely known. Currently, rocket

engines are used mostly in missiles and boosters.

There are severe limitations in current propulsion systems that render sustained air-breathing hypersonic flight unachievable and contemporary turbojet engines cannot single-handedly propel an aircraft to Mach 3+. As the vehicle speeds up, stagnation temperature and pressure significantly rise and strong shockwaves take place at the inlet. This leads to a rapid increase in static temperature and pressure, strong flow detachment on the compressor vanes and temperatures beyond material limits. As a result, less heat can be added in the burner while temperatures at the end of the combustion process must be below the metallurgic limits of the turbine vanes.

High-velocity air-breathing propulsion still remains, to this day, one of the most demanding tasks in hypersonics. Air-breathing engines outperform conventional rockets in regards to specific impulse, safety and maneuverability. For simplified air-breathing cycles, ramjet and scramjet are the most promising concepts [32].

The most powerful, proven, reusable high-speed air-breathing engine conceived to date is the Pratt & Whitney J58, which powered the Lockheed SR-71 ”Blackbird” up to Mach 3 with technology developed 60 years ago. This could only be possible with a high bypass afterburner at a very high fuel burn rate, effectively making it a turbo-ramjet engine. Furthermore, the engine required significant maintenance upon landing to re-fly.

Currently, the only way to achieve higher speeds from static launch takeoff conditions is through rocket engines, with a heavy penalty on payload capacity. As such, performance across a broad range of operating speeds is a major limitation. As of now, propulsion systems are either very limited for such a large mission profile, too heavy or not mature enough to be a proven technology.

### 2.1.4 Materials

Hypersonic flight through the atmosphere generates extremely high temperatures as the result of two phenomena over the vehicle surface:

- Conversion of coherent kinetic energy to internal energy of the gas, as shockwave deceleration across the hypersonic structure takes place;
- Large entropy increase and viscous dissipation over the vehicle surface due to the boundary layer downstream of the leading edge shock

As such, air properties have a strong influence on the temperatures at the vehicle surface. For instance, the Space Shuttle orbiter re-entry velocity at an altitude of 120km was equivalent to Mach 25 and the downstream of the bow shock produced temperatures capable of reaching 7,000 K. However, the effect of these extreme temperatures was balanced by strong air rarefaction. For atmospheric flight, where ambient pressure and density are much higher, these temperatures would be unbearable for any material known so far.

Hence, sustained hypersonic flight is strongly limited by the materials deployed on the airframe. To survive this flight regime, they must be strong enough to withstand high heat fluxes, temperatures and

temperature gradients. Furthermore they must provide shielding against oxidation and erosion while supporting strong aerodynamic loads. Critical conditions takes place on the vehicle leading edge, where these parameters reach their peak value. Temperature requirements on a sharp leading edge for a cruise hypersonic vehicle are in the order of 2000-3000° C compared with current shuttle reinforced carbon-carbon leading edge materials which withstand approximately 1650 ° C [33].

### 2.1.5 Thermal Protection Systems

Thermal protection systems (TPS) incorporate different technologies that help the vehicle resist excess heat in hypersonic flight. They are not only dependent on the material properties but also other mechanisms that can be implemented to alleviate thermal loads. Over time, new TPS concepts have been proposed for high speed flight and these can be grouped in separate categories depending on their fundamental working principle.

Different types of thermal management are implemented depending on the mission profile and, subsequently, the aerodynamic heating profile. The same vehicle can bear different TPS for its many subcomponents, as each may be exposed to unique hypersonic conditions. In general, TPS can be divided in three categories: passive, semi-active and active. [34, 35].

- Passive TPS makes use of materials that are able to cool the surface through radiation, withstanding high temperatures while minimizing heat flow to the internal structure. Passive TPS has been the go-to technology for atmospheric re-entry and other extreme heat conditions since the dawn of the Space age: they are fairly simple to design and support moderate heat loads. However, as the heat load increases, so does the required TPS weight, rendering them unfeasible and unpractical for a variety of mission profiles. Passive TPS mechanisms can be further split in different concepts: heat sinks, hot structures and insulation.
  - The heat sink concept is designed to absorb the incident heat load. The maximum heat capacity is determined by the initial temperature of the structure, the amount of TPS material and its properties (i.e., specific heat capacity, maximum service temperature). Because high heat loads translate to a heavier TPS, this concept is not suitable for large surface areas. Nevertheless, it is a very simple, reliable design which has been implemented on the afterbodies of the Mercury and Gemini reentry vehicles;
  - The principle behind hot structures relies on heat re-radiation by applying a high emissivity surface or coating. These TPS systems operate near adiabatic temperatures and therefore there is no net energy absorption through the vehicle skin. The radiation equilibrium temperature is determined by the emissivity of the TPS top surface and can reach very high temperatures;
  - Insulation TPS effectively acts as part hot structure, part heat sink. It works by interposing a high temperature, low thermal conductance insulator between hot skin and the airframe. Usually ceramics are used but their high rate of porosity and low fracture toughness impose considerably restraints on its application.

- Semi-active TPS rely upon a working fluid to remove heat, without requiring any external system for its circulation. Unlike the previous concept, this type of TPS can withstand higher thermal loads and is therefore appropriate for more prolonged mission envelopes. There are two main semi-passive TPS concepts, heat pipes and ablators:
  - Heat pipe TPS relies on highly efficient thermal conductivity through internal convection, effectively distributing intense localized heat from one area to cooler locations, to be rejected or stored. They are suitable for regions of extremely high, localized heating, relatively close to a cooler region (e.g., wing leading edge, fuselage nose);
  - Ablators work by applying a single-use coating that stores heat by combination of chemical and endothermic phase changes and/or mass loss by evaporation. They are very practical and attractive concepts and were used in the Apollo and Soyuz capsules. Nevertheless, despite its successful implementation in small areas, it is not a viable concept for large vehicle surfaces.
- Active TPS requires an external system to continuously supply coolant to alleviate heat loads to the structure. These systems add complexity to the vehicle design (i.e., aerodynamic performance) and mission design (i.e., additional coolant weight decreases payload capacity). There are three main concepts for active TPS: transpiration, film and convective cooling.
  - In transpiration and film cooling, a fluid is ejected from the vehicle surface; by traveling alongside it, the fluid evaporates when absorbing the atmospheric heat, mitigating its effect on the surface;
  - In convective cooling, fluid circulates through passages and small gateways in the airframe to remove heat from the freestream flow.

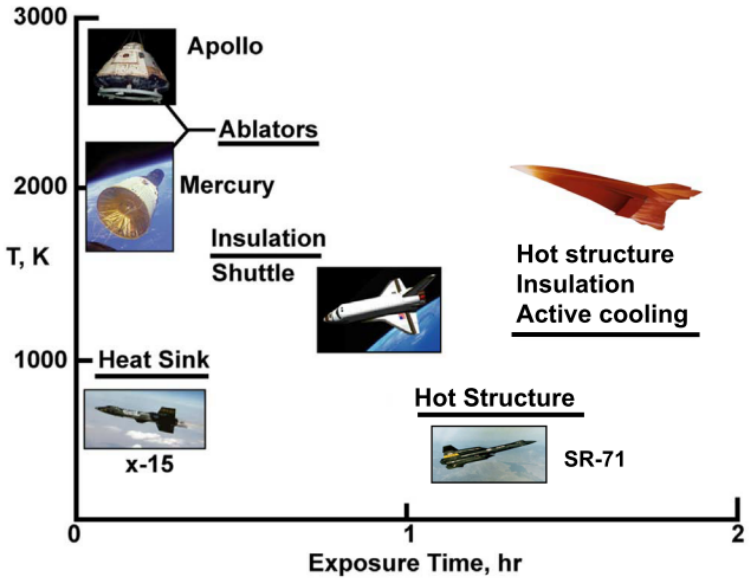


Figure 2.1: TPS application map [36]

The correct choice of TPS results from a balance between the heat fluxes exerted on the vehicle and the exposure time, as clarified in Figure 2.1. Further evidence for this statement is provided in Chapter 8 upon comparing different mission profiles.

While semi-active and active TPS concepts can accommodate larger heat fluxes for extended periods of time, they have to overcome design challenges and working constraints before becoming fully-matured technologies. That is why passive TPS, through its multiple concepts, is used to a much greater extent.

State-of-the-art TPS has been applied to expendable, re-entry spacecraft, such as the PICA heat shield used on Stardust, capable of withstanding heat fluxes of 1500 $W/cm^2$ [37]. In the spectrum of reusable mechanisms, the Space Shuttle TPS, composed primarily of TUFI ceramic tiles, could sustain multiple re-entries [38]. However, upon landing, panels would require significant maintenance, resulting in high turnaround times and repair costs. Ultimately, mechanical failure (i.e., very low impact resistance) was the main reason behind the fatal Challenger disaster in 2003.

### 2.1.6 Control

Guidance, Navigation and Control (GNC) systems are critical enabling technologies for a safe and efficient hypersonic operation. These must be reliable, robust but also highly sensitive to minimal changes in the environment and/or working conditions. In hypersonics, any small perturbation in freestream flow can rapidly propagate and result in viscous instability, which is amplified as the air moves downstream [39]. Moreover, the displacement of the center-of-gravity location in hypersonics requires small trim corrections which, at such speeds, need to be applied within a short time scale to prevent instability [40].

Currently there are numerous designs for hypersonic flight control, whose main task is to deal with the system uncertainty and guarantee the stability of the closed-loop system. Control design can be based on different methodologies such as small perturbations, input/output linearization or back-stepping. The latter, back-stepping, is a powerful tool for non-linear controllers, based on recursive design. It is used quite extensively in hypersonic flight control since hypersonic dynamics is in cascade form [41].

One of the biggest accomplishments in GNC systems dates back to the 80s, when then Soviet Union managed to launch and land Buran, a fully automatic spaceplane, an extraordinary feat considering how rudimentary GNC theory and technology was back in this age. Buran was the first space shuttle to perform an unmanned flight and still holds the record of the largest aircraft to orbit and land unmanned [42]. Recently, there has been progress in the hypersonic GNC field, such as demonstrations for the Boeing X-51 scramjet-powered aircraft. Nevertheless, one of the most advanced GNC systems of today must be that of the Boeing X-37. Operated by the Defense Advanced Research Projects Agency (DARPA), this secretive spaceplane is taken to LEO through expendable rocket engines, where it then conducts classified missions before performing a fully autonomous re-entry and landing.

### 2.1.7 Engineering tools

Hypersonics is a major engineering challenge. To assist in technology development and subsequent application in vehicle design, powerful tools are required. These can take the form of Computational Fluid

Dynamics (CFD) software, Multi-Disciplinary Optimization (MDO) tools or databases (among others). Their task is to provide accurate predictions of important engineering parameters, which will determine the success of a certain design. However, when during the conceptual phase of a new project, there is a need for flexible and quick tools that analyze the trade-offs between technologies and designs, pointing towards the most viable options. The goal in this preliminary phase is to spend very few time in heavy computational calculations and only use these tools for fine-tuning and final concept validation. This preliminary analysis is dependent on multi-fidelity tools and enhancing these capabilities is an important contribute towards successful hypersonic aircraft design. R&D activities in MDO will not be mentioned in this work but there are tools capable of performing in this preliminary environment. Nevertheless, the proposed roadmap output will apply directly to upgrading a multi-fidelity analysis tool in Chapter 7.

## 2.2 Vehicles

There is an extraordinary small number of vehicles to have successfully performed in hypersonic conditions. A majority are only technology demonstrators and were used as testbeds for a larger hypersonic agenda. As of 2018, there is no vehicle that can continuously accelerate from takeoff to hypersonic speed without using an auxiliary propulsion system. Nevertheless, technology has matured in several areas and upon looking at the last five years, there have been major advances in hypersonic full-scale aerial systems.

### 2.2.1 Boeing X-51

The Boeing X-51 ”WaveRider” was an experimental aircraft, developed from a cooperation effort between USAF, DARPA, NASA, Boeing and Pratt & Whitney Rocketdyne. It was originally commissioned as part of the endothermic fueled scramjet engine flight demonstrator program in December 2003, being renamed X-51 in 2005. With a length of approximately 8 meters and an empty weight of 1,800 kg, the X-51 was an hypersonic air-breathing propulsion demonstrator. Before scramjet engine ignition, the X-51 was carried by a B-52 to an altitude of 15 km at subsonic speed and then accelerated to Mach 4.5 by a solid rocket booster, which would detach from the airframe as soon as the scramjet engine ignited.

The waverider design provides the vehicle with a substantial amount of lift without being dependent on the wings. When the X-51 travels at high speeds, the increased heat can damage the metal portions of the airframe by melting them. In order to avoid damage, the hypersonic combustion is used to produce cycling water behind the engine cowl and sidewall edges, thereby cooling the surfaces.

After two failed tests, in 2013, the Rocketdyne SJY61 scramjet engine performed successfully for 210 seconds over Mach 5, becoming the longest duration powered hypersonic flight. The test signified the completion of the program [43].

### 2.2.2 IXV

The Intermediate eXperimental Vehicle (IXV) was an experimental suborbital re-entry vehicle developed by ESA. This spacecraft was a prototype to validate ESA's work in the field of lifting-body technology and TPS. It consisted of a wingless spacecraft and lift was generated by its own fuselage. At the rear, two flaps were used to steer the vehicle during re-entry.

IXV was launched on February 2015, on board of the Vega launch vehicle. After reaching a peak altitude of 412 km, it began its re-entry at 120 km, with a speed of 7.5 km/s, simulating a typical re-entry path from LEO spacecraft. Prior to re-entry, the IXV made use of its lifting body to glide and land over the Pacific Ocean.

The spacecraft belly was covered in protective heat-resistant panels made of carbon-fibers, woven into a ceramic matrix. Through an infrared camera and a large array of sensors on the heat shield, it was possible to map the heat flow on the belly during re-entry. Following the major IXV success, a new test has been scheduled for 2019-2020, this time with a runway landing planned.

(a) Boeing X-51 "WaveRider" (b) IXV after splashdown

Figure 2.2: State-of-the-art hypersonic vehicle demonstrators [43, 44]

### 2.2.3 DF-ZF and Kinzhal

Shifting East, there have been major advances in China and Russia with successful military demonstrations.

The DF-ZF is an hypersonic missile delivery vehicle being developed by China and expected to enter service by 2020. Several tests have taken place since its maiden flight in 2014, with the most recent in late 2017. There is little information on this hypersonic glider but it is believed it can reach speeds between Mach 5 and 10. A vehicle like the DF-ZF could be fitted into intercontinental ballistic missiles, extending range from 8,000 to 12,000 km. Analysts suspect that the DZ-ZF will first be used in shorter-range roles as an anti-ship missile and for other tactical purposes to address the problem of hitting a moving target with a ballistic missile [45, 46].

Russia has announced in March 2018 a new hypersonic cruise missile, to be launched from a MiG-31 aircraft. This missile is said to travel at Mach 10 and have a range of 2,000 km, through rocket propulsion. Despite a public announcement stating the technology readiness, no further information has been disclosed [47].

# Chapter 3

# Roadmap requirements

This chapter initializes the building process for the hypersonic technology roadmap. The tools for developing the roadmap are described in Section 3.1. The essential conditions, boundaries and focus for this roadmap are set from Sections 3.2 to 3.5. The critical system requirements are briefly described in Section 3.6. Finally, the major technology drivers and targets are listed in Section 3.7.

## 3.1 Framework for development assessment

### 3.1.1 Roadmap methodology

A technology roadmap is a tool to support strategic and long-range planning by matching both short and long term goals to specific technology solutions. Therefore, a major part of it consists on scouting and forecasting emerging technologies to be used in the development of a certain product. In the particular case of innovative markets and/or products, roadmaps are of significant importance to provide a financially-detached overview (even though it can be coupled with other corporate foresight methods). These are valuable tools to measure progress and manage a common vision towards the application goals in a high uncertainty environment.

There are clear benefits associated with the development of such roadmaps, regardless of company size and/or status:

- Setting a common vision across disciplines and stakeholders;
- Matching goals with specific technology solutions, applied to new products or processes;
- Setting needs and technologies required to achieve them;
- Providing a framework that forecasts, monitors and coordinates technology development.

For the purpose of this work, the model in use is adapted from the Defense Logistics Agency of the United States Department of Defense [48]. It consists of three main phases, each one built from smaller activities. Table 3.1 lists all the phases and activities detailedly.

| Phase | Activity | Description |
|---|---|---|
| I: Preliminary Assessment | Identify essential conditions | Define customers, suppliers and other essential groups. Clarify what the conditions are and who takes actions to meet them |
| | Provide leadership/sponsorship | Define who is responsible to drive the roadmapping process |
| | Define scope and boundaries | State and the develop the context and vision for the roadmap. Delimit boundaries to refine roadmap needs and level of detail |
| II: Roadmap Development | Identify the product focus | State common product needs |
| | Identify critical system requirements | State requirements that provide an overall framework for the roadmap. Requirements must be of high-level dimensions. State targets for each requirement |
| | Identify major technological areas | Link major technological areas to the critical system requirements |
| | Identify main technology drivers | Transform the critical system requirements into technology drivers, specifying the targets set to each one of them. |
| | Identify technology alternatives | Link technology alternatives to meet targets set in previous step. Identifies a timeline for each alternative |
| | Recommend alternatives to follow | Determine which technology alternative should be pursued by gathering information and consensus from experts |
| | Create the technology roadmap report | Build the roadmap |
| III: Follow-up activity | Validate and accept the roadmap | Periodical review and update to assess technology progress and compare it with roadmap prediction |

Table 3.1: Technology roadmap model (adapted) [48]

### 3.1.2 Technology Readiness Level scale

Among other readiness scales such as the business readiness level and the manufacture readiness level, the technology readiness levels (TRL) was selected as a reference scale for this project, particularly for the construction of the roadmap. TRL is a method of estimating and comparing the maturity of a set of critical technology elements enrolled in a wider program/project.

The TRL scale was developed during the 1970s for NASA when it was concluded from observation that the research and development (R&D), operational and planning communities were facing difficulties in communication and synchronization of their own progress scales during development; this in turn had

a significant impact in performance, scheduling and budget, especially as it regarded high-complexity technological systems. By using a standard TRL, the common assessment of individual technologies allows for risk reduction both in budget and planning processes. Even though it is not exempt from flaws, it is widely used, albeit adapted to better fit the needs of the organization enforcing it. For the purpose of this dissertation, the same TRL standard as that of the European Space Agency [49] for Space product development is used, as it closely resembles the original NASA TRL. It is comprised of nine different levels, all of which are specified in Appendix A.1.

## 3.2 Essential conditions

Hypersonic aerospace activities are a challenging endeavor, whose complexity is dictated by the entanglement of vastly different and strongly conflicting design parameters (aerodynamics vs. sonic signature, TPS vs. aircraft weight, etc). While at low hypersonic flight there can be a certain degree of separation between airframe and propulsion manufacture (approachable to current production methodologies), the problem worsens at high hypersonic speeds when airframe/propulsion integration is unavoidable to attain satisfactory performance.

The main actors in the hypersonic aerospace market are the users that benefit from high-speed atmospheric/orbital transport, through both passenger and cargo transportation. These services have to be provided by airliners and future spaceliners. These companies build up their fleets with certified aircraft and spacecraft built by aircraft and engine manufacturers, each conceived with different flight envelopes depending on its final application. New hypersonic aircraft and spacecraft therefore depend on R&D centers for technology maturation and regulatory agencies for certification.

## 3.3 Leadership and Sponsorship

Currently, technological advances on the field of hypersonics have come from companies with vastly different backgrounds, state or private-owned, with focus on single or multiple technological areas. Hypersonics is still undergoing a massive development phase and only now tangible results are being presented. Agencies responsible for national and international airspace monitoring (e.g., FAA, ICAO, EASA) must be included in the loop and properly advise and provide feedback on any new regulatory issues that will inevitable come forward. Furthermore, for these concepts to become a reality, an increasing level of integration must be achieved so that economical, legal and organizational readiness can be synced to technology development and maturation.

## 3.4 Scope and boundaries

The creation of this roadmap is fully justified by a strong R&D effort towards a viable hypersonic market. Even though hypersonics has been under intensive studies since the 1960s, only now technology has reached a point where practical applications have become somewhat viable and successful hypersonic

demonstrations in complex fields such as air-breathing propulsion have already taken place. There have been numerous studies on hypersonics and hypersonic technology roadmap proposals in the past [50, 51]; however without constant maintenance and revision, they may become outdated and useless as new technologies emerge and current technologies either mature or fail to deliver. The creation of this particular roadmap is further driven by the will of Embraer R&D department to have a tool that can assess and comprehend the potential of new technologies and map synergies established among them.

Therefore, the main vision leading this project is that of a wide international hypersonic market for civilian activities by 2050, expanded beyond Earth's atmosphere into sub-orbital and orbital domains. As such, the purpose of this roadmap is to map/identify hypersonic applications, how they can be conceptually materialized, what obstacles stand in their way and what technologies should be used to overcome said obstacles. The technology scope focuses on the main areas behind hypersonic flight, including aerodynamics, thermodynamics, stability and control, propulsion and material design.

This roadmap is intended to provide an overall view of enabling technologies towards routine hypersonic market while refraining from venturing into unrealistic or overly conceptual technologies which have not yet been properly demonstrated to a minimum extent.

## 3.5 Hypersonic product focus

There are two main necessities for an hypersonic product: cost-effectiveness and safety. Any future hypersonic applications, whether military or civilian, atmospheric or suborbital/orbital, need to be financially viable and this effort must take place at different operational levels. Firstly, the product must perform efficiently throughout the entire mission envelope, including subsonic and supersonic segments. Secondly the product should be able to carry relevant payloads to become more versatile and flexible and therefore expand rapidly as a business. Finally, sustainability must also be taken into consideration to maximize product life cycle. This allows for amortization of initial purchase through multiple flights albeit maintenance costs must be included in the equation.

Hypersonic applications must follow strict safety rules and comply with regulatory agencies, either national, supranational or international. These organizations are responsible to monitor and enforce very high standards for airlines and future spaceliners. Current airliners and manufacturers are subjected to very demanding safety rules which contribute to the low fatality rate and risk associated with commercial aviation. For future hypersonic products, where the environment presents a much higher threat, these demands must not be downgraded.

## 3.6 Critical system requirements

From analyzing state-of-the-art hypersonic technology and current technological gaps, it is possible to conclude there are many critical systems with a high degree of integration; however, any effort to fully map hypersonic requirements may become too extensive given the size constraints for this dissertation. Therefore, to simplify and streamline the mapping process, the list of critical system requirements was

narrowed down to refer to practical engineering problems, excluding developments on analysis and design tools. A list of the critical system requirements to be evaluated in this work can be found on Table 3.2, alongside a brief description and corresponding targets.

It should be noted however, that despite not being mentioned in this work, design and analysis tools (e.g., CFD software, material databases, experimental facilities, plasma numerical models, preliminary analysis software) are critical to understand how different subsystems behave and how their integration in a larger aircraft design affects its performance. To cut down time and costs associated with the development of new technologies, these tools must be improved to generate accurate performance estimates. This notion is reinforced in Chapter 6 when SUAVE is used for preliminary analysis of a generic hypersonic vehicle.

| Critical system | Description | Targets |
|---|---|---|
| Heat management | Extreme heat loads produced by aerothermodynamics on critical vehicle subsystems | Withstand high heat fluxes and temperatures |
| Thrust | Continuous, unassisted powered flight through all flight phases until hypersonic | Mach 0 - Mach 5+ |
| Design | Efficient, aerodynamic, quiet design | Sonic boom and wave drag mitigation; full or partial integration of major subsystems |
| Integrity | Extreme mechanical loads when subjected to hypersonic environment | Extended subsystem life cycle |
| Control | Hypersonic vehicles highly sensitive to changes in flight conditions | Powerful GNC and efficient mechanisms to prevent instability |

Table 3.2: Critical system requirements and respective targets

## 3.7 Technological areas, goals and enablers

To address the issues raised in Section 3.6, all technology alternatives must be properly sorted according to the needs and/or requirements they fulfill. This results in a cleaner structure and contributes to a more efficient roadmapping process.

The first step is to identify the main technological areas which address the critical system requirements. For the hypersonic problem, there are six distinct technological areas this work focuses on: propulsion, materials, thermal protection systems, guidance and navigation control, aerodynamics and sonic signature. However, because these are broad categories, each area is split among different drivers which can have specific goals associated.

Upon examining existing literature, the work has been structured according to Table 3.3. Each driver is associated with a specific reference, which will be necessary to comprehend which technological alternatives apply to it.

| Technological Area | Drivers | Goal |
|---|---|---|
| A. Propulsion | (A1) Subsonic to low hypersonic acceleration | High performance Mach 0 to Mach 3 |
| | (A2) Acceleration to hypersonic cruise speed | Mach 3 to Mach 5+ |
| | (A3) Orbital insertion | Minimum speed 6 km/s |
| | (A4) Continuous propulsion | Integrated propulsion systems |
| B. Materials | (B1) Leading edge | Temperatures up to 3000 K [52] |
| | (B2) Control surfaces | Lightweight, strong mechanical properties |
| | (B3) Engines | High strength-to-weight and heat resistance [53] |
| | (B4) Airframe | Lightweight, high fracture toughness |
| C. TPS | (C1) Leading edge | Heat flux up to 500 $W/cm^2$ [54] |
| | (C2) Acreage | Lightweight, strong mechanical properties |
| | (C3) Internal insulation | Lightweight, high conductivity |
| D. Aerodynamics | (D1) High lift configuration and low drag | Maximize L/D |
| E. Sonic signature | (E1) Sonic boom mitigation | Sonic boom below 90db [31] |
| F. GNC | (F1) Hypersonic control systems | Reliability, robustness, high sensitivity |

Table 3.3: Technology drivers and goals

# Chapter 4

# Novel technologies and concepts

This chapter is tasked with providing technology alternatives for a generic hypersonic product that attend to the technological drivers set in Section 3.7. Technology alternatives are categorized by their main technological area, represented from Sections 4.1 to 4.6. A final summary is presented in Section 4.7.

## 4.1 Propulsion

### 4.1.1 Dual-mode ramjet engine

Dual-mode ramjet (DMR) engines are purely supersonic propulsion systems that can attain both subsonic and supersonic combustion, effectively working as either a ramjet or a scramjet engine. By integrating both engines in a single design, the propulsion system is fundamentally lighter as the same flow path is used. Therefore, DMR are dependent on individual ramjet and scramjet performance, as well as final integration design.

Ramjets engines have been successfully applied to missile designs. The most notable example of a ramjet-powered missile is the BrahMos [55], a medium-range ramjet supersonic cruise missile and a joint venture between India and Russia in service since 2006. This is the world's fastest anti-ship cruise missile in operation, capable of reaching Mach 3.0 at an altitude of 14,000 meters. To achieve supersonic speed it is initially powered by a first-stage rocket and only then switches to its second-stage liquid-fueled ramjet. This second stage, despite introducing a certain degree of complexity in its design, has better fuel efficiency and the BrahMos range is almost triple of modern conventional missiles.

More recently, advances in scramjet-powered vehicles took place with the successful test of the Boeing X-51 "WaveRider", a collaboration between Boeing, USAF, DARPA, NASA and Pratt and Whitney Rocketdyne. The vehicle was designed to be carried to a high altitude by an auxiliary plane, accelerated through rocket propulsion beyond the scramjet start velocity and only then turn on the scramjet engine. Rocket auxiliary propulsion structure was ejected before scramjet start. Three different models were built and flown between 2010 and 2013; the X-51 reached Mach 5+ while in scramjet-mode and broke the record for the longest scramjet-powered flight. Other scramjet projects are under development in Brazil, India and Australia. Given latest developments on this technology, a TRL 6-7 is proposed.

### 4.1.2 Continuous Rotating Detonation Engine

The Continuous Rotating Detonation Engine (CRDE) is a type of pressure-gain combustion engine where the combustion process relies on detonation instead of traditional deflagration. As a result, the propagation speed is much higher and thus tied to a coupled shock effect. This results in pressure and temperature rise, providing a much more efficient thermal process. Furthermore, detonation allows a more intense and steadier combustion, which in turn reflects in a smaller combustor design for high thrust generation [56]. There are three different processes for detonation-based engines: standing detonation, pulse detonation and continuously rotating detonation. For aircraft propulsion and in particular for high-speed flight, CRDE is the most promising concept.

CRDE can be thought of as a infinite number of small pulse detonations running at very high frequency. CRDE engines utilize an annular combustion chamber closed on one side and opened at the other end chamber. The closed head has numerous micro nozzles through which the fuel is injected. While the flow transverses in the axial direction,the combustion reaction creates detonation waves which propagate in the circumferential direction, normal to the direction of injection. Downstream of the detonation wave, the exhaust gas has a greater temperature and pressure and, through a series of expansion waves, these burnt products flow out of the combustion chamber in a near axial direction into the exit nozzle. The transverse detonation wave propagates in a small layer of fresh mixture near the injection wall and, to allow for a continuous process, the layer of combustible mixture ahead of the transverse detonation wave must be constantly renewed [57].

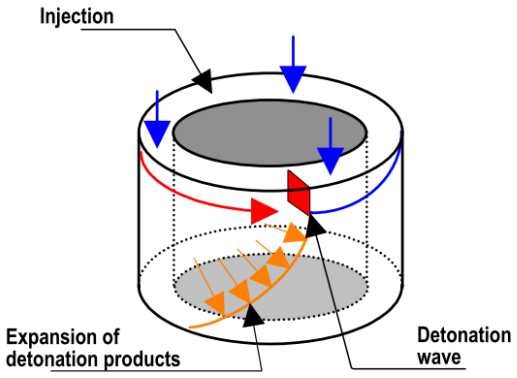


Figure 4.1: Simplified diagram of a CDRE combustion chamber. [57]

In recent years in Russia, researchers at the Institute of Hydrodynamics achieved continuous liquid and gas fuel detonations in combustors of different shapes, using different injection systems. Tests were carried with fuels such as hydrogen, kerosene, gasoline, propane and methane and a maximum specific impulse as high as 200 seconds was achieved with a kerosene-oxygen mixture. This experience also studied techniques to capture the flow field inside the CRDE and provide a stable detonation wave throughout the combustion process. [58]

In Europe, the leading work has been developed by MBDA-France, with the support of French National Center for Space Studies (CNES), which not only conducted theoretical studies but also designed

and performed ground tests on a full-size CRDE model to address issues of a continuous detonation rocket engine using LH2/LOX mixture [59]. In 2011, the company announced the Perseus supersonic missile system, due to enter service in 2030. With a comparable performance to that of the BrahMos missile, its efficiency savings by using CRDE technology estimate a launch mass reduction over 70% and a corresponding body length decrease of 40%, carrying a 200 kg payload at Mach 3+.

In the United States, Lu et al. [60] from University of Texas at Arlington analyzed the challenges of CRDE and performed feasibility studies on the burner performance when integrated in an engine cycle. They concluded that the detonation annulus of the combustion chamber can be directly connected to an axial inlet systems allowing the air to mix with fuel between detonation waves. Moreover, comparisons between air-breathing pulse detonation engines and CRDE simulations in this study showcase CRDEs superior capabilities on high-speed flight.

On the industrial level, companies such as Pratt & Whitney Rocketdyne and GHKN/Aerojet have also begun experimental work on this promising technology. Given current development stage and known research projects, a final TRL 4-5 is attributed, for supersonic/hypersonic segments and subsonic segments, respectively.

### 4.1.3 Combined cycle engines

A versatile hypersonic vehicle must be able to continuously accelerate from static to hypersonic conditions. However, propulsion systems introduced so far have a limited Mach range; only rocket propulsion can deliver this capability at the expense of carrying oxidizer on-board. Therefore, any combination of these cycles is an attractive option.

Combined cycle propulsion systems can be split into three categories [61]:

- Turbine Based Combined Cycle (TBCC)
- Rocket Based Combined Cycle (RBCC)
- Turbine Rocket Based Combined Cycle (TRBCC), also known as TriJet engines

TBCC engines are a combination of turbine-based engines (usually turbojets) with ramjet/scramjets. The turbojet is used to accelerate the vehicle to a specific speed from which ramjet operation can take over. The turbojet is mounted on a separate duct with its own flow path to isolate it from the high enthalpy flow of hypersonic flight, which could result in critical damage to the turbo-compressor. Turbojet is responsible for all subsonic operations, including take-off, ferrying and landing. However, if it is not properly sized, there can be ”thrust trap” between turbo and ramjet modes: this happens when flight speeds are too high for turbojet operation but not high enough to obtain significant ram compression [62].

RBCC engines follow the same schematics of a TBCC but replacing the turbojet with a rocket engine. Rocket thrusters have the advantage of being mounted within the high speed flow path and function as ejector ramjets, therefore excluding the need for a separate flow path altogether. This results in a

significantly lower installed weight. However, specific impulse provided by RBCC engines falls short of its TBCC and even its turbojet counterpart.

Finally, TRBCC (also known as Turbo-Aided Rocket-Augmented Combined Cycle) are a merger of the last two concepts. The turbojet cycle can be sized to provide efficient subsonic operation. The rocket cycle can be used to assist the turbojet in transonic acceleration, where the parasite drag is higher. [62].

For the three concepts, hypersonic flight is usually provided by a dual mode ramjet engine, where an isolator installed between the inlet and the combustion chamber adequately separates ramjet from scramjet operation. Currently, TRL for TBCC is 5-6, with Lockheed planning to implement them on the SR-72 reconnaissance aircraft. RBCC have been studied by NASA, with plans for technology demonstrators around 2030, with a current TRL 3-4 estimate. TRBCC are the most complex design of three as they encompass three different propulsion systems in one; while there have been some studies and proposed designs (i.e., TriJet [63]), this concept has a lower TRL of 2-3.

### 4.1.4 Magneto-hydrodynamic engines

Magneto-hydrodynamic engines are strong contenders for single flow path alternatives to current combined-cycle systems. Magneto-hydrodynamic energy-management techniques have the possibility to extend the flight Mach envelope of conventional engines, through the use of a magneto-hydrodynamic drive (MHD) generator. As such, this technology can be applied to regular air-breathing engines with minimum penalties on airframe/engine integration, as exemplified in Figure 4.2. The MHD generator is a device responsible for transforming thermal and kinetic energy into electricity, by means of hot conductive plasma moving through a magnetic field.

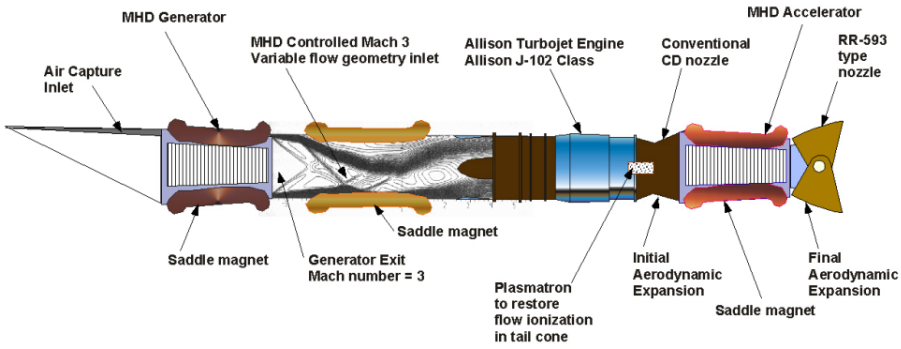


Figure 4.2: General arrangement of MHD-controlled turbojet high-Speed propulsion engine [26]

In a generic configuration, an MHD generator is placed between the inlet and the burner. By converting kinetic energy into electric power, enthalpy is extracted from the flow and bypasses the engine flow path. As a consequence, the overall static temperature rise due to flow deceleration in the inlet can be pro-actively constrained, supporting a higher stagnation enthalpy in the inlet (and subsequently, higher freestream Mach number) [64]. As it stands, the concept works if freestream stagnation enthalpies are high enough to ionize the freestream airflow, which would require the vehicle to be traveling at high-hypersonic speeds. However, the electric power extracted from the flow can then be used in a

pre-ionizer placed downstream of the inlet, allowing for continuous thrust from static conditions. Hence, there are major advantages brought by the MHD engine bypass concept [65]:

- No mode transition: turbo-machinery operates continuously over entire Mach range;
- Single flow path: refraining from a combined-cycle methodology eliminates dead weight and useless machinery;
- MHD power generation: Power can be extracted from the flow and used on other vehicle systems (i.e., weakly ionized gases can be used for shock-wave interference and modification of the flow around the aircraft. This would result in an apparent variable-geometry and could offer shock-free interaction with high speed inlet flows);
- MHD inlet control: through dynamic magnetic contraction, recovery losses can be minimized even when flow-field is at off-design conditions.

USA and Russia are the main players exploring this technology. NASA has been conducting recent studies on the prospects of MHD engines [66] but the original concept is Russian and dates back to the 1960s in the form of Ayaks, a project for a Soviet spaceplane intended to fly at an altitude between 50 and 85 km. In this atmosphere layer called mesosphere, the air is ionized due to solar radiation and the MHD generator would be allowed to work without extensive assistance from a pre-ionizer. The MHD generator would slow down the incoming ionized flow and generate electricity to be applied in the magnetoplasmadynamic thruster at the nozzle exit, creating additional thrust. Air capture area would not be a problem regardless of high speed because the plasma funnel derived from the magnetohydrodynamic forces would increase the effective inlet diameter [67]. No new information has been given regarding the status of the Ayaks program ever since. A TRL 2-3 estimate is attributed.

### 4.1.5 Pre-cooled jet engines, SABRE and Scimitar

An air-breathing vehicle cruising at Mach 5 through the atmosphere experiences stagnation temperatures close to 1320 K and the high compression that takes place in the inlet results in elevated temperatures on the engine internal flow path. Turbojet engines cannot realistically operate at these speeds: it is impractical to compress the air directly to even higher pressures and the resulting compressor delivery temperature would surpass current turbo-machinery limits. The solution can come by installing a precooler station between the inlet and the compressor. A cryogenic fuel could also be used as coolant to simplify integration with other aircraft systems and avoid unnecessary weight penalties. By precooling the air, the flight envelope of the vehicle is extended beyond Mach 4, reducing the compressor exit air temperature. Thrust is also increased because less power is required to compress a now cooler and denser air [68].

The concept of pre-cooled jet engines was first described by Robert P. Carmichael in 1955 and gave birth to other related concepts such as LACE, which would cool and liquefy the air. [69, 70] More recently, major research and development activities have been taking place in Japan and Europe.

The ATREX (air-turbo ramjet engine) project began in Japan in 1988 under guidelines from the Institute of Space and Astronautical Science, ancestor of the Japan Aerospace Exploration Agency (JAXA). [71]. Funding was eventually shifted to JAXA's current hypersonic precooled propulsion project, the Pre-Cooled Turbojet Engine (PCTJ). For this design, a small single-spool turbojet is used as a core engine and a precooling system and reheat burner are attached. This engine was successfully operated at sea level static condition in 2008 using liquid hydrogen as fuel and coolant. In 2010, the first supersonic test was conducted: to achieve such speeds, the engine dived from an auxiliary balloon-based operation vehicle at an altitude of 40 km. The engine was ignited and operated for 20 seconds in supersonic flight environment [68]. More recently, Mach 4 propulsion wind tunnel experiments were performed, where the precooler design was improved and it could now be shielded from particles flowing into the engine. Future plans include Mach 5 ground experiments, where core engine operation will be tested [72]. Given these developments, a TRL 4-5 estimate is given.

In Europe, Reaction Engines Limited is developing a pre-cooled combined cycle engines intended for ascent and re-entry vehicles: SABRE (Synergetic Air-Breathing Reaction Engine). It incorporates rocket propulsion in the main turbojet cycle to expand the flight range and improve fuel efficiency, with the goal of delivering SSTO capabilities. Unlike ATREX, SABRE uses two fluids for the refrigeration cycle. This is the case because while a simple hydrogen-air cooling system is in theory the simplest method to cool and provide fuel to the air flow, by interposing an intermediate fluid one can prevent issues related to hydrogen embrittlement and provide an additional safety layer between fuel and oxidizer. For SABRE, helium is the fluid of choice; it is an inert gas that can span the temperature difference between air and hydrogen without condensation, as its specific thermal capacity is between that of air and hydrogen.

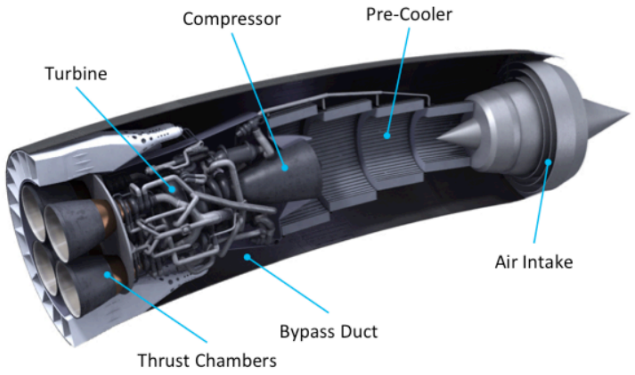


Figure 4.3: Synergistic Air-Breathing Rocket Engine (SABRE) [73]

In order for SABRE to work, it requires a high-performance precooler. Reaction Engines engineers have designed a novel heat exchanger which can, in theory, cool the air from 1300 K to 120 K in 0.1 seconds, with a mass flow rate of 400 kg/s under Mach 5.0, effectively removing 400 MW of heat energy. All this is accomplished with a shell-and-tube-type heat exchanger, composed of over 300,000 micro-tubes [74]. In 2012, the cooling capabilities of the heat exchanger were successfully demonstrated on a small scale; operation below 173 K for over 5 minutes was sustained, while showing complete thermal, mechanical and aerodynamic integrity [75]. In 2015, the cooling concept passed a theoretical feasibility review conducted by the United States Air Force Research Laboratory (AFRL). Furthermore,

a new rocket engine test facility is currently under construction, expected to become active in 2020 and, recently, Reaction Engines was contracted by DARPA to build a high-temperature airflow test facility in Colorado, USA. The facility is going to be designed to assess SABRE precooler heat exchanger technology, with the first tests scheduled to begin in late 2018 [76, 77]. For SABRE, given success on their precooler function demonstration, a TRL 3 is attributed.

## 4.2 Materials

### 4.2.1 Ultra-high temperature ceramics

Ultra-high temperature ceramics (UHTC) are an emerging class of materials which have been under development since the 1970s. Nearly all UHTCs are binary compounds, resulting of a combination of boron, carbon or nitrogen with transition metals such as zirconium, hafnium and niobium . Thus, strong covalent bonds are generated between the transition metals, resulting in superior mechanical properties and high melting temperatures. By merging metal and ceramic-like properties, UHTCs can withstand extreme heat fluxes, mechanical loads and other conditions beyond the capabilities of existing structural materials [78]. Borides, in particular, have high thermal conductivity, resulting in good thermal shock resistance.

For the aerospace industry, the diaborides of hafnium ($HfB_2$) and zirconium ($ZrB_2$) are of particular interest for sharp leading applications, where high structural stability at extremely high temperature resistance is required [79]. Both materials have very high melting temperatures (3380$^\circ$ C and 3245$^\circ$ C, respectively). Nevertheless, pure UHTCs are brittle and therefore silicon carbide (SiC) can be added to boride powers to increase fracture toughness by promoting refinement of the micro-structure, despite lowering its thermal conductivity [33].

Future challenges for UHTC deployment are likely improving fracture toughness (through fiber reinforcement), providing better oxidation resistance, understanding catalytic behavior and enhancing modeling capabilities to shorten development time. Table 4.1 displays current research activities in UHTC development. R&D projects are scattered throughout the world and focused on specific properties and issues. Current UHTC development leads to a TRL 5-6 estimate.

| Organization | Country | $ZrB_2$ based | $HfB_2$ Reinforcement | Fiber Properties | Catalytic Properties | Oxidation | Modeling |
|---|---|---|---|---|---|---|---|
| AFRL | USA | X | | X | X | X | X |
| NASA | USA | X | X | | | X | X |
| Imperial College | UK | X | | | | | |
| CNR-ISTEC | Italy | X | X | | X | X | |
| Harbin Institute Technology | China | X | | | | X | |
| Naval Surface Warfare Center | USA | X | X | | X | X | |
| Universidad de Extremadura | Spain | | X | | | | |

Table 4.1: Research and development centers throughout the world, separated by field of research [33]

### 4.2.2 Ceramic Matrix Composites

Ceramic matrix composites (CMC) are a subgroup of both ceramics and composite materials and consist of ceramic fibers embedded in a ceramic matrix. The matrix and fibers can be of any ceramic material and typical CMCs comprise SiC-based matrix reinforced by SiC fibres, with a moderately weak fibre/matrix interface. Carbon fibers can also be used to reinforce SiC matrices, resulting in a high-strength C/SiC material, at the cost of reduced lifetime.

CMCs have superior mechanical properties when compared to traditional ceramics. These materials are about 30% lighter than superalloys and thus have high specific strength. Moreover, the integration of ceramic fibers increases fracture toughness and CMCs display a non-linear stress-strain behavior, effectively acting in a quasi-plastic manner. In traditional ceramics, high stresses are generated because of high Young's modulus and low elongation capability, resulting in cracks and brittle fractures. Because fiber displacement in CMCs bridges over these cracks, the material can show no macroscopic damage even if the matrix has cracked locally. Therefore, unlike traditional ceramics, CMCs are damage-tolerant and notch-insensitive [80].

Europe has been leading the effort on CMC and currently TRL for CMC materials is higher than that of USA (estimate of TRL 7) One of their main applications is shingle design TPS.

Snecma Propulsion Solide, part of the Safran group, has developed a CMC shingle TPS, separating the mechanical and the thermal functions. Several tests have been conducted on vibration, acoustics and thermal-mechanical handling. The TPS was capable of sustaining 1500 K behind the leading edge while, structure-side, this value would not be any higher than 400 K, demonstrating the thermal efficiency of the concept [52].

The same concept was later applied to IXV project, which used a CMC hot structure. A thin, heat resistant shell made of CMC is designed to withstand mechanical loads due to extreme heat fluxes while maintaining the outer aerodynamic line of the vehicle. Layers of insulation material underneath this skin absorb the heat load, and protect the cold structure from high temperatures. The IXV was successfully retrieved in 2016, after performing a sub-orbital re-entry [44].

### 4.2.3 Polymer Matrix Composites

Polymer Matrix Composites (PMC) are a potential solution for many aircraft subsystems given their strength to weight characteristics and heat resistant properties. Reinforced carbon-carbon (RCC) which has been originally developed for intercontinental ballistic missiles is a unique material in the way it handles thermal loads while maintaining high mechanical performance at high temperatures.

Carbon–carbon has been used by NASA for the Space Shuttle orbiter design and, because of its exceptional mechanical properties, it was the only material in the the entire orbiter design that also served a structural and aerodynamic role simultaneously. While it is less brittle than many other ceramics, it lacks impact resistance; Space Shuttle Columbia was destroyed during atmospheric re-entry after one of its RCC panels was broken by the impact of a piece of foam insulation from the Space Shuttle External Tank. On the other hand, Toyota has been developing polymer nanocomposites as three-phase

composite systems: fiber reinforcement, matrix and nanofillers. These nanocomposites are composed of nanoparticles such as nanosilica, montmorillonite and nanoclays with surface insulation elements for improving integrity and toughness; this results in superior thermal stress and mechanical impact load capabilities. Whereas carbon-carbon has already been demonstrated in a real scenario, new polymer nanocomposite TRL is estimated at 3-4.

### 4.2.4 Metallic Matrix Composites

Metallic Matrix Composites (MMC) are composite materials with one additional constituent (a reinforcing material) besides its metallic component (metal matrix). This matrix is a monolithic material into which the reinforcement constituent is embedded. For high-temperature applications, the metallic matrix is usually made of cobalt or cobalt-nickel alloys. The reinforcement adds to the structural strength but also modifies other material properties such as thermal conductivity or wear resistance.

MMCs have been used in aircraft components and other high-end equipment (e.g., automotive industry). However, these materials are more expensive than the conventional ones they are replacing and more affordable manufacturing costs are required to increase the scope of applications. Furthermore, one of the main concerns in its application is that mechanical properties start to weaken as temperatures increases for a lower temperature range compared to CMCs. That may explain, at least partially, why there has been intensive research in alternatives such as ceramic-based materials. Nevertheless, MMCs have been used on the external skin of hypersonic aircraft, but also within the engine and other internal structures [53]. During the 80s, NASA conducted extensive research on titanium-based MMCs. These tests demonstrated the potential of the technology, as they proved capable of withstanding thousands of hours of cyclic loading in an oxidative environment, at temperatures as high as 2000 K. However, current manufacturing problems mentioned above prevent the capability of producing complex shaped components [81].

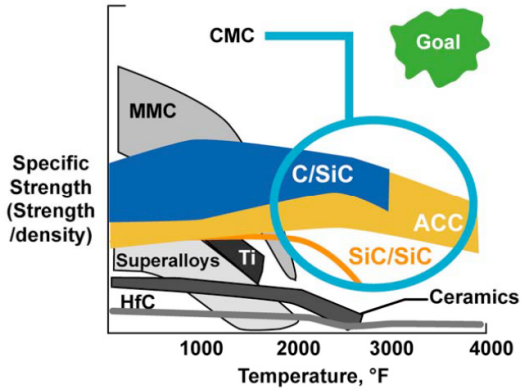


Figure 4.4: Specific strength over a temperature range for different materials [53]

### 4.2.5 Boron nitride nanotubes

Boron nitride nanotubes (BNNT) are a recent discovery (1995) and are comparable to more traditional carbon nanotubes (CNT). Both have a high aspect ratio and are considered the strongest light-weight nanomaterials, with Young's modulus higher than 1 TPa. Furthermore, they are both great thermal conductors. BNNTs outperform CNTs because of their higher oxidation resistance and thermal stability, making them top candidates for mechanical reinforcement applications.

NASA produces BNNTs but the manufacture price is its major downside, set at around $1,000/gram. This value is too high for widespread commercial applications (i.e, carbon nanotubes cost about $10-28 / gram). Nevertheless, BNNTs can be the standard manufacturing material for hypersonic airplanes in the next decades provided enough is produced to lower the manufacturing costs. Therefore, it may be rated with a current TRL 4 estimate.

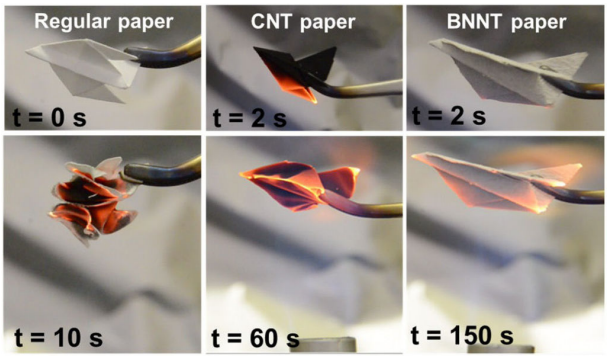


Figure 4.5: Comparative flame test of airplanes made of cellulose, carbon buckypaper and BN nanotube buckypaper [82]

## 4.3 Thermal Protection Systems

### 4.3.1 Toughened Uni-Piece Fibrous Reinforced Oxidation-Resistant Composite

Toughened Uni-Piece Fibrous Reinforced Oxidation-Resistant Composite (TUFROC) is an insulation-based TPS which represents a leap in reusable TPS technology. It is a lightweight, low catalytic efficient TPS composed of two different pieces with different materials for distinct uses. The combination of materials applied in TUFROC can help provide structural integrity during reentry as well as survive extreme heating. The upper layer includes a high-temperature, low density, carbonaceous, fibrous material whose surface is treated to slow oxidation and keep emissivity high ($\epsilon \approx 0.9$). As such, it can re-radiate most of heat, maintaining the outer mold line while sustaining temperatures up to 1900 K. Remaining heat is then absorbed and conducted to the second layer. The mechanical design is arranged specifically so that thermal expansion differences in the component materials are tolerated. As such, this TPS can be applied to wing leading edge and/or nose caps of hypersonic vehicles [83, 84]

TUFROC has been developed by NASA's Thermal Protection Materials Branch. It was tested on arc jet facilities and modified to provide better thermal shielding. This led to advanced TUFROC designs

which have been applied successfully to the wing leading edge tiles of the Boeing X-37. This spacecraft performed its first spaceflight on 2010 and has been conducting secret missions for the USAF ever since. TUFROC scored outstanding results and performed better than expected as demonstrated by successful re-flights of this spacecraft (TRL 9) [83].

### 4.3.2 High-performance heat pipes

For extreme heat fluxes and temperatures, when considering re-usability, non-passive TPS must be implemented. Heat-pipe-cooled leading edges are a semi-passive TPS that works as two-phase heat transfer device. The concentrated heat input is conducted to a different section where it is absorbed by the evaporation of the working fluid. The now heated vapor is directed towards a slightly cooler section of the heat pipe where it condenses again and returns its stored heat. Finally, this heat is conducted towards the wick/working-fluid matrix and rejected. The cycle is completed with the liquid condensate returning to the heated region by capillary pumping. This mechanism is able to cool the stagnation point where temperatures are most critical by isothermal heat transfer towards cooler regions. When applied to leading-edge cooling, heat pipes operate by accepting heat at a high rate over a small area near the stagnation region and radiating it at a lower rate over a larger surface area [52].

Thermacore is an American company which has been developing heat pipes for various applications over the last decades. More recently, in 2014, they completed testing a heat pipe assembly at the NASA Ames Arc Jet Complex, operating a hypersonic leading-edge heat pipe simulation, in a joint project with Lockheed Martin. There, they tested a 15-centimeter-wide, 25-centimeter-deep module fully integrated into a static edge of a the wing mounting structure. was accomplished within the static edge of the wing mounting structure. The assembly was subjected to high heat fluxes at speeds ranging from Mach 5 to 20. The test was used to validate thermal models and performance characteristics. The module is ready for prototyping in an operational environment for spacecraft and hypersonic vehicles (TRL 6) [85].

### 4.3.3 Structurally Integrated Thermal Protection System

Structurally Integrated Thermal Protection System (SITPS) is a dual-purpose sandwich panel designed to carry thermal and mechanical loads simultaneously with a high integration degree and, as consequence, a higher structural efficiency. The concept is dependent on an outer and inner wall, where the outer surface is a robust, heat-resistant material. The inner and outer walls are designed to carry the airframe loads while the inner wall is kept cooled through insulation. Thermal and load bearing performance integration helps reducing the number of seals, surface gaps and parts, contributing to an overall lighter structure.

This concept is being developed by NASA's Armstrong research team and albeit recent, it has made significant progress in recent years. To date, advantages of future SITPS are only theorized. Mechanical tests have been conducted on small concept panels, together with a material database of SITPS strength and thermal performance. As such, a TRL 3-4 is attributed. Other sandwich core designs have also been studied [86].

### 4.3.4 Electron transpiration cooling

Even in the realm of active TPS, current mechanisms struggle to provide efficient, lightweight cooling capabilities. For instance, since the high stagnation pressure at the leading edge can pose a significant challenge to coolant flow through the pores, transpiration may be an inefficient process.

One of the most innovative concepts is electron transpiration cooling, which could theoretically outperform traditional transpiration cooling devices. This alternative relies on thermionic materials which, upon exposure to high convective heating rates, would emit a current of electrons which could then be used for cooling purposes. The efficiency of this transpiration cooling effect could be further magnified as there is no longer a requirement for a porous material: this prevents propagation of hypersonic turbulent boundary layer. The work principle for this concept is called thermionic emission, which occurs when there is a thermal energy surplus compared to the binding potential of the surface material [87]. This is a very recent concept and therefore most work performed so far has been purely conceptual. The first detailed models for electron emission are currently being developed in China and the USA. As such, an approximate TRL 2 is attributed.

### 4.3.5 Opacified Fibrous Insulation and Internal Multi-screen Insulation

Shingle TPS is an option fo stand-off thermal protection system, capable of withstanding multiple reentries. The shingle design has the advantage of allowing a different contour from the outer shell with regards to the aircraft support structure, adding versatility to the design. Similar to tile TPS concepts like TUFROC, the shingles are much larger in dimension and act effectively as the aircraft skin. However, the shingles alone are not sufficient to sustain high heat fluxes, and an additional layers of insulation material underneath is required to absorb the heat load and protect the cold structure from high temperatures. Because insulation occupies a significant volume in the vehicle design, it must be light-weight and very capable when it comes to thermal performance, as it is designed to sustain extreme temperatures for prolonged periods of time. Therefore, high heat capacity and low thermal conductivity are properties of choice. Generally, high-temperature fibrous insulation is often chosen [52].

The Opacified Fibrous Insulation (OFI) is developed by Steve Miller and Associates Research Foundation, based in Arizona. They use opacified silica/zirconia/alumina felts capable of sustaining temperatures up to 1700 °C encased in a fabric cloth. Depending on the exact configuration, nominal densities can vary from 96 to 384 $kg/m^3$. Model verification and experimental tests in 2010 concluded that low-pressure applications OFI was the most efficient insulation with the lowest product of density and thermal conductivity, compared with other available insulation materials (TRL 4) [88].

The Internal Multi-screen Insulation (IMI) is a high-temperature multi-layer insulation designed by MT Aerospace, a German company. The high-temperature variant is able to sustain temperatures up to 1600°C. Parametric studies on numerical model of IMI were conducted in 2007 and showed good agreement with experimental values (TRL 4) [89].

## 4.4 Aerodynamics

### 4.4.1 I-shape plane

Recently, a 2017 study from the Chinese Academy of Sciences [90] unveiled a new category of design configurations named Hypersonic I-shaped Aerodynamic Configuration (HIAC), with two separate wings connected through the airframe and attachment struts. The name derives from the cross-section shape. The theory relies on two different wing designs: a forward swept wing on the fuselage center line and a swept delta wing on top of the rear fuselage. The purpose of the additional wing is not only to provide extra lift but also redirect the shockwaves from the lower wing to improve flight performance and stability, reducing drag and turbulence effects. Small scale wind tunnel results have shown improvements of up to 20% in maximum $L/D$ and of up to 58% in maximum lift coefficient, for Mach numbers ranging from 5 to 7. This recent and possibly groundbreaking concept has been attributed a TRL 2-3.

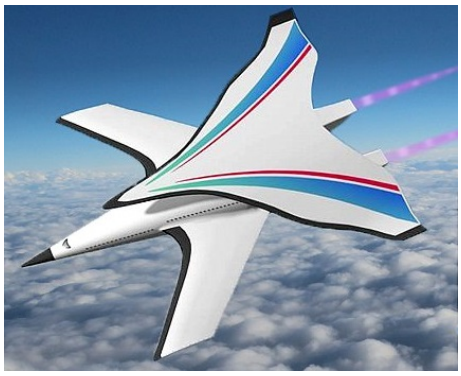

Figure 4.6: HIAC concept [90]

### 4.4.2 Distributed roughness

Distributed roughness laminar flow is a technology enhancement developed by NASA whose purpose is to distribute bumps on aircraft surfaces to create acoustic disturbances out of phase with cross-flow disturbances. This results in a prolonged laminar flow on swept wings, which in turn leads to a higher $L/D$ and increased efficiency at supersonic/hypersonic Mach flight. This technology is still in its initial development phase (TRL 3) and it is not expected to be functional before 2030 [91].

## 4.5 Sonic boom mitigation

In the field of sonic boom mitigation, some technologies have progressed while new options have been theorized.

Using variable sweep outboard wing panels technology allows for a shifting wing sweep using pivots and/or other mechanical systems, which not only provides a better aerodynamic performance during critical flight phases but also reduces the sonic signature. This technology has already been fully demonstrated in full-scale flight (TRL 9).

Hypersonic configuration shaping makes use of advanced MDO techniques to properly and efficiently shape the vehicle to close fore and aft shock, resulting in a much weaker sonic signature. MDO tools for hypersonic flight are still underdeveloped and therefore this is only a promising technology for a mid-term implementation (TRL 1-2).

Finally, following the AYAKS working principle, plasma boom optimization technology can also be used to implement a virtually shock-free supersonic/hypersonic flight. This can be accomplished by using plasma generators to change airflow at key locations, therefore mitigating/dissipating the shock (TRL 2-3) [91].

## 4.6 Stability and control

There's a strong effort towards hypersonic control systems in China, Russia and USA. Available theoretical studies in control literature for hypersonic aircraft focus primarily in longitudinal dynamics; from a flight stability point of view, a successful longitudinal controller is crucial. However, an efficient design must strike the perfect balance between performance and robustness. Linear-model based approaches such as the $H_\infty$ and $\mu$-synthesis are highly conservative with undesirable compromise in performance. An alternative to classic control theory is the introduction of stochastic robustness in nonlinear systems. This is a statistical measure of robustness that can be described as the probability of instability; it directly uses statistics of physical parameter variations and therefore provides an intuitive and precise response, avoiding over-conservative or insufficiently robust designs [92]. It is important to note that, for all these possible designs, the controller only applies to a certain flight condition but it should be able to adapt to learn information on the fly. This display of intelligent control is highly dependent on speed and useful machine learning might provide a new to way to deal with hypersonics. This can be a useful tool to work with the large flight envelope of hypersonic aircraft, with vastly different dynamic characteristics given the extremely wide range of operating conditions and rapid change of mass distributions [41].

The integration of longitudinal aero-propulsive models could be further improved upon by adding directional dynamics. A more comprehensive model implies a larger number of states, inputs and outputs, which has a negative impact on performance, particularly for air-breathing propulsion systems which introduce various new control parameters. For an integrated design, the controller must include engine effectors commanding fuel flow as well as inlet/diffuser area ratio variations, besides conventional control surfaces. All of this should be commanded via an integrated mechanism that processes information from the aerodynamic and propulsive parameters, to maximize performance.

## 4.7 Summary

An user-friendly interpretation of this chapter can be seen consulted on Table 4.2. Each alternative addresses a specific technological driver, through the driver references specified in Section 3.7. Furthermore, current TRL is also displayed, using the TRL scale defined in Section 3.1.2. Projected Timeline for technology implementation is also included, using manufacturer references.

To add to the conclusions extracted from this chapter and complement the analyses presented thus far, each technology alternative is also associated with a predicted timeline for actual implementation. It differs from the projected timeline as it is loosely based on manufacturer references and it also takes into account the author's judgment on the prospects of certain technologies. These assumptions are based on previous timelines for similar technologies, publication date of current timeline references and historical knowledge of technology maturation levels for specified technological areas. For instance, there are development roadmaps for TBCC from USAF as recent as 2017 [93] and therefore the likelihood of project delay is significantly shorter compared to older roadmaps proposed by NASA on the same subject [94]. In this case, the predicted timeline would try and correct the timeline to a more accurate value given the absence of new information. For highly theoretical concepts (e.g., I-plane shape, plasma boom optimization) there are no available references on expected delivery, which was estimated in a very moderate manner. In general, this interpretation provides a more conservative estimate. This is attributed, in part, to the strict certification procedures for the aerospace industry. The effect is aggravated by the high-degree of innovation introduced in some of these technology concepts.

| Technological Area | Driver | Technology | Current TRL | TRL 8 (Projected) | TRL 8 (Predicted) |
|---|---|---|---|---|---|
| Propulsion | (A1) | High-speed turbine | 6 | 2019 [93] | 2020 |
| | | Continuous Rotating Detonation | 5 | 2024 [95] | 2030 |
| | (A2) | Dual-mode scramjet | 7 | 2020 [94] | 2020 |
| | | Continuous Rotating Detonation | 4 | 2024 [95] | 2030 |
| | (A3) | Rocket-based combined cycle | 3-4 | 2025 [95] | 2035 |
| | | Turbine-rocket based combined cycle | 2-3 | 2030 [96] | 2040 |
| | | SABRE | 3 | 2030 [97] | 2040 |
| | (A4) | Turbine-based combined cycle | 5-6 | 2023 [93] | 2025 |
| | | Rocket-based combined cycle | 3-4 | 2025 [95] | 2035 |
| | | Turbine-rocket based combined cycle | 2-3 | 2030 [96] | 2040 |
| | | Magneto-hydrodynamic drive | 3 | 2025 [95] | 2030 |
| | | SABRE | 3 | 2030 [97] | 2040 |
| 2030 [97] | 2040 | | | | |
| | | Pre-cooled turbojet | 4-5 | 2025 [98] | 2030 |
| Material | (B1) | Ultra-high temperature ceramics | 5-6 | — | 2025 |
| | | Ceramic Matrix Composites | 7 | 2025 [99] | 2025 |
| | (B2) | Ceramic Matrix Composites | 7 | 2025 [99] | 2025 |
| | | Metallic Matrix Composites | 7 | 2023[94] | 2023 |
| | | Polymer nanocomposites | 3-4 | 2023 [94] | 2023 |
| | | Metallic Matrix Composites | 7 | 2023 [94] | 2023 |
| | (B3) | Ceramic Matrix Composites | 7 | 2025 [99] | 2025 |
| | | Metallic Matrix Composites | 7 | 2023[94] | 2023 |
| | | Reinforced Carbon Carbon | 9 | — | — |
| | (B4) | Ceramic Matrix Composites | 7 | 2025 [99] | 2025 |
| | | Boron nitride nanocomposites | 4 | — | 2030 |
| TPS | (C1) | High-performance heat pipes | 6 | — | 2030 |
| | | Electron transpiration cooling | 2 | — | 2040 |
| | (C2) | Structurally Integrated TPS | 3-4 | 2021 [94] | 2025 |
| | | TUFROC | 9 | — | — |
| | (C3) | Opacified Fibrous Insulation | 4 | 2024 [94] | 2024 |
| | | Internal Multi-screen Insulation | 4 | 2024 [94] | 2024 |
| Aerodynamics | (D1) | I-plane | 3 | — | 2040 |
| | (D1) | Distributed roughness | 3 | — | 2040 |
| Sonic signature | (E1) | Variable swap outboard wing panels | 9 | — | — |
| | (E1) | Configuration shaping | 1-2 | — | 2030 |
| | (E1) | Plasma boom optimization | 2-3 | — | 2040 |

Table 4.2: Technology alternatives, current TRL and timeline

# Chapter 5

# Roadmap proposal

Upon listing and individually reviewing the major hypersonic R&D activities, a prioritizing process must be pursued to select the best candidates that fulfill the drivers set in Section 3.7. The reasoning behind this triage process is clarified in Section 5.1 and a condensed timeline is displayed in Section 5.2.

## 5.1 Technology Recommendation

### 5.1.1 Propulsion

Depending on the desired application, different propulsion systems may be better suited to operate for certain mission profiles. This can be further accentuated as different vehicles can be used for the same application; whether an engine is attached to an ARV or a CAV, it will have to behave differently to satisfy the mission requirements.

For hypersonic missile design, the most cost-effective solution relies on rocket propulsion, optionally complemented with scramjet engines for certain segments of the mission (e.g., BraHmos II, Kinzhal). However, for reusable cruise vehicles, both military and civil, there are more compelling options. First of all, to become fully reusable, there is a desire to fly continuously and efficiently from take-off up to Mach 4+, with no expendable components. This can be achieved with combined cycle engines, particularly turbine-based combined cycles for atmospheric flight. This choice is also driven by a current considerable understanding of the technologies involved in its design. Compared to more radical solutions which are in early stages of their R&D cycle (e.g., CRDE, MHD engines), TBCC are a solid options when also looking at development costs and timeline for delivery. These combined cycles can be merged with precooled jet flow concepts to provide very versatile and capable engines, such as PCTJ. While the precooler component still requires extensive tests to verify its performance in an operational environment, these concepts are very promising and may not require the same high-degree of aero-propulsive integration of its TBCC counterpart.

While it is less likely to see rocket engines applied to atmospheric flight, they are necessary in the propulsion cycle to achieve orbital speed and altitude. With the goals of continuous propulsion and SSTO-capabilities, combined-cycle engines are also the most promising concepts; in particular SABRE

uses precooled flow to obtain an optimal performance during almost all flight stages. This contrats with Virgin Galactic SpaceShipOne [100], the world's first air-launched rocket-powered spacecraft, which needs to be carried to an altitude of 15 km by another aircraft before rocket engine ignition.

### 5.1.2 Materials

The selection of appropriate materials for aircraft design depends on its mission profile and flight envelope. The system the material is being applied onto is also relevant as not all vehicle parts are subjected to the same freestream conditions.

In general, CMC represents a significant gain not only in terms of mechanical and thermal performance but also structural weight; therefore, it should be implemented in vehicle components such as acreage and control surfaces, similar to the X-43 [52]. For leading edge and nose design, more thermally-capable materials are necessary; UHTC are one of the most promising concepts, even though issues with fracture toughness still need to be addressed. Finally, boron nitride nanocomposite manufacturing must be improved drastically in the future to become a viable alternative, even though they can be applied in large structures such as vehicle fuselage.

### 5.1.3 Thermal Protection Systems

For prolonged and repeated heat exposure, single-use TPS is the least efficient solution. However, from the many proposed reusable TPS concepts, their application is driven by the expected heat fluxes and loads from its mission profile. Nevertheless, leading edge high-performance heat pipe technology seems like a very promising concept that can be applied to both orbital and atmospheric cruise vehicle, as it can dissipate a significant heat flux from the freestream flow. Given its flexibility in mission design, it represents a major leap forward in regards to more traditional, passive TPS. Nevertheless, the prospects of shock-free hypersonic flight presented by electron transpiration cooling make it a high-priority target to be pursued. For acreage TPS, structurally integrated TPS technology still needs to mature as it is in its early readiness stage but it can become a very useful concept. As such, the effort should go to shingle-like TPS, in particular CMC shingle concepts (and subsequent additional insulation requirements).

### 5.1.4 Aerodynamics

Hypersonic aerodynamics have not suffered major practical updates in the past years; theoretical concepts like the wave rider and lifting body have been proposed decades ago but have been held back due to engineering constraints. They have been recently put to the test successfully and are likely candidates for future reusable vehicles. Further improvements on aerodynamic shapes may come from advanced computational fluid simulations and databases. Particularly for atmospheric cruise profiles, ellipsoid shapes are generally though to yield the best aerodynamic/thermodynamic performance in sustained hypersonic flight, positioning themselves in between the traditional blunt shapes of re-entry vehicles and the aerodynamically-efficient sharp edge configurations of atmospheric flight. Nevertheless, the Hyper-

sonic I-shaped Aerodynamic Configuration promises to revolutionize hypersonic flight, increase MTOW and reduce fuel weight needed; investment on this innovative technology is strongly encouraged.

### 5.1.5 Guidance and Navigation Control

New GNC systems for aircraft due to enter serve in twenty to thirty years will inherently have much more computational power supporting them and should be much better prepared to deal with complex control systems. Nevertheless, any development on current/new algorithms and mechanisms to accurately model aircraft systems and hypersonic conditions are recommended and will have a considerable impact on the final performance.

### 5.1.6 Sonic boom mitigation

The design of a mission profile has a significant impact in shock wave strength. However, the possible benefits in terms of sonic boom mitigation from flying at higher altitudes are counterbalanced by a much less efficient aerodynamic performance. Therefore, future work towards sonic boom mitigation relies on configuration shaping and ultimately plasma boom optimization. However, given current TRL for these technologies, an approximate delivery date is still a long-term solution. Plasma injection has potentially huge benefits with the prospect of an entirely shock-less flight and therefore its development should not be discarded.

## 5.2 Final roadmap report

The technology roadmapping process is now complete. The scope and boundaries of this roadmap have been set in Chapter 3; an extensive library of hypersonic technology initiatives has been provided in Chapter 4; finally, recommendations on which technologies should be applied for specific hypersonic products have also been listed in Chapter 5. According to Table 3.1, there is a third phase of a standard technology roadmap, related to any follow-up activity. Here, the roadmap is constantly updated and re-validated to keep up with technological progress and guarantee the initial objectives are still being pursued. However, this does not fall under the premise of this dissertation.

To conclude this process, Figure 5.1 represents a predicted hypersonic timeline comprising all technology alternatives and relevant demonstrators, as well as an estimate for its various applications. It neatly condenses in a single diagram the predictions presented in Table 4.2. However, this timeline should be taken with a grain of salt, as countless other hypersonic roadmaps and demonstrators have been proposed throughout time [70, 101, 102] and have systematically failed to predict the hypersonic breakthrough. It is interesting to note, however, that despite misstep after misstep, some of the projects that were based of these roadmaps were pivotal for later successful endeavors in the aerospace industry (e.g, Boeing X-20 ”Dyna-Soar” did not even fly but still served as a testbed for materials such as Q-felt insulation, later redirected towards the Space Shuttle program). For a broader view of hypersonic development, Appendix B maps the most significant hypersonic R&D players around the world.

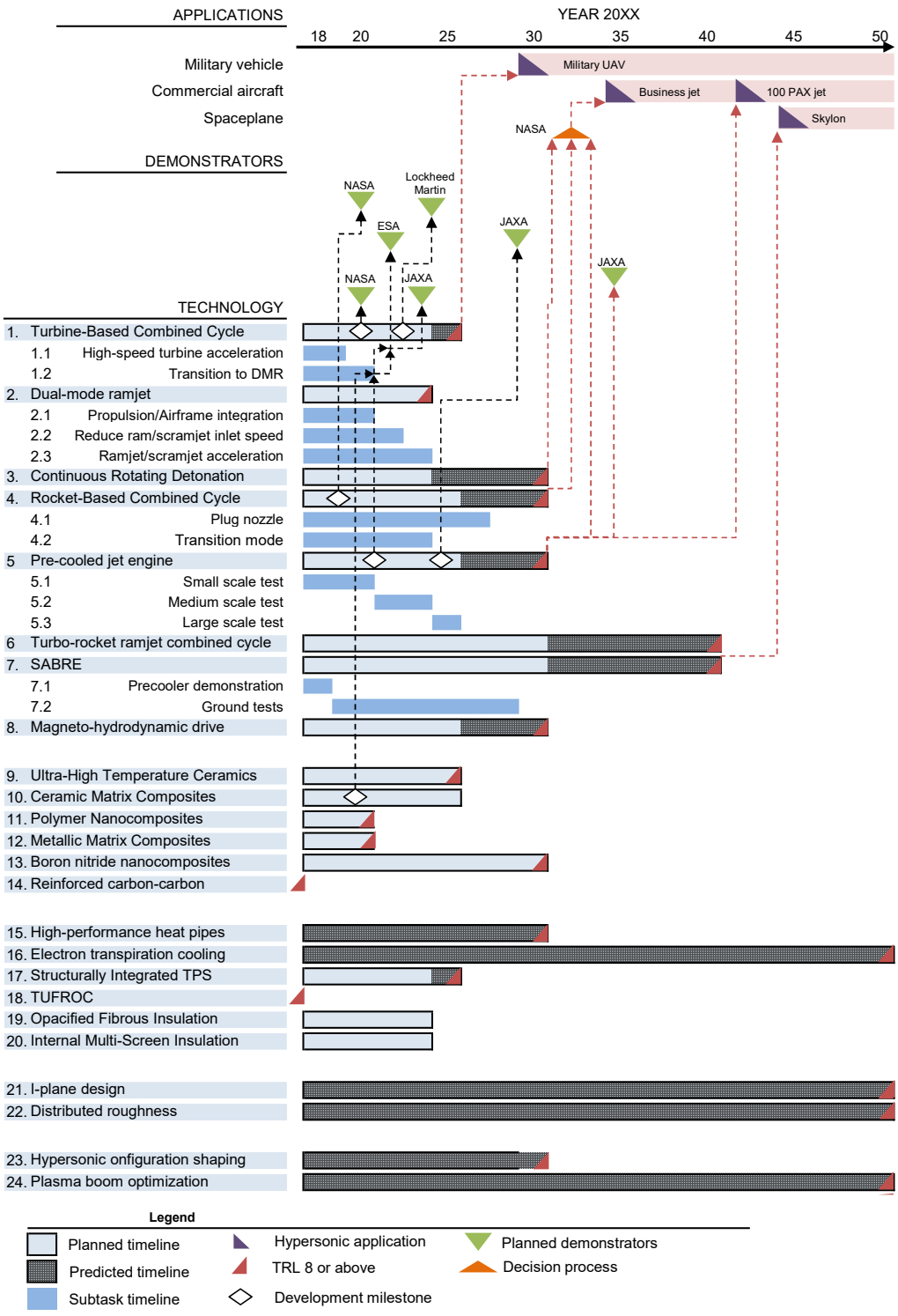


Figure 5.1: Hypersonic technology and applications timeline display

# Chapter 6

# Preliminary hypersonic vehicle design

Work so far has been focused exclusively on research and development activities for hypersonic technologies and applications. On Chapter 2, a brief demonstration of hypersonic concepts was provided and Chapters 4 and 5 have explained what is currently being developed to meet the requirements of hypersonic flight. Moving towards a more practical approach, this chapter assesses the impact of hypersonic technologies in aircraft performance, through a preliminary analysis of generic hypersonic vehicles. This is done by accomplishing two things: first by translating the extreme conditions of hypersonic flight into tangible engineering variables; second by demonstrating the feasibility of some of the emerging technologies in hypersonics highlighted in Chapter 5.

## 6.1 Objective

The main objective for this test case is to assess the impact of emerging hypersonic technologies in determining the minimum requirements to transport a specified payload. Since the main focus of this analysis is placed in the individual performance of hypersonic technologies, there is a need for a vehicle-oriented assessment rather than mission-oriented; that is, the vehicle geometry is fixed and the main subsystem performance parameters are tweaked to yield the best possible mission profile. In this case, the ideal mission profile tries to maximize the range and minimize the flight duration.

To provide a more robust analysis, the same vehicle is applied to two different test cases, encompassing distinct flight conditions and making use of different technologies: an air-breathing cruise vehicle and an air-breathing single-stage ascent and re-entry vehicle.

## 6.2 Tools

### 6.2.1 SUAVE

The preliminary design analysis is performed using Stanford University Aerospace Vehicle Environment (SUAVE), an open source conceptual level aircraft design tool, developed by Stanford University's

Aerospace Design Lab and Embraer. The main goal of SUAVE is to provide a robust environment for analysis and optimization of aerospace vehicles, with a high degree of flexibility for easy implementation of futuristic designs and advanced technologies and concepts. Aircraft performance assessment in a given mission can be done to support arbitrary levels of fidelity; that is, by integrating the relevant equations of motion directly, the simulation of a mission is independent of the level of fidelity of the supporting data. An analysis in SUAVE is performed on a segment-by-segment basis via a pseudo-spectral collocation method and relies on the user-provided or internally calculated mass properties, aerodynamic information, and propulsion system data. Code architecture and description can be found on multiple publications [103, 104, 105].

However, SUAVE is not equipped with any hypersonic models and this is the first attempt at incorporating these flight conditions and specifications into the program. Therefore, the scope of this use case must be narrowed down to the verification and implementation of new hypersonic models in crucial technological sectors. For that reason, stability analysis has been discarded as part of this dissertation and the main focus will be in aerothermodynamics and propulsion.

### 6.2.2 OpenVSP

Taking advantage of its architecture, Open Vehicle Sketch Pad (OpenVSP) was used to complement SUAVE, providing visualization capabilities. This geometry modeling tool is capable of rapidly creating aircraft configurations without the expertise required for traditional Computer Aided Design programs. This tool was developed by NASA and is publicly available. OpenVSP was also chosen given its compatibility with SUAVE [106].

## 6.3 Vehicle Design

### 6.3.1 Sizing

For the academic test case, a small hypersonic aircraft is envisioned, hereby referenced as Hypersonic Multi-purpose Vehicle (HMV). Both the CAV variation and the ARV variation (hereby referenced as HMV-CAV and HMV-ARV, respectively) share the exact same design. In reality, this would not be the case as both vehicles are meant to operate in different environments; however, for a direct performance comparison, this assumption is considered valid. For its initial sizing, the Lockheed SR-72 was used as baseline for length, wingspan and height, as seen in Table 6.1.

| Aircraft | Length $[m]$ | Wingspan $[m]$ | Height $[m]$ | Number of engines | PAX |
|---|---|---|---|---|---|
| SR-72 | 30.0 | 16.0 | 5.0 | 2 | 0 |
| HMV | 30.0 | 20.0 | 4.0 | 2 | 0 |

Table 6.1: Baseline parameters for model geometry

After fixing the basic aircraft specifications, three main components were added: fuselage, wing and a vertical stabilizer. The geometry file was written in SUAVE and imported to OpenVSP to visualize the

final result. Specific airframe geometry for the SR-72 is not publicly available and approximations were made to resemble the original reference. OpenVSP was used to calculate the wet area and volume of the different airframe components. Table 6.2 provides more detailed information on the model geometry. The nose radius was initially estimated to be approximately a quarter of the body diameter.

(a) Wing and tail parameters

| Parameter | | Main Wing | Vertical stabilizer |
|---|---|---|---|
| Aspect Ratio | [-] | 1.37 | 0.56 |
| Span | $[m]$ | 20.00 | 2.50 |
| Root chord | [-] | 27.27 | 6.00 |
| Tip chord | $[m]$ | 2.00 | 3.00 |
| Sweep angle | $[^\circ]$ | 65.00 | 30.00 |
| Reference Area | $[m^2]$ | 292.75 | 11.25 |
| Wet Area | $[m^2]$ | 444.79 | 20.98 |
| Volume | $[m^3]$ | 144.27 | 2.50 |

(b) Fuselage parameters

| Parameter | | Value |
|---|---|---|
| Fineness nose | [-] | 1.20 |
| Nose radius | [m] | 0.30 |
| Fineness tail | [-] | 1.20 |
| Fuselage length | [m] | 30.0 |
| Fuselage width | [m] | 3.50 |
| Fuselage height | [m] | 3.00[1] |
| Wetted area | [$m^2$] | 200.56 |
| Volume | [$m^3$] | 140.43 |

Table 6.2: HMV geometry parameters

The final vehicle geometry is displayed in Figure 6.1. Because the SUAVE - OpenVSP portability is not overtly developed, the vehicle geometry had to be simplified. Nevertheless, there is sufficient information for providing basic aerodynamic analysis.

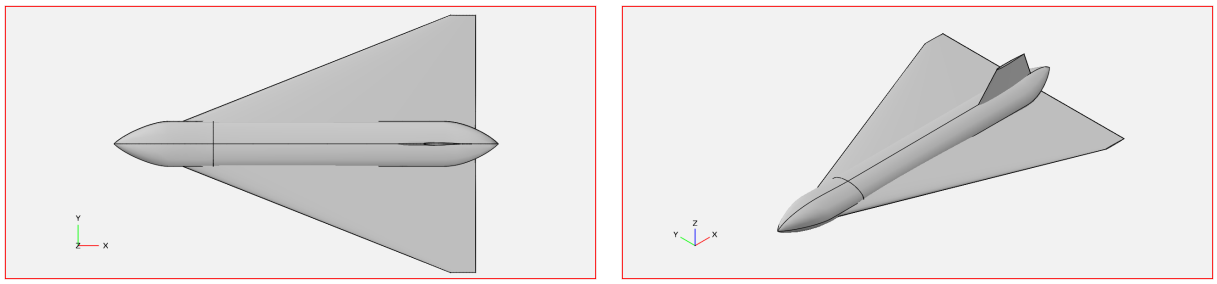

(a) Top view (b) Isotropic perspective

Figure 6.1: HMV final design on OpenVSP

### 6.3.2 Propulsion

Upon concluding the technology roadmap, turbine-based combined cycle engine were selected as one of the preferred solutions for smaller hypersonic cruise aircraft. To showcase the possible benefits from applying this technology, HMV-CAV is going to be equipped with two of these engines, with separate flow paths for turbojet and DMR operation. Because no stability analysis is being performed, their exact position relative to the airframe is not discussed.

For the HMV-ARV, multiple propulsion concepts in Chapter 5 are eligible. Independently of the model chosen for this use case, rocket propulsion is necessary to achieve high speeds and altitudes of an ascent and reentry trajectory; the decision is if and how rocket propulsion is coupled with the air-breathing cycles for the first stage of the ascent trajectory. Whichever solution is selected, it must interfere minimally with the previously established vehicle geometry, to the point where further impact from its integra-

[1] With landing gear retracted

tion may be neglected in terms of aerodynamics; for this reason, a vertical launch system was discarded for it would require significant geometry modifications. As such, and to establish a closer link with the HMV-CAV, a TRBCC engine is selected; this allows for a direct comparison of the initial climb stage prior to the rapid climb to orbital altitude.

### 6.3.3 Weight distribution

The total weight is split among aircraft empty weight (EW), payload weight (PW) and fuel weight (FW). All these contributions summed together yield the gross take-off weight (GTOW).

The first step is to estimate a value for GTOW and then assess how the aircraft performs with that constraint; if necessary, this value should be iterated. For now, let us consider a GTOW of 50,000 kg. This reference value is aligned within the range of GTOW of similar sized aircraft [107] and therefore serves as an initial estimate. Since the purpose here is to enhance the mission profile as much as possible, the same vehicle is used for cruise and re-entry scenarios. It should be noted that these scenarios are widely different from one another and therefore so are the aircraft requirements. Nevertheless, for the sake of simplicity, the most pessimist weight assumption is used as reference for both test cases. Finally, because the goal here is to compare payload transport performance at different operating conditions, PW is the same for the HMV-CAV and the HMV-ARV.

As a reference value, the weight distribution of the LAPCAT MR2 vehicle is used. The GTOW of the LAPCAT MR2 is almost ten times bigger than that of the HMV but it can be used as an initial estimator; for this Mach 8 hypersonic CAV-like vehicle, EW and PW represent nearly 40% and 15% of the GTOW respectively [11]. For a more conservative approach, the payload capacity for the HMV is downsized to 10% of the GTOW. The initial estimates are displayed in Table 6.3. Further on, EW is refined using an appropriate hypersonic sizing tool in Section 7.1 to obtain the final weight distribution.

| | $EW_0$ | $PW_0$ | $FW_0$ | $GTOW_0$ ($\sum$) |
|---|---|---|---|---|
| % $GTOW$ | 40.0 | 10.0 | 50.0 | 100.0 |
| Value (kg) | 20,000 | 5,000 | 25,000 | 50,000 |

Table 6.3: HMV initial weight estimate

## 6.4 Mission profiles

Despite being designed to fulfill the same goal, HMV-CAV and HMV-ARV operate in very different regimes given the clear distinction in freestream properties each vehicle faces.

In the case of the HMV-CAV, it has an apparently similar mission profile to that of a regular subsonic airliner: it takes off horizontally, climbs to cruise altitude where it stays for most of flight duration before initiating its descent; the main changes compared to the hypersonic cruiser are in the magnitude of airspeed and altitude. However, the climb segment is usually done at constant dynamic pressure to avoid excessive loads on the vehicle structure during this high-speed maneuver. This parameter mustn't

be neither too high to prevent critical structural failure, nor too low to allow the engine to function properly. Therefore, there is a climb ”corridor” for air-breathing maneuvers, with a dynamic pressure $q$ situated between 25 and 95 KPa, as seen in Figure 6.2.

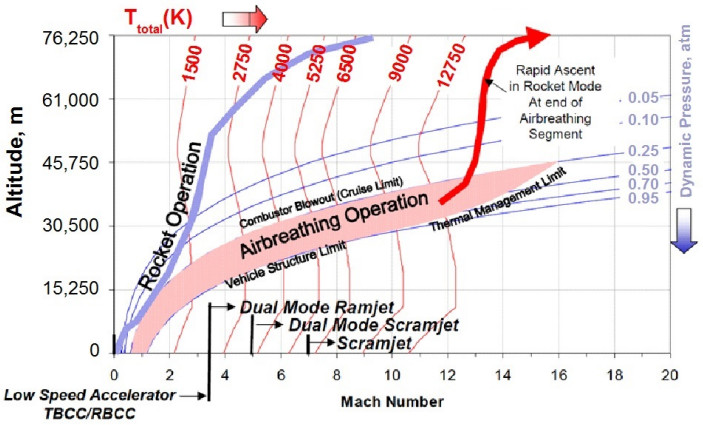


Figure 6.2: Airbreathing and rocket vehicle flight envelopes [7]

For the HMV-ARV, given the engine selected in Section 6.3.2, the spacecraft will follow a similar trajectory to that of the HMV-CAV during the initial climb phase, at constant dynamic pressure. Upon reaching a sufficiently high Mach number, air-breathing operation is shut down and the rocket engine kicks in; this marks the beginning of a final ascent phase up until maximum altitude is reached. From here, the reentry phase takes place. During the entire climb segment, the conservative assumption of constant $1g$ acceleration is used. Furthermore, the gravity turn segment is neglected during the final ascent, considering instead that the spacecraft pitches down immediately for a descent glide. These assumptions are inherently conservative and a more detailed analysis taking into account more precise orbital mechanics may lead to a better performance than the one predicted here. As a first approach in the scope of this dissertation, the analysis was constrained to these simple assumptions. Further work should be carried in continuation projects, extending the complexity of the mission profile.

Mock-up trajectories have been plotted in SUAVE for the HMV-ARV and HMV-CAV to visualize the assumptions listed above.

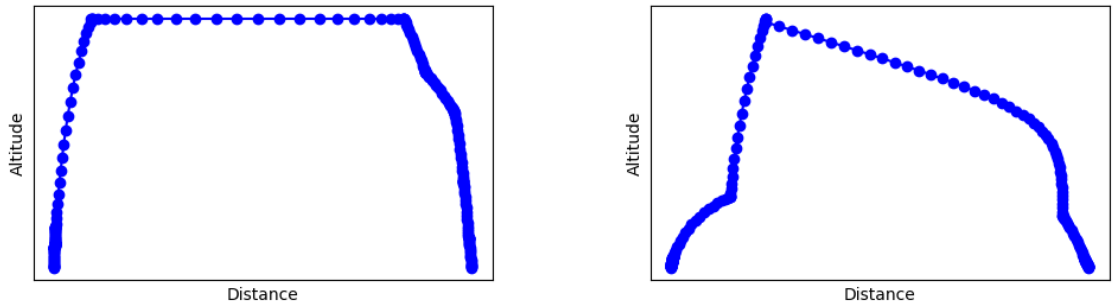


(a) HMV-CAV mock-up mission profile

(b) HMV-ARV mock-up mission profile

Figure 6.3: Predicted trajectories generated in SUAVE

# Chapter 7

# Numerical methods

After identifying the new technologies to be implemented in the academic use case, SUAVE is now the new focus of this dissertation. As previously discussed, SUAVE is able to perform subsonic and, to some extent, supersonic vehicle analysis with various degrees of fidelity, supported by OpenVSP aerodynamic toolbox. This analysis is integrated in several aircraft design levels, including aerodynamics, propulsion, weights and stability. However, SUAVE does not incorporate any numerical methods targeting hypersonic flight in particular. Current supersonic capabilities extend to propulsion and aerodynamic correlations based on empirical or semi-empirical laws. Therefore, after analyzing the actual SUAVE capabilities and cross-checking them with the basic requirements to run the academic test case proposed in Chapter 6, a number of numerical methods were labeled as necessary to perform a basic hypersonic analysis.

## 7.1 Weight distribution

Hypersonic aircraft require complementary structures that enable them to fly at such speeds (e.g., TPS, cryogenic storage tanks, structural reinforcements). As such, the empirical relations currently used for subsonic aircraft design might fail to correctly estimate EW. SUAVE has several different methods for aircraft weight estimation depending on airframe design (i.e., tube and wing, blended wing body), even accounting for out-of-the-ordinary propulsion systems (i.e., human and solar-powered). Because none of them fit the test case requirements, the Hypersonic Aerospace Sizing Analysis (HASA) weight estimation method was used [108].

The aircraft is divided in three main weight categories: structures, propulsion and subsystems. Structural weight is split amongst body, wing, tail, TPS, landing gear and thrust structure; propulsion weight is split amongst engines and fuel tanks; subsystem weight is split amongst hydraulics, avionics, electrical systems and equipment. Because wing weight is dependent on the aircraft empty weight, the initial estimate $EW_0$ is used and the algorithm is iterated until convergence is achieved.

For the SUAVE model, a few simplifications were assumed to streamline the process:

- Fuel tank weight was neglected on the first approach;

- Thrust structure weight (the structure that supports the engines) is a function of the total momentum thrust and is calculated differently for air-breathing and rocket engines. Both HMV-CAV and HMV-ARV share a common air-breathing propulsion cycle, so the most pessimist approach was used to model both instances; HASA also states that "for vehicles with several propulsion systems, it is unclear how each individual system would vary" [108]. For this reason, the scramjet weight function was selected to calculate the engine weight;

- Subsystem weight was assumed as 5% of the total gross weight, following the recommendations on HASA.

The individual contribution of each component is described in Appendix B.1. The final empty weight is given by the sum of all the component weights:

$$EW = W_{bd} + W_{wg} + W_{tl} + W_{tps} + W_{lgr} + W_{thr} + W_{eng} + W_{sys} \tag{7.1}$$

## 7.2 Propulsion models

Thrust can be calculated by delimiting a control volume around the propulsion system and applying the mass and momentum conservation equations. These can be manipulated to obtain the general thrust equation:

$$F = \dot{m}_a(u_e - u_\infty) + u_e\dot{m}_f + A_e(P_e - P_\infty) \tag{7.2}$$

The first two terms relate to the momentum change of the air mass flow across the engine and the momentum change of the fuel mass flow. The last term refers to the acceleration of the exit flow in the nozzle. However, to evaluate and compare different propulsion systems regardless of size, there are better performance indicators. The most commonly used are fuel-to-air ratio, specific thrust and specific impulse (Equations 7.3 to 7.5 respectively) as they provide basic information on engine performance independent of air mass flow rate [109].

$$f = \frac{\dot{m}_f}{\dot{m}_a} \tag{7.3}$$

$$F_{sp} = \frac{F}{\dot{m}_a} = u_\infty\left[(1+f)\left(\frac{u_e}{u_\infty} - 1\right)\right] + \frac{A_e}{\dot{m}_a}(P_e - P_\infty) \tag{7.4}$$

$$I_{sp} = \frac{F}{\dot{m}_a \cdot g} = \frac{F_{sp}}{g} \tag{7.5}$$

For general propulsion performance, the stream thrust concept is also used. This is a variation of the general thrust equation based on the impulse function, where the final thrust is the algebraic sum of the individual impulse contributions of each engine component. The axial force imposed upon the flow between two axial stations is often most conveniently calculated using Equation 7.6 [110].

$$Sa = u\left(1 + \frac{RT}{u^2}\right) \tag{7.6}$$

The final thrust is the algebraic sum of the individual impulse contributions of each engine component. When applied to the a control volume comprising the entire engine and through algebraic manipulation, Equation 7.4 can be rewritten as:

$$F_{sp} = (1+f)Sa_e - Sa_\infty - \frac{R_\infty T_\infty}{u_\infty}\left(\frac{A_e}{A_\infty} - 1\right) \tag{7.7}$$

Finally, to determine the actual thrust, SUAVE uses a sizing function where the inputs are altitude, speed and thrust. The program proceeds to calculate the specific thrust at sizing conditions and determines the air mass flow necessary to produce the sizing thrust. For conditions other than sea level, the air mass flow is corrected according to Equation 7.8. An iterative throttle parameter is used to adjust thrust to mission segment conditions, according to Equation 7.9.

$$\dot{m}_a{}^{corr} = \dot{m}_a \cdot \frac{\sqrt{T/T_{ref}}}{P/P_{ref}} \tag{7.8}$$

$$F = \zeta \cdot \dot{m}_a{}^{corr} F_{sp} \tag{7.9}$$

### 7.2.1 LOX/LH2 rocket engine

Rocket engines do not use the freestream air in the propulsion cycle. The exhaust gas is a mixture of oxidizer and fuel (described by the oxidizer to fuel ratio, $O/F$) and the general thrust equation is slightly adapted:

$$F = u_e \dot{m}_{prop} + A_e(P_e - P_\infty) \tag{7.10}$$

To design a low-fidelity model for preliminary rocket performance, simplified equations are needed to calculate flow properties along the engine. In this manner, the ideal rocket theory [111] is applied; it consists on a set of physical assumptions that streamline the performance calculations:

1. Rocket engine is divided in two separate components: a combustion chamber and a convergent-divergent nozzle;
2. Propellant has constant homogeneous chemical composition and behaves as perfect gas;
3. Propellant is not under any external forces in the nozzle and has a negligible velocity in the combustion chamber;
4. Nozzle flow is steady, isentropic and one-dimensional, flow velocity is purely axial.

The building blocks behind the ideal rocket theory are the mass, energy and momentum conservation and ideal gas equations. This theory also assumes the propellant conditions in the chamber are known

along with its composition and characteristics. The theory predicts that specific impulse is a function of a drag coefficient, $C_D$, a thrust coefficient, $C_F$, and acceleration of gravity, $g$ [112].

$$I_{sp} = \frac{C_F}{C_D \cdot g} \tag{7.11}$$

The drag coefficient is solely dependent on the propellant composition and the combustion temperature (Equation 7.12), which is assumed as the adiabatic flame temperature. The thrust coefficient is also dependent on the propellant composition (through specific heat ratio, $\gamma$, and exhaust gas constant, $R_m$) but must also be tied to the nozzle performance (through expansion ratio $\kappa$ in Equation 7.13). $C_F$ is also dependent of the Vandenkerckhove function, $\Gamma(\gamma)$.

$$C_D = \left(\frac{2}{\gamma+1}\right)^{\frac{\gamma+1}{2(\gamma-1)}} \cdot \sqrt{\frac{\gamma}{R_m \cdot T_{t_c}}} \tag{7.12}$$

$$C_F = \Gamma(\gamma)\sqrt{\frac{2\gamma}{\gamma-1}\left[1-\left(\frac{P_e}{P_c}\right)^{\frac{\gamma-1}{\gamma}}\right]} + \kappa \cdot \frac{P_e - P_\infty}{P_c} \tag{7.13}$$

$$\Gamma(\gamma) = \sqrt{\gamma\left(\frac{1+\gamma}{2}\right)^{\frac{1+\gamma}{1-\gamma}}} \tag{7.14}$$

Assuming the combustion parameters and the propellant chemical composition remain unchanged, the pressure at the nozzle exit is constant because the nozzle expansion ratio is also fixed. It can be calculated implicitly through Equation 7.15.

$$\kappa = \frac{A_e}{A_t} = \frac{\Gamma(\gamma)}{\sqrt{\frac{2\gamma}{\gamma-1}\left(\frac{P_e}{P_c}\right)^{\frac{2}{\gamma}}\left[1-\left(\frac{P_e}{P_c}\right)^{\frac{\gamma-1}{\gamma}}\right]}} \tag{7.15}$$

To fill in this model, the relevant variables must be identified. At first, it seems that the only independent design variables are the choice of propellant and the nozzle expansion ratio. However, chamber pressure and oxidizer-fuel ratio are vital for the engine performance and dictate how other parameters behave. For instance, specific gas constant, molecular weight and adiabatic flame temperature change drastically for the same propellant under different pressures and/or mixture proportions. Given the complex relations between variables, a single model for liquid rocket propulsion was created using exclusively a propellant combination of LOX and LH2. Combustion parameters are set based on Braeuning [113]: using available plots of adiabatic flame temperature, gas molecular weight and specific heat ratio with respect to chamber pressure and $O/F$, polynomial and logarithmic functions were built using EXCEL and used for interpolation. These can be consulted in Appendix C.1.

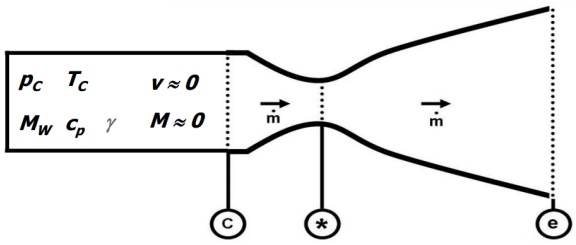


Figure 7.1: Ideal rocket theory schematics [111]

### 7.2.2 Ramjet

The ramjet model was expanded upon the existing turbojet network available in SUAVE. New constraints were added (e.g., thermal choking) and underlining simplifications were assumed. For instance, the flow is considered steady, quasi-one dimensional, purely axial and behaves as perfect gas. The engine is comprised of a diffuser, burner and exit nozzle, as seen in Figure 7.2.

By examining Equation 7.4, values for exit velocity, pressure and area are necessary to compute model performance. To do so, it is necessary to start at the first engine component, calculate the flow properties after they interact, move to the next component and repeat the process.

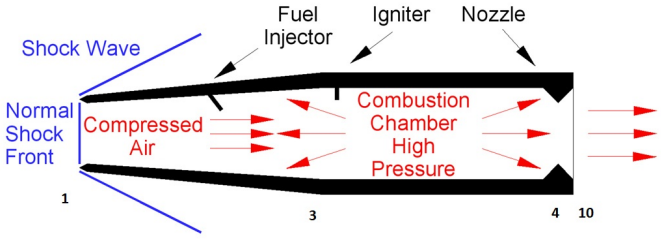


Figure 7.2: Ramjet engine schematics [114]. The numbers represent the different stations of the engine.

In traditional ramjet engines, compression is usually accomplished in several steps through multiple oblique shocks due to the geometry of the vehicle fore-body and the diffuser itself, followed by a final normal shockwave before entering the burner to achieve subsonic combustion. For the purpose of this demonstration, a simple diffuser design is implemented, using only one normal shock to decelerate the flow. This initial approach is much less efficient and results in a conservative estimate for the diffuser performance. Equations 7.16 and 7.17 determine flow properties downstream the shock front.

$$M_{ii} = \frac{(\gamma - 1)M_i^2 + 2}{2\gamma M_i^2 - (\gamma - 1)} \tag{7.16}$$

$$P_{recovery} = \frac{P_{t_{ii}}}{P_{t_i}} = \left[\frac{(\gamma + 1)M_i^2}{(\gamma - 1)M_i^2 + 2}\right]^{\frac{\gamma}{\gamma - 1}} \left[\frac{\gamma + 1}{2\gamma M_i^2 - (\gamma - 1)}\right]^{\frac{1}{\gamma - 1}} \tag{7.17}$$

There are two efficiency parameters inherent from the diffuser geometry: adiabatic efficiency, $\eta_d$, and pressure ratio, $\pi_d$. Both have an impact in the loss of stagnation pressure and temperature. Static

temperature and pressure can be calculated from the isentropic flow equations (see Appendix B.2).

$$\frac{P_{t_3}}{P_{t_\infty}} = \pi_d p_{recovery} \tag{7.18}$$

$$\frac{T_{t_3}}{T_{t_\infty}} = 1 - \eta_d \left[ 1 - \left( \frac{P_{t_3}}{P_{t_\infty}} \right)^{(\gamma/(\gamma-1))} \right] \tag{7.19}$$

The burner is responsible for fuel injection, mix and burn. Fuel-to-air ratio is calculated with energy conservation through Equation 7.20. The burner exit stagnation temperature, $T_{t_4}$, depends on the material limitations of the next component, $T_{mtl}$. For turbojets, this is a high pressure turbine, where mechanical and thermal stresses are very high due to rotation; for a ramjet engine, this is the exit nozzle, which withstands much higher temperatures. Furthermore, the burner exit stagnation temperature can also be limited due to thermal choking from the Rayleigh equations [115] (Equations 7.21 and 7.22).

$$f = \frac{T_{t_4} - T_{t_3}}{\dfrac{Q}{C_p} - T_{t_4}} \tag{7.20}$$

$$\frac{P_{t_4}}{P_{t_3}} = \frac{1 + \gamma M_3^2}{1 + \gamma M_4^2} \left( \frac{1 + \dfrac{\gamma - 1}{2} M_4^2}{1 + \dfrac{\gamma - 1}{2} M_3^2} \right)^{\frac{\gamma}{\gamma - 1}} \tag{7.21}$$

$$\frac{T_{t_4}}{T_{t_3}} = \left[ \frac{1 + \gamma M_3^2}{1 + \gamma M_4^2} \right]^2 \left[ \frac{M_4}{M_3} \right]^2 \frac{1 + \dfrac{\gamma - 1}{2} M_4^2}{1 + \dfrac{\gamma - 1}{2} M_3^2} \tag{7.22}$$

To maintain subsonic combustion throughout the burner, $M_4 \leq 1.0$. Therefore, there is a maximum value for the stagnation temperature according to Rayleigh, $T_R$, calculated using Equation 7.22 with $M_4 = 1.0$. An increase in $T_R$ can be obtained by decelerating the incoming flow. This may be accomplished by placing a divergent duct between the diffuser and the burner. After calculating $T_R$, SUAVE compares it with $T_{mtl}$ and proceeds to select the lowest of the two limits to work with.

$$T_{t_4} = \begin{cases} T_R & \text{if } T_R < T_{mtl} \\ T_{mtl} & \text{if } T_R \geq T_{mtl} \end{cases} \tag{7.23}$$

Finally, the flow exits through the expansion nozzle. Similarly to the diffuser, this component has two performance parameters inherent from its geometry: adiabatic efficiency, $\eta_n$ and pressure ratio, $\pi_n$. To further simplify the calculations, exit flow is considered fully expanded.

$$\frac{P_{t_{10}}}{P_{t_4}} = \pi_n \tag{7.24}$$

$$\frac{T_{t_{10}}}{T_{t_4}} = 1 - \eta_n \left[ 1 - \left( \frac{P_{t_{10}}}{P_{t_4}} \right)^{(\gamma/(\gamma-1))} \right] \tag{7.25}$$

The nozzle exit velocity can now be calculated using isentropic conditions in Appendix B.2.

### 7.2.3 Scramjet

To design a low-fidelity model of scramjet engine, core assumptions were considered to reduce the number of constraints to the problem:

- Flow behaves as a perfect gas, is steady and quasi-one dimensional, velocity is purely axial;
- Burner is assumed long enough for the supersonic combustion process to take place;
- Engine is divided in three separate components (Figure 7.3): inlet nozzle, combustion chamber and exit nozzle. Other components such as the isolator were discarded given their complexity for quasi-one dimensional analysis;

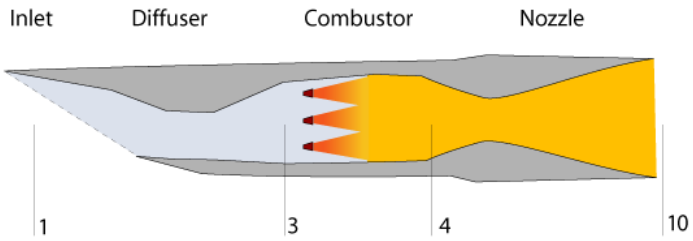


Figure 7.3: Scramjet engine schematics[116]. The numbers represent the different stations.

Using the concept of cycle static temperature ratio, $\psi$, it is possible to estimate inlet compression while bypassing specific geometry details [117].

$$\psi = \frac{T_3}{T_0} \tag{7.26}$$

The stagnation pressure is constant across the multiple shocks that take place in the inlet. Therefore, through algebraic manipulation of the isentropic equations, $M_3$ is attainable through Equation 7.27. Inlet exit pressure is obtained through Equation 7.28. Isentropic flow relations are used to calculate other flow properties such as $P_{t_3}$ and $u_3$. Finally, by applying the mass conservation (Equation 7.29), the area ratio $A_3/A_\infty$ is obtained.

$$M_3 = \sqrt{\frac{2}{\gamma - 1}\left[\frac{1}{\psi}\left(1 + \frac{\gamma - 1}{2}M_\infty^2\right) - 1\right]} \tag{7.27}$$

$$\frac{P_3}{P_\infty} = \left[\frac{\psi}{\psi(1 - \eta_d) + \eta_d}\right]^{C_p/R} \tag{7.28}$$

$$\frac{A_3}{A_\infty} = \psi \frac{P_\infty}{P_3}\frac{u_\infty}{u_3} \tag{7.29}$$

The burner is modeled after Heiser and Pratt [117], using a constant-pressure process. This assumption also takes in consideration a stoichiometric combustion. Following this approach, several performance factors are introduced to model supersonic combustion: burner drag coefficient, efficiency and fuel injection velocity. Flow properties at the burner exit are calculated using Equations 7.30 to 7.32.

$$u_4 = u_3 \left[ \frac{1 + f\frac{u_{fx}}{u_3}}{1+f} - \frac{C_{D_b}}{2(1+f)} \right] \tag{7.30}$$

$$T_{t_4} = \frac{T_3}{1+f} \left[ 1 + \frac{1}{C_{p_b} T_3} \left( \eta_b f Q + f C_{p_b} T_{ref} + \left[ 1 + f\frac{u_f^2}{u_3^2} \right] \frac{u_3^2}{2} \right) \right] \tag{7.31}$$

$$T_4 = T_{t_4} - \frac{u_4^2}{2C_{p_b}} \tag{7.32}$$

The flow at the exit nozzle is considered to be fully expanded ($P_{10} = P_\infty$). The output temperature and velocity can be calculated from Equations 7.33 and 7.34. By applying the mass conservation, the area ratio is determined using Equation 7.35 and the stream thrust concept is directly applicable. Station 10 corresponds to the nozzle exit, $e$.

$$T_{10} = T_4 \left[ 1 - \eta_n \left( 1 - (\frac{P_{10}}{P_\infty}\frac{P_\infty}{P_4})^{R/C_{p_n}} \right) \right] \tag{7.33}$$

$$u_{10} = \sqrt{u_4^2 + 2C_{p_n}(T_4 - T_{10})} \tag{7.34}$$

$$\frac{A_{10}}{A_\infty} = (1+f) \left( \frac{P_\infty}{P_{10}} \frac{T_{10}}{T_\infty} \frac{u_\infty}{u_{10}} \right) \tag{7.35}$$

## 7.3 Aerothermodynamic model

The heat flux permeating the aircraft surface is the result of a thermal energy balance between the vehicle and atmosphere and it is equal to the net energy transferred by contact with the gas minus that which is re-radiated by the vehicle surface. There are several aerothermodynamic models that help predict temperatures and heat fluxes across all sections of an airframe. Higher-fidelity models rely on CFD software but are unnecessarily computational-heavy for preliminary design. To better understand how aerothermodynamic models are built, some key concepts regarding heat and how it is produced must be clarified. Surface heat is measured by heat rate and heat load; heat rate is the instantaneous heat flux at a point on the vehicle whereas heat load is the heat rate integral with time over a trajectory. Heat itself has different origins and it can be classified as convective, catalytic and radiative.

- Convective heating derives from heat flux to the vehicle from conduction;
- Catalytic heating occurs due to surface chemical reactions and it is, by convention, lumped with convective heating;
- Radiative heating comes mostly from radiation produced by excited atoms and molecules in the shock layer.

For a simpler approach, the aerothermodynamic analysis in SUAVE will be performed based on semi-empirical laws. One of the most known is the Fay-Riddell correlation, which established that the

stagnation-point convective heating could be calculated given vehicle radius, velocity and freestream density. However, solving for this correlation is not a simple task as other variables are required, among them the Lewis number (the ratio of thermal diffusivity over mass diffusivity) or enthalpy of mixture. In the extreme, perhaps the simplest method for estimating hypersonic aerodynamic heating is to use Equation 7.36, an approximation for trans-atmospheric vehicles derived from Anderson [3]. This is a powerful design tool that can be used to approximate heating from a small number of CFD "anchor points" and provide an estimate of the order of magnitude of the heat flux at the stagnation point. This approximation already takes into account convective and radiative heating, even though the effects of the latter are negligible for speeds below 9 km/s.

$$q_w = {\rho_\infty}^{0.5} \cdot {V_0}^3 \cdot 1.83 \times 10^{-8} \cdot {r_{crv}}^{-1/2} \tag{7.36}$$

$$Q_W = \int_{t=0}^{t=t_f} q_w dt \tag{7.37}$$

## 7.4 Atmospheric re-entry

In SUAVE, mission profiles are built from different segments, properly arranged in climb, cruise, hover or descent categories. During analysis, each segment is split in a predefined number of control points at which the equations of motion are put together and the vehicle operational conditions (e.g., thrust, throttle, aircraft weight) are calculated through an iterative process [103]. With this information, it is also possible to plot the distance traveled:

$$x = x_0 + u_0 t + \frac{a_o t^2}{2} \tag{7.38}$$

$$u = u_0 + a_0 t \tag{7.39}$$

For atmospheric operations there are plenty of mission segments to choose from but there are none available for spacecraft-specific trajectories, including re-entry. For the HMV-ARV, it is necessary to create such segments to study heat flux distribution during re-entry. One important notion for reentry trajectories is the concept of ballistic coefficient, $\beta$, which measures the ability to overcome air resistance in flight.

$$\beta = \frac{M}{C_D A} \tag{7.40}$$

There are two main reentry trajectories to be considered: ballistic and lifting. While both are applicable to un-powered vehicles, ballistic trajectories neglect the effect of lift as the body is in free-fall, with a specific reentry angle. For an efficient gliding re-entry, a ballistic trajectory is undesirable; if used correctly, aerodynamic lift can provide a controlled, gradual and precise descent. Because orbital insertion takes place over a very short horizontal distance, a large portion of the spacecraft range develops over

re-entry and, to maximize it, a gliding trajectory is necessary. Therefore, the lifting re-entry is selected.

There are four main forces being exerted on the aircraft: weight, drag, lift and centripetal force. Through a series of simplifications (e.g., very shallow constant glide, constant $L/D$, constant drag coefficient) and algebraic manipulation [118], it is possible to obtain expressions for velocity and acceleration throughout re-entry:

$$v = v_{re} \cdot \left[ 1 + \frac{\rho_o R_{Earth}}{2\beta} \frac{L}{D} e^{-h/h_s} \right]^{-\frac{1}{2}} \tag{7.41}$$

$$n = -\frac{1}{\frac{2\beta}{\rho_o R_{Earth}} e^{h/h_s} + \frac{L}{D}} \tag{7.42}$$

By analyzing both equations, one may conclude there are four design variables for an Earth re-entry. Two of them (L/D and $\beta$) are related to vehicle design whereas the other two ($v_{re}$ and $h$) are only dependent on trajectory information. It can also be concluded that a higher L/D results in a smaller deceleration and a longer glide. Together with Equations 7.38 and 7.39, it is possible to determine altitude gradient, elapsed time and range.

## 7.5 Verification and Validation

In this section, each new numerical model is individually tested and compared against other numerical tools and/or experimental data to assess their behavior before their final implementation in the use case.

### 7.5.1 Weight distribution

The HASA methodology applied in SUAVE is specific to hypersonic vehicles and has been certified by NASA. Nevertheless, its results are compared with two other algorithms for weight distribution. The first one is the default tube and wing methodology available in SUAVE, based in the work of Kroo and Shevell [119]. The second one is the Weight Analysis for Advanced Transportation Systems (WAATS) methodology applied to the LAPCAT MR2 project [10, 120].

Tube-and-wing and HASA methodologies are applied to HMV vehicle and can be directly compared. This means the 50,000 kg GTOW and all the design parameters in Table 7.1 are used for the weight calculation. Then, the relative GTOW weights are compared to that of LAPCAT MR2 using the WAATS method.

As expected, the default tube-and-wing methodology underestimates EW as it fails to account for the higher structural requirements. This clearly demonstrates the need for a new weight distribution methodology to be implemented in SUAVE. From comparing WAATS and HASA, there are differences for certain subsystems but overall the empty weight percentage with respect to GTOW is very similar and also more conservative The subsystem discrepancy can be attributed to the non-linearity of scaling effects in aircraft design: LAPCAT MR2 is a much larger aircraft than the HMV.

| Component | Tube-and-Wing | | | HASA | | | WAATS | |
|---|---|---|---|---|---|---|---|---|
| | kg | %EW | %GTOW | kg | %EW | %GTOW | %EW | %GTOW |
| Structural | 11,252 | 65.7 | 22.5 | 14,446 | 69.6 | 28.9 | 66.6 | 24.5 |
| Propulsion | 4,000 | 23.4 | 8.0 | 5,182 | 25.0 | 10.4 | 29.8 | 10.9 |
| Systems | 1,880 | 10.9 | 3.8 | 1,111 | 5.4 | 2.2 | 3.6 | 1.3 |
| Sum | 17,132 | 100.0 | 34.3 | 20,739 | 100.0 | 41.5 | 100.0 | 36.7 |

Table 7.1: Weight distribution verification

### 7.5.2 LOX/LH2 rocket engine

When describing the rocket model, three main variables were identified: combustion pressure, $O/F$ and nozzle expansion ratio. As such, information on these parameters was compiled for a series of existing LOX/LH2 engines [121, 122, 123, 124]. The engine sample is wide and diverse, contemplating not only engines from different decades but also purposefully built with distinct on-design conditions (i.e.g, RD-0120 is a first-stage engine whereas Vulcain 2 is a second-stage engine). The next step was to use information compiled from Braeuning to calculate specific propellant properties to obtain values for specific impulse, which were then compared to experimental data on each engine, both at sea level (if applicable) and vacuum. A table comprising rocket design parameters is displayed in Appendix C.1. Figure 7.4 provides a visual representation of the validation process for all engines:

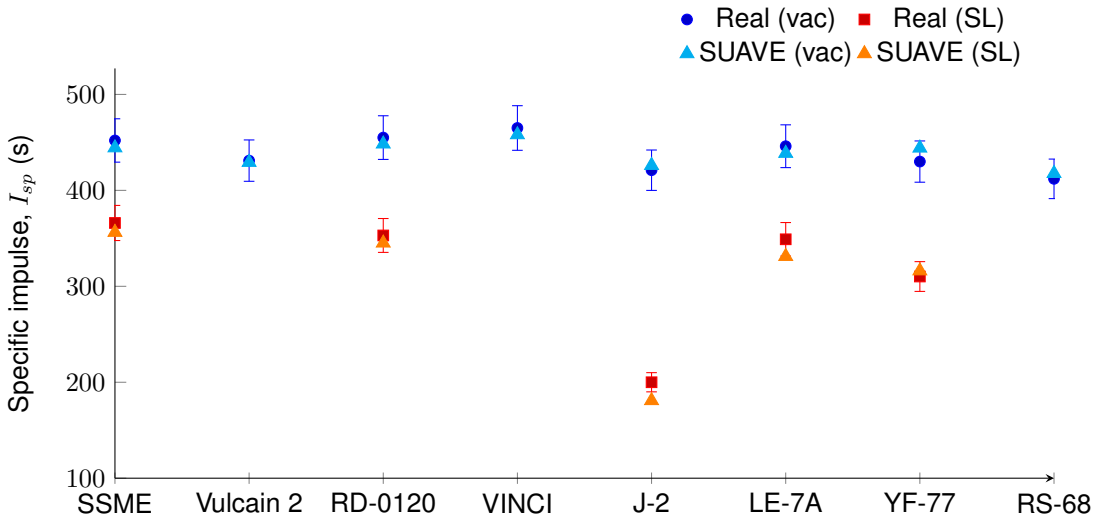


Figure 7.4: LOX/LH2 rocket engine model validation, error bars of 5%

The results are surprisingly accurate, especially when noting the ideal, one-dimensional premise involved in these calculations. The newly implemented SUAVE LOX/LH2 rocket module succeeds at predicting the specific impulse of various engines at different operating conditions, with a maximum error margin of less than 10%.

### 7.5.3 Ramjet

The new SUAVE ramjet model is verified with theoretical quasi-one dimensional performance predictions of specific impulse.

Firstly, a range of $I_{sp}$ for ramjet engines was obtained for hydrocarbon and hydrogen fuels. Then, general SUAVE efficiencies were set, the same for both fuel types. These values ranged from 95 to 100%. To compare the numerical model with the expect $I_{sp}$ range, JP-7 and LH2 were chosen for the simulation; that is, data on the fuel combustion heat, stoichiometric fuel-to-air ratio and energy density was collected [125, 126].

A list of inputs and the final verification graph is displayed in Figure 7.5. The dashed lines delimit the range for hydrocarbon (square markers) and hydrogen (triangle markers) operation.

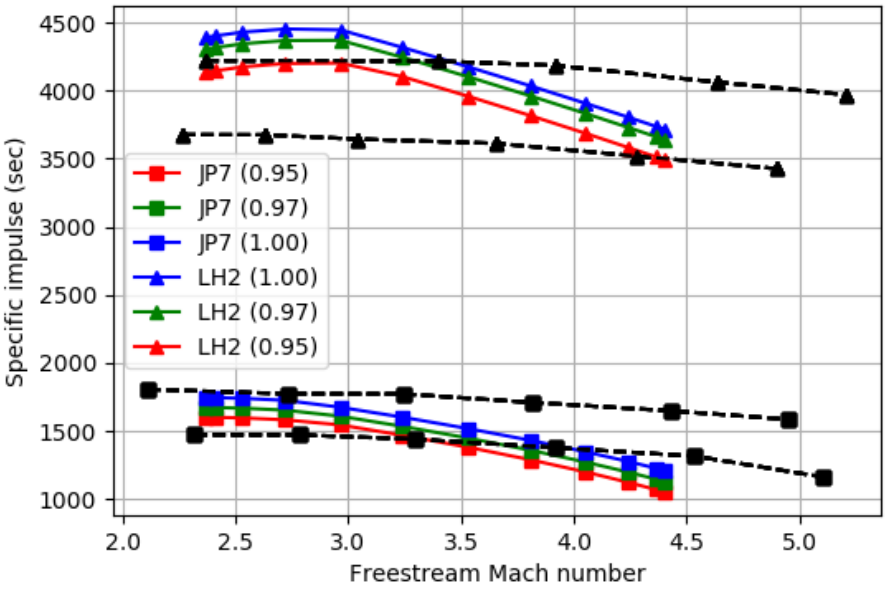


Figure 7.5: Ramjet model verification

It is important to notice that, as mentioned before, a single normal shockwave was chosen as the only compression mechanism in the SUAVE model for simplification; in reality, spikes are incorporated in the inlet design to induce one or multiple oblique shock waves prior to the final normal shock. Albeit more complex, this allows for a higher pressure recovery factor which may help explain the small deviation from the expected range. This difference can also be aggravated by small changes to the heat of combustion of the simulated fuels, which may differ depending on the exact circumstances the engine is operating at. Nevertheless, given the low-fidelity nature of the desired analysis and noting that the SUAVE offset does not exceed 10% of the predicted range, the ramjet model is sufficient for the test case implementation.

### 7.5.4 Scramjet

Since scramjet technology is still an active, high-priority research topic, there is a lack of publicly available experimental data to validate this model. There are, nonetheless, numerous scramjet numerical models

available. For the verification process, three different scramjet codes were used.

The Ramjet Performance Analysis Code (RJPA), considered an industry standard, was developed by the Applied Physics Laboratory at John Hopkins University. Like SUAVE, it separates the flow path into separate sections, which are modeled individually as a control volume. The combustion process is simulated in extreme detail including thermo-chemical equilibrium. However, program access is very restricted.

The Simulated Combined-Cycle Rocket Engine Analysis Module (SSCREAM) is an object-oriented code written in C++ that uses quasi-one dimensional flow analysis through several components. It was created for the conceptual launch vehicle design environment by the Georgia Institute of Technology.

Finally, VTMODEL is a detailed quasi one-dimensional analysis tool, developed by Virginia Tech University. It is a very robust code as it models the isolator shock train and also provides various options to calculate the performance of its different subcomponents.

All the codes mentioned above are private and/or have very restricted access. As such, for the verification process, data was gathered from different publications in the same operating conditions [127]. These constraints were then fed or adapted into SUAVE for proper comparison. For instance, cycle static temperature ratio is not a parameter in any of the previous models; instead, its value was estimated to provide the same starting Mach number of all the other models, according to Equation 7.27.

The verification process used liquid hydrogen as fuel with stoichiometric fuel-to-air-ratio. The SUAVE model parameters and the numerical model comparison can be visualized in Figure 7.6.

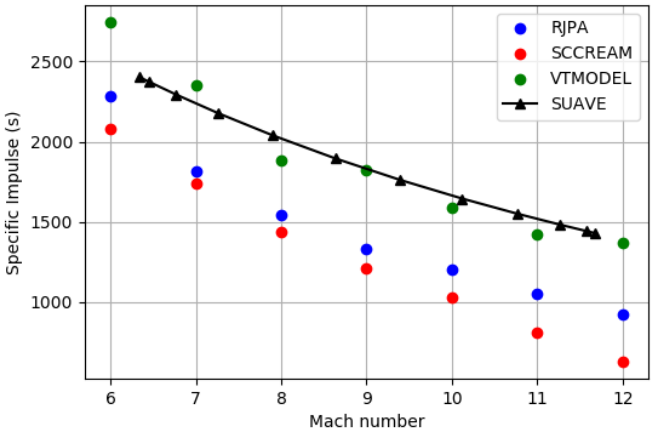


| Parameter | Value |
|---|---|
| $\eta_d$ | 0.985 |
| $\psi$ | 2.333 |
| $u_{f_x}/u_3$ [1] | 0.500 |
| $C_{D_b}$ [1] | 0.500 |
| $u_f/u_3$ [1] | 0.100 |
| $\eta_b$ | 0.900 |
| $\eta_n$ | 0.985 |
| $f$ | 0.293 |

Figure 7.6: Scramjet model verification

The results highlight some of the discrepancies that exist between other numerical models and demonstrate the scramjet sensibility to minor modifications in flow properties and component efficiency. It is important to note that the efficiency parameters used for the SUAVE model may not be exactly the ones used for the other numerical codes. Nevertheless, the newly implemented SUAVE scramjet model provides a specific impulse estimate either within the expected range or with a small deviation from it, which is sufficient for a preliminary design analysis.

[1] Parameters assumed from Heiser and Pratt [117] as they have no equivalent to any of the codes used for comparison

## 7.6 Atmospheric reentry and heat flux

The IXV spacecraft was used as reference to validate both the atmospheric reentry and the aerothermodynamic model and to do so requires vehicle and trajectory information. Vehicle geometry, mass and $L/D$ were extracted from IXV references [128]. For hypersonic flight, an initial estimate for drag coefficient places it between 0.4 and 0.7 [129], depending on the exact geometric shape. Reentry altitude and speed were set according to trajectory parameters [130]. The leading edge radius was approximated to a quarter of the body diameter and the area was approximated to width multiplied by length. The ballistic coefficient was calculated accordingly with Equation 7.40. Information is compiled in Table 7.2.

| Parameter | | Value | |
|---|---|---|---|
| Vehicle parameters | | | |
| | Length | $[m]$ | 5 |
| | Width | $[m]$ | 2.2 |
| | Height | $[m]$ | 1.5 |
| | Mass | $[kg]$ | 1,845.0 |
| | $C_D$ | [-] | 0.4 - 0.7 |
| | $L/D$ | [-] | 0.70 |
| | $r_{crv}$ | $[m]$ | 0.38 |
| | $A$ | $[m^2]$ | 11.00 |
| | $\beta$ | $[kg/m^2]$ | 670.91 |
| Trajectory parameters | | | |
| | $h_re$ | $[km]$ | 90.0 |
| | $v_re$ | $[km/s]$ | 7.50 |

Table 7.2: IXV validation parameters

The final results of the validation process are displayed in Figure 7.7. The reentry profile matches the actual flight data (expected reentry time of $\approx$ 20 minutes) and the maximum experimental heat flux is of 65 $W/cm^2$, which corresponds to a 4.6% relative error for a $C_D = 0.4$.

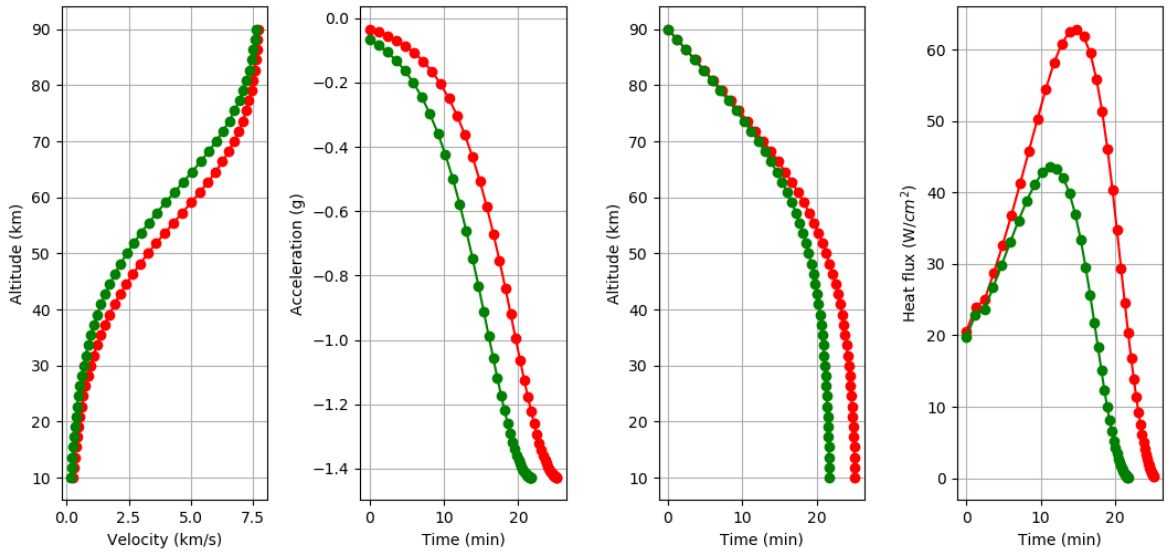


Figure 7.7: Atmospheric and aerothermodynamic model validation, for $C_D = 0.4$ (red) and $C_D = 0.7$ (green)

# Chapter 8

# Results

After verifying each new numerical model independently, all of them were used in the test case defined in Chapter 6 to finally obtain the performance of a generic hypersonic vehicle, for both HMV-CAV and the HMV-ARV. The main focus is in the comparison of mission profile requirements for these distinct cases and, therefore, a large portion of the aircraft setup is shared and detailedly described in Section 8.1. Specific results for the HMV-CAV and the HMV-ARV are shown in Sections 8.2 and 8.3, respectively.

## 8.1 Final setup

### 8.1.1 Weight distribution

Upon reviewing the hypersonic weight breakdown process, the empty weight obtained through HASA in Section 7.5.1 was rounded and the final weight distribution is listed in Table 8.1.

| EW (kg) | FW (kg) | PW (kg) | GTOW (kg) |
|---|---|---|---|
| 20,750 | 24,250 | 5,000 | 50,000 |

Table 8.1: HMV final weight distribution

### 8.1.2 Propulsion

To create the common air-breathing cycle, the existing turbojet model was merged with the newly created dual-mode ramjet. However it is necessary to choose an appropriate criteria to dictate when transition between operational modes takes place. To simplify this issue, and because there are very clear Mach ranges for each individual engine, the freestream Mach number is chosen as a criteria; as such, each engine model comes associated with a transition Mach number that determines when said engine begins to work. The only difference is in the rocket transition, which is imposed exclusively to the specific orbital ascent segment. The final propulsion parameters are listed in Table 8.2. The left table represents the parameters for the air-breathing cycle, including the transition Mach numbers; the right table represents the final parameters for the rocket cycle. For the ramjet and scramjet engines, these were either chosen

based on Heiser and Pratt [117] or approximated to SUAVE values for turbojet propulsion. The sizing conditions were either based on current engines or inferred based on drag estimates. For the dual-mode ramjet engine, only one of the operational modes is required for the sizing process.

(a) Airbreathing cycle parameters

| Parameter | | Turbojet | Ramjet | Scramjet |
|---|---|---|---|---|
| $\eta_d$ | | 0.96 | 0.90 | 0.90 |
| $\pi_d$ | | 0.98 | 0.96 | 0.96 |
| $\psi$ | | — | — | 2.00 |
| Fuel | | JP-7 | LH2 | LH2 |
| $\eta_b$ | | 0.99 | 0.90 | 0.90 |
| $T_{t_{mtl}}$ | $[K]$ | 1450 | 2400 | — |
| $C_{D_b}$ | | — | — | 0.10 |
| $u_{f_x}/u_3$ | | — | — | 0.50 |
| $u_f/u_3$ | | — | — | 0.50 |
| $\eta_n$ | | 0.95 | 0.90 | 0.90 |
| $\pi_n$ | | 0.99 | 0.96 | 0.96 |
| $F_{sizing}$ | $[N]$ | 150,000 | — | 24,000 |
| $h_{sizing}$ | $[km]$ | 0.00 | — | 18.00 |
| $M_{sizing}$ | | 0.00 | — | 5.00 |
| $M_{transition}$ | | 0.00 | 1.80 | 4.50 |

(b) Rocket cycle parameters

| Parameter | | Rocket |
|---|---|---|
| Oxidizer | | LOX |
| Fuel | | LH2 |
| $\kappa$ | | 69.0 |
| $p_c$ | $[bar]$ | 206.4 |
| $O/F$ | | 6.00 |
| $F_{sizing}$ | $[kN]$ | 1,860 |
| $h_{sizing}$ | $[km]$ | 0.00 |
| $M_{sizing}$ | | 0.00 |

Table 8.2: Final propulsion parameters

## 8.2 Air-breathing cruise (HMV-CAV)

### 8.2.1 Mission profile selection

For a general hypersonic CAV, climb is done at constant dynamic pressure, calculated through Equation 8.1. When this parameter is fixed, the cruise altitude (influenced by the freestream density) automatically determines the cruise speed. On the other hand, for hypersonic flight, the cruise Mach number must be at least higher than 4.0. Therefore, by examining Figure 6.2, there is range of values for dynamic pressure (between 25 and 80 KPa) and cruise altitude (between 20 and 25 km) that fulfill all the requirements.

$$q = \frac{1}{2}\rho V^2 \tag{8.1}$$

From a performance standpoint, there is a general interest in reducing the flight duration but also maximizing the flight range, with a fixed amount of fuel. The optimum cruise design point is therefore chosen based on the best trade-off between these two variables, represented by the utility function, $U$, shown in Equation 8.2. For each coordinate $(q, h)$, the values for the maximum and minimum range and duration are stored and the cruise distance is iteratively increased until a final fuel margin of $(2.50 \pm 0.30)$% is reached. For each pair $(q, h)$, $U$ returns a value from 0 to 1, where 1 is the best possible result and 0 is the least favorable. The function is plotted in Figure 8.1 for 225 coordinates.

$$U(q,h) = \frac{1}{2} \cdot \frac{X - X_{min}}{X_{max} - X_{min}} + \frac{1}{2} \cdot \left(1 - \frac{t - t_{min}}{t_{max} - t_{min}}\right) \tag{8.2}$$

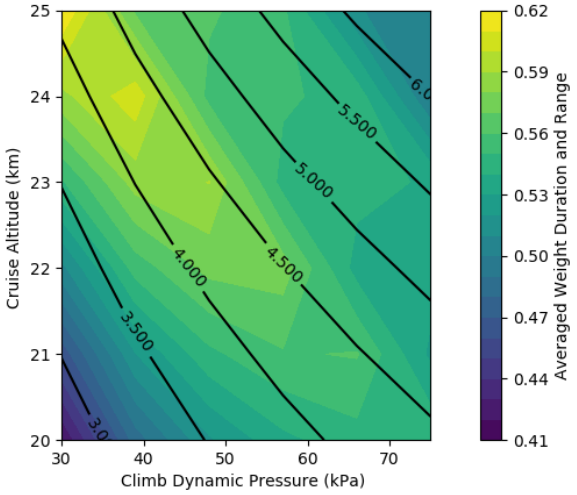


Figure 8.1: HMV-CAV utility function. Contour lines represent cruise Mach number, $M$

It is important to note that this utility function not only takes into account the cruise conditions (altitude and dynamic pressure) but also the extra fuel necessary to climb to each new cruise altitude. From here, the design point can be selected. If $M_{cruise} = 5$ is chosen, the best coordinate pair sits around the area of 45-50 KPa at an altitude of 20-25 Km. The final climb design conditions are set to 45 KPa and 25 km.

### 8.2.2 Baseline solution

The final mission profile is displayed in Figure 8.2. The top graphs show the altitude over time and distance, as well as speed and Mach number. The aircraft reaches Mach 5.0, which, according to the transition Mach numbers set in Table 8.2, means all engine operational modes are activated. The bottom left graph shows the acceleration felt during the entire trajectory, measured in $g$. Finally, on the bottom right, dynamic pressure is shown which is consistent with the range portrayed in Figure 6.2.

Propulsion performance is demonstrated in Figures 8.4 and 8.5. Figure 8.5 displays specific propulsion parameters such as $I_{sp}$, $F_{sp}$ and $f$. These plots provide a clear indication of the engine operation transition points, represented by abrupt spikes in the function output. Values for specific impulse and specific thrust match theory predictions. Figure 8.4 displays the thrust at all points of the mission and the throttle value that was iterated to provide said thrust. From this figure, throttle exceeds 100% in certain mission segments which indicates that the engine is not sized correctly; that is, it's producing a higher thrust than what it is capable of. This calls for a corrected solution, presented below in Section 8.2.3.

Weight distribution is shown in Figure 8.3 alongside fuel consumption and demonstrates the prerequisites set for the test case. Finally, the heat flux distribution at the stagnation point of the vehicle nose is demonstrated in left graph of Figure 8.6. This point in particular is chosen as it undergoes some of the most severe heating conditions. In the right graph of Figure 8.6, $L/D$ is plotted over time; the red-dashed line represents the Küchemann empirical relation [131] for $L/D_{max}$ in hypersonic flight.

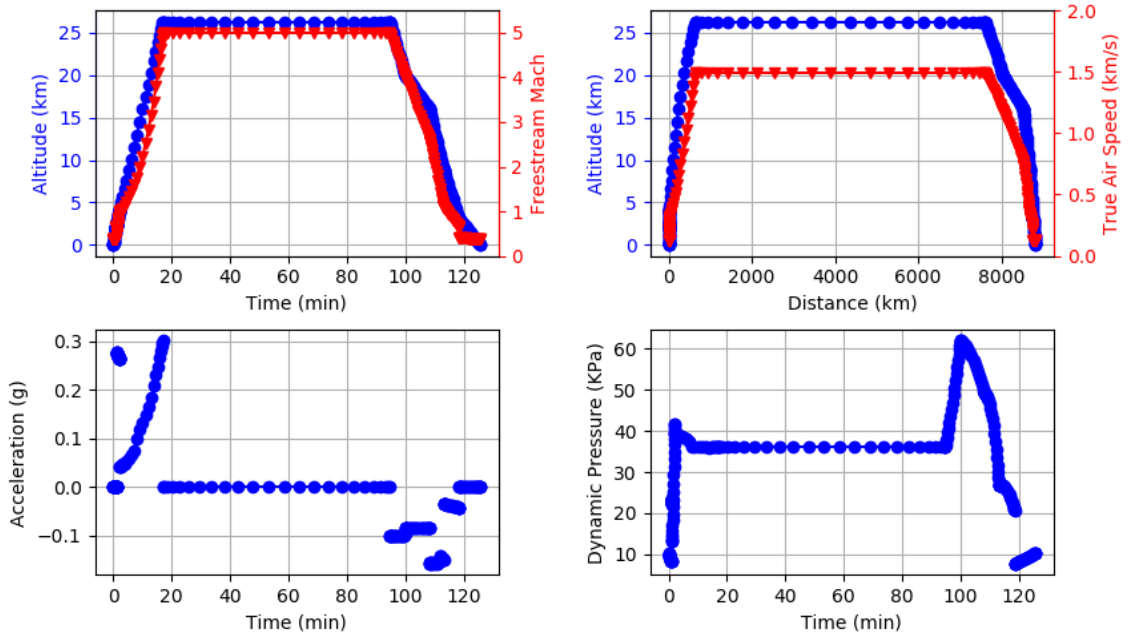


Figure 8.2: HMV-CAV mission profile

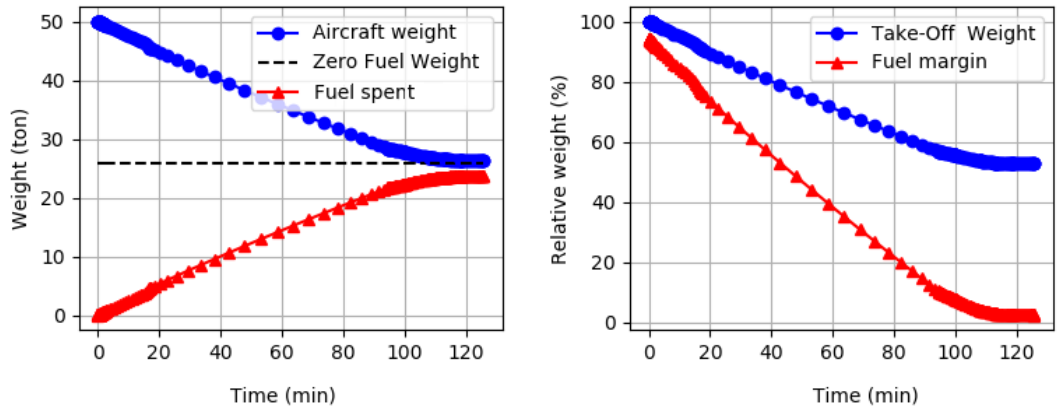


Figure 8.3: HMV-CAV weight distribution

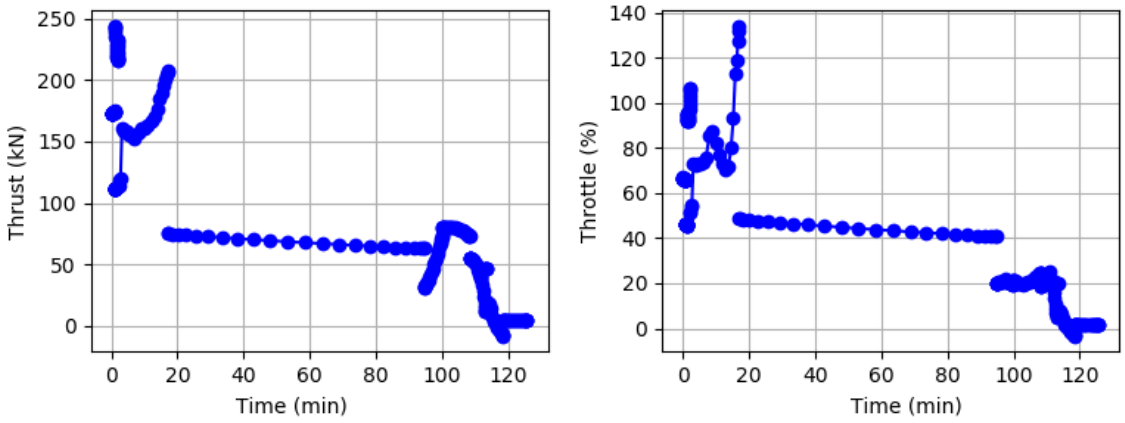


Figure 8.4: HMV-CAV propulsion general parameters

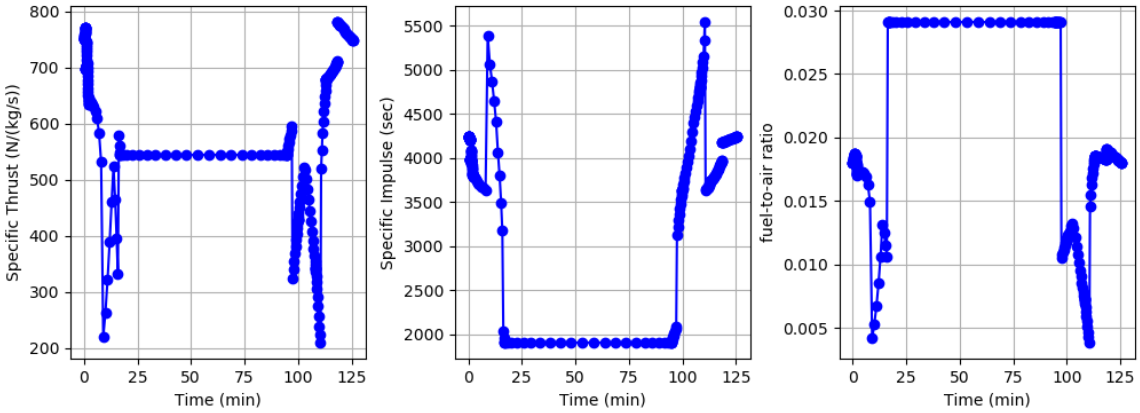


Figure 8.5: HMV-CAV propulsion specific parameters

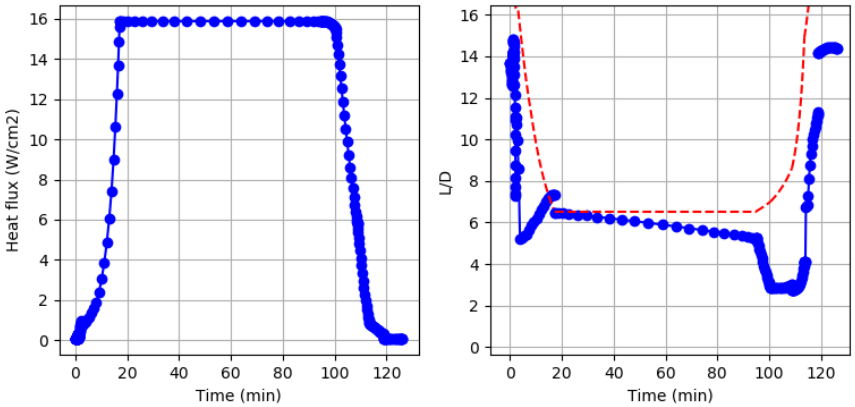


Figure 8.6: HMV-CAV aerothermodynamic and aerodynamic analysis

### 8.2.3 Enhanced solution

As mentioned above, while in general the results obtained for the baseline solution are satisfactory, there is a misrepresentation of the engine performance expressed in the throttle function; that is, SUAVE concluded the engines were not able to produce sufficient thrust by themselves to propel the aircraft through the entire climb segment. There are various options to deal with this situation, for instance changing the mission profile itself or increasing the sizing thrust. However, the most fruitful and elegant solution is to tweak the efficiency parameters of all the subcomponents of the engine network as it can also serve as a discussion point for hypersonic propulsion technology maturation. The parameters which have been modified are shown in Table 8.3. This combination of new efficiencies, with partial effort on the combustion process, is the minimum necessary to obtain a valid flight for this mission profile in particular, and represents the progress required for engine subsystems to allow it. While a few modifications were made to the inlet and nozzle parameters, the main performance gains were attributed to the combustion process, in an effort to simulate future combustion technology enhancement, a major area of development in hypersonic propulsion.

By running a simulation for the new parameters and the same mission profile, the superior propulsion performance is evident in Figures 8.7 and 8.8. The maximum throttle is now below 100% and, in

| Parameter | Ramjet | Scramjet |
|---|---|---|
| $\eta_d$ | 0.92 | 0.92 |
| $\pi_d$ | 0.97 | 0.97 |
| $\eta_b$ | 0.95 | 0.95 |
| $T_{t_{mtl}}$ | 2600 | — |
| $\eta_n$ | 0.92 | 0.92 |

Table 8.3: HMV-CAV updated propulsion parameters

particular, the improved $I_{sp}$ translates into significantly lower fuel consumption, which in turn leads to a fuel margin increase at the end of the mission to up to 13%. This can be interpreted in one of two ways:

- For the same final fuel margin, the aircraft could have carried twice the payload, which corresponds to an extra 5,000 kg;
- For the same payload, the optimized aircraft could fly longer distances and longer periods of time.

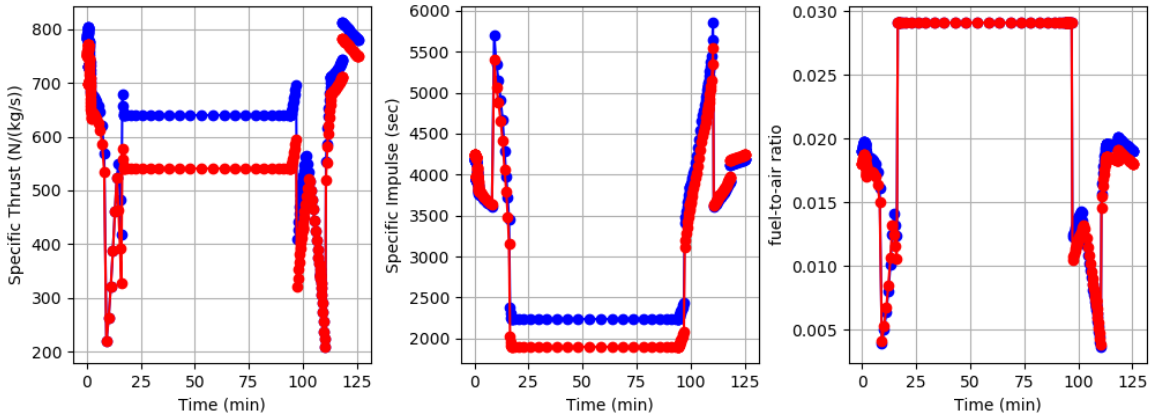


Figure 8.7: Comparison of propulsion specific parameters (in blue, the updated simulation)

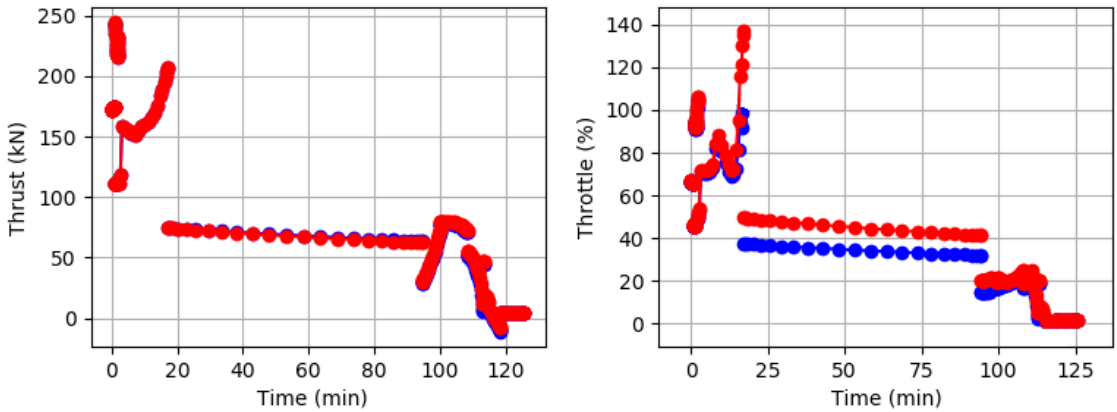


Figure 8.8: Comparison of propulsion general parameters (in blue, the updated simulation

For the second case, using the extra fuel may lead to new values for the utility function, which is recalculated to obtain a new cruise design point for the same fuel margin. $U_{opt}$ is plotted in Figure 8.9

and, upon inspection, there hasn't been a significant change in its value; therefore, the same design cruise point as before is chosen, only this time range is expected to be considerably larger. The relevant results are shown in Figure 8.10. It is now approximately 12,000 km and the flight duration is 150 minutes. Acceleration and dynamic pressure variations are exactly the same as experienced in the baseline case and are not displayed. The heat flux distribution is also equivalent to the baseline solution but the total heat load is higher due to an increase of flight duration.

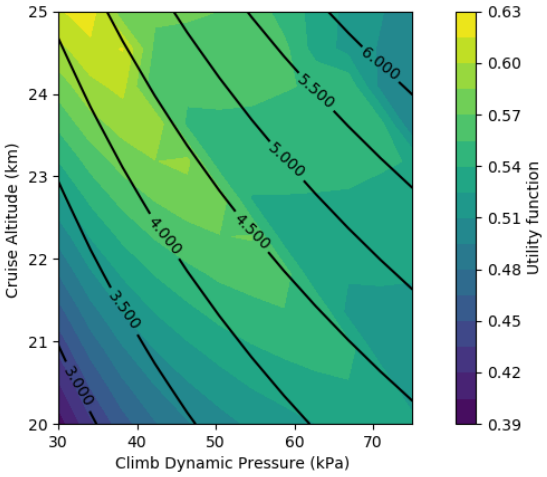


Figure 8.9: Optimized HMV-CAV utility function. Contour lines represent cruise Mach number, $M$

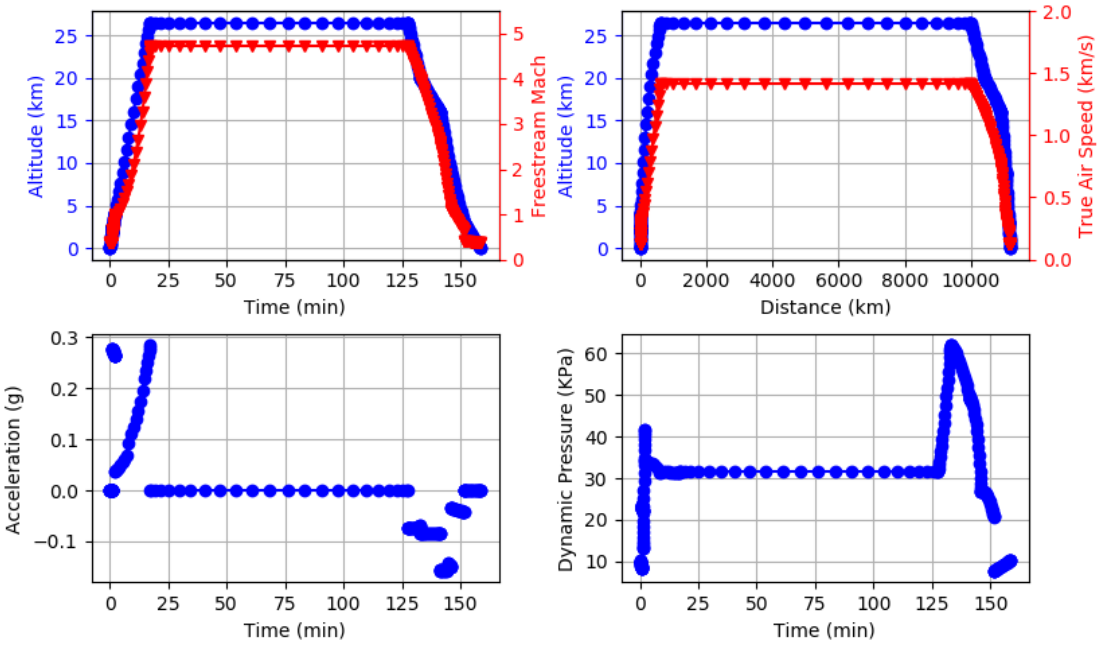


Figure 8.10: HMV-CAV optimized mission profile

## 8.3 Air-breathing ascent and reentry (HMV-ARV)

### 8.3.1 Mission profile selection

For a generic hypersonic ARV-like vehicle, there is a higher interest in maximizing the flight range given that the ascent phase always develops over a small time frame. In this manner, for fixed aircraft properties (e.g., area, $L/D$, $C_D$), range may be significantly increased by achieving a higher altitude and/or speed at the end of the ascent phase since most of the flight range develops over the reentry process. Therefore, through the built-in SUAVE optimization functions, it is possible to plot the range for an array of initial reentry altitude and speed, $(h, v)$. As mentioned in Section 6.4, for the purpose of this test case, the reentry segment takes place immediately after the completion of the orbital ascent segment and, therefore, these input conditions are simultaneously the final climb altitude and speed, respectively.

To simulate the reentry segment, estimates for $L/D$ and $C_D$ had to be provided. For $L/D$, an initial estimate sits between the value for IXV ($L/D \approx 0.7$) and the Space Shuttle orbiter ($L/D \approx 0.714$ at 100 km). An intermediate value of 0.710 is selected. For $C_D$, the final value of 1.10 is chosen according to the same Space Shuttle Orbiter references [132].

Unlike the HMV-CAV cruise design trade-off, there is no point in using a similar utility function because the final ascent to orbit develops over a relatively small period of time when compared to the total flight duration; on the other hand, any additional seconds during the final ascent may lead to considerable changes to the final aircraft range, as seen in Figure 8.11: the maximum flight duration gap is of approximately 10 minutes whereas the maximum range gap is nearly 3500 km. Therefore, only the range is used as a selection criteria. Please note that, in Figure 8.11, the final descent segment after reentry is being neglected for the climb design choice. This approximation is valid given the fact that during the landing descent there is a negligible range development and only a very small fraction of fuel is consumed. The climb parameters used for the HMV-ARV are the same that have been selected for the HMV-CAV, including constant dynamic pressure for the air-breathing climb segment. The final climb design point has a final orbital speed of 6.0 km/s at an altitude of 100 km.

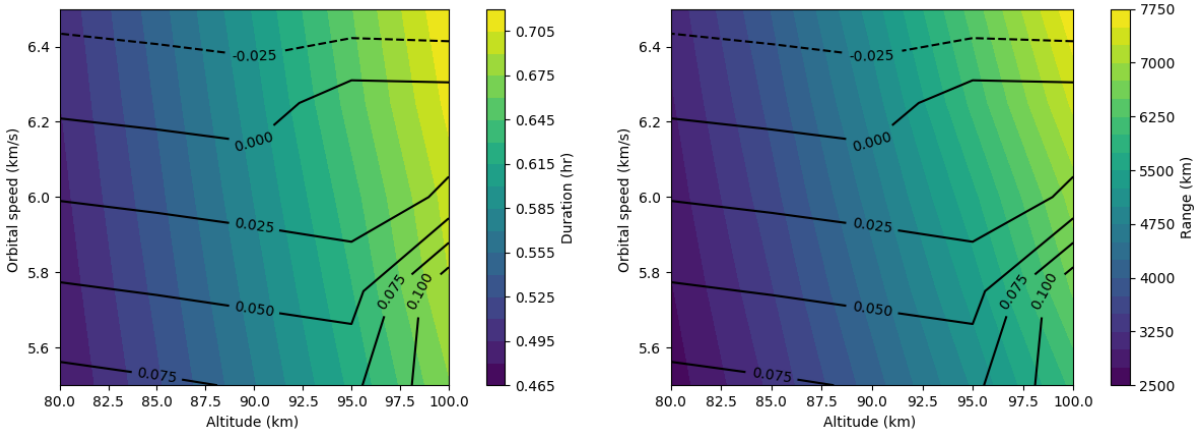


Figure 8.11: Range and duration for the HMV-ARV. Contour lines represent fuel margin

### 8.3.2 Baseline solution

The final mission profile is represented Figure 8.12. Most of the climb segments are the same as that of the HMV-CAV except for the final ascent to orbit; because no gravity turn segment exists in SUAVE, this is replaced by a linear climb at linear Mach numbers. The dynamic pressure exerted on the vehicle does not vary much from the previous case, whereas the accelerations are much more meaningful. In these conditions, the aircraft is able to reach 6.0 km/s, almost comparable to the Space Shuttle orbiter reentry speed (see Figure 1.2).

Weight distribution is shown in Figure 8.13. For the most part, fuel consumption is moderate, in line with the HMV-CAV case, until rocket operation kicks in near the 18-minute mark; now the propellant consumption is rapidly increasing as both on-board oxidizer and fuel are being used. The heat flux distribution at the stagnation point of the vehicle nose is also plotted in Figure 8.14, to the left. While the flight duration is considerably shorter than the HMV-CAV, the maximum heat flux is higher. For such a mission profile, there are two different peak heat fluxes. The first one takes place midway through the orbital ascent while the second one takes place midway during reentry. These result from a combination of hypervelocity flight and moderately rarefied atmosphere and, as the aircraft climbs further, heat rate decreases in magnitude. In the right graph of Figure 8.14, $L/D$ is plotted over time; the red-dashed line represents the Küchemann empirical relation for $L/D_{max}$ in hypersonic flight.

Propulsion performance is demonstrated in Figures 8.15 and 8.16. As mentioned before, the reentry segment is completely un-powered and therefore no propulsion parameters were plotted here. The main concern from the HMV-CAV base solution is replicated: the engine is poorly sized for the mission profile and throttle overshoots by 50%. This calls for an enhanced solution, which is discussed in further detail in Section 8.3.3 . In the fuel-to-air ratio graph in Figure 8.15, the red plot represents the rocket segment; it is highlighted to keep in mind that, given the absence of air, it represents the inverse of O/F.

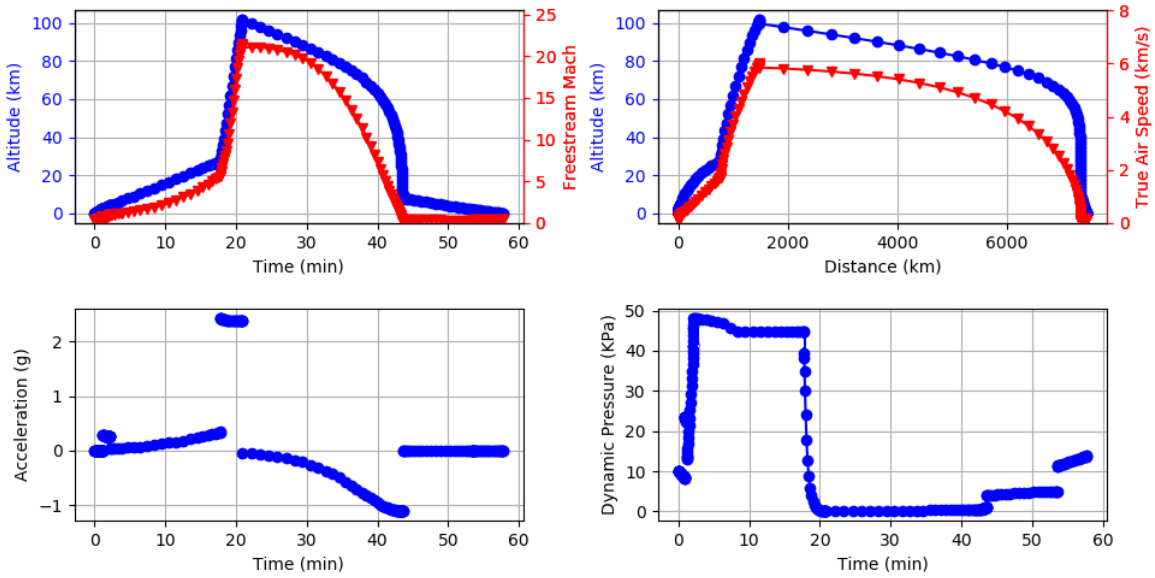


Figure 8.12: HMV-ARV mission profile

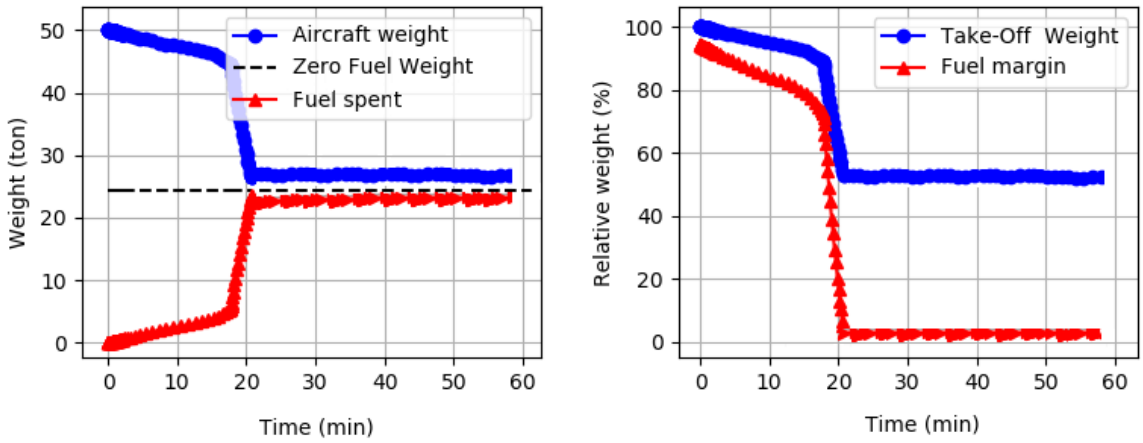


Figure 8.13: HMV-ARV weight distribution

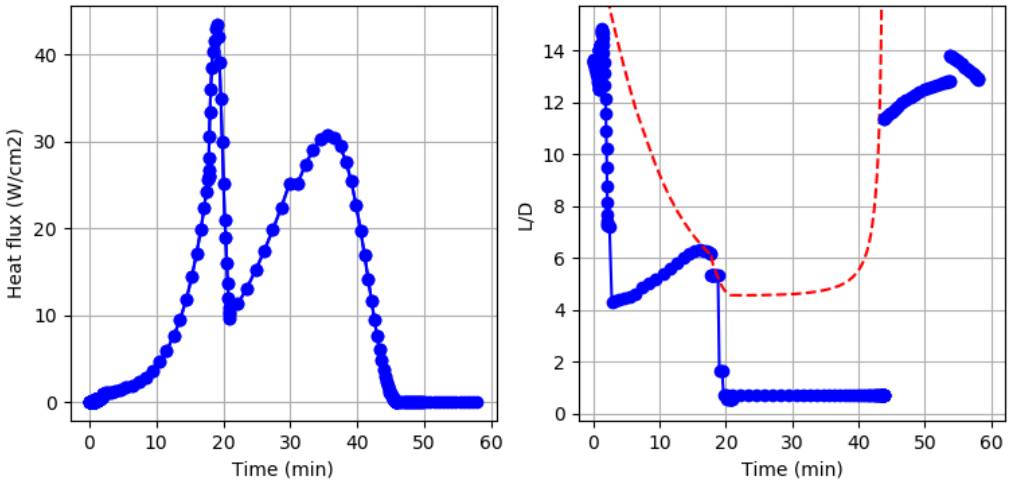


Figure 8.14: HMV-ARV aerothermodynamic and aerodynamic analysis

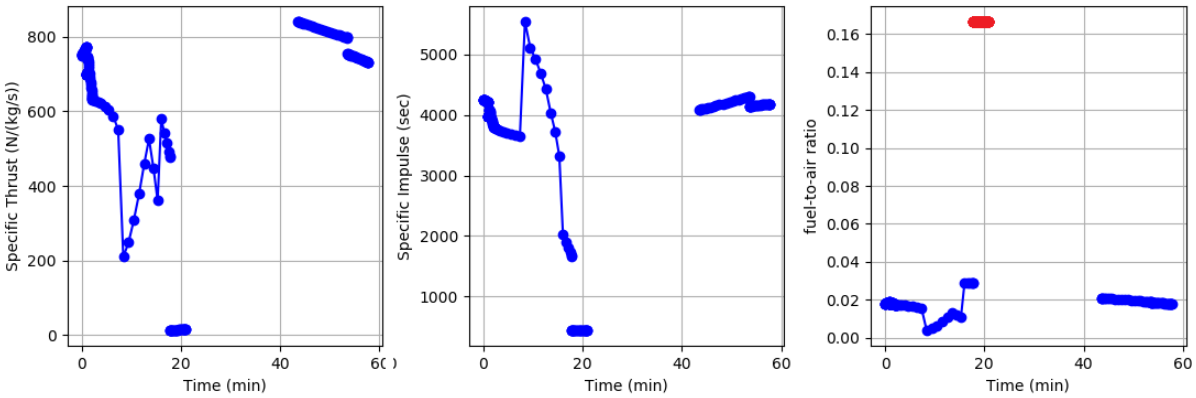


Figure 8.15: HMV-ARV propulsion specific parameters

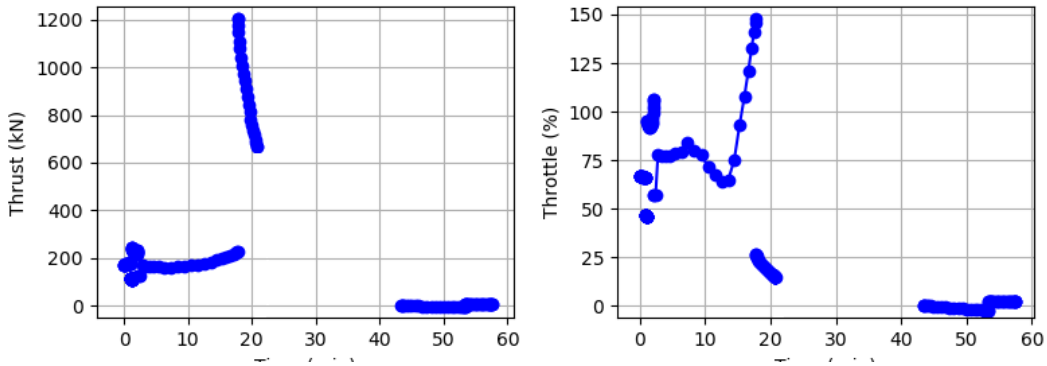


Figure 8.16: HMV-ARV propulsion general parameters

### 8.3.3 Enhanced solution

For the enhanced solution, the same logic from the HMV-CAV optimization case applies; that is, the burner parameters were improved to obtain a more efficient combustion. In this way, it may be possible to properly size the engine and correct the throttle issue from the previous subsection. Through fuel savings it may also be possible to reach higher speeds and significantly increase the spacecraft range. For the common air-breathing cycle, the improvements are exactly the same presented for the HMV-CAV test case, listed in Table 8.3; rocket parameters remain unaltered. Rockets are extraordinarily sensible to weight and therefore any fuel savings are predicted to have a significant impact in the spacecraft performance. Upon improving the individual component efficiencies, the new climb design conditions are set for a final climb speed of 7.5 km/s (similar to the IXV flight test) at an altitude of 100 km.

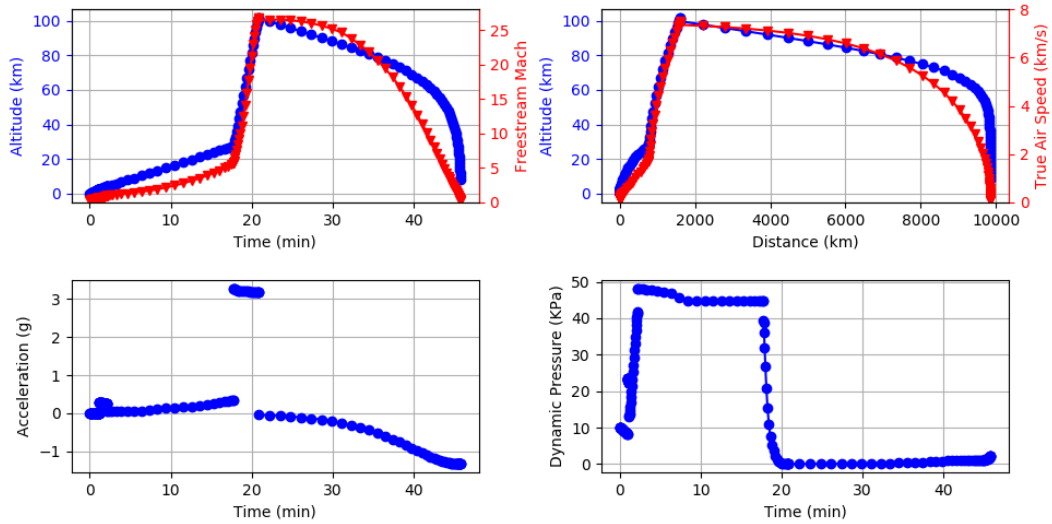


Figure 8.17: HMV-ARV optimized mission profile

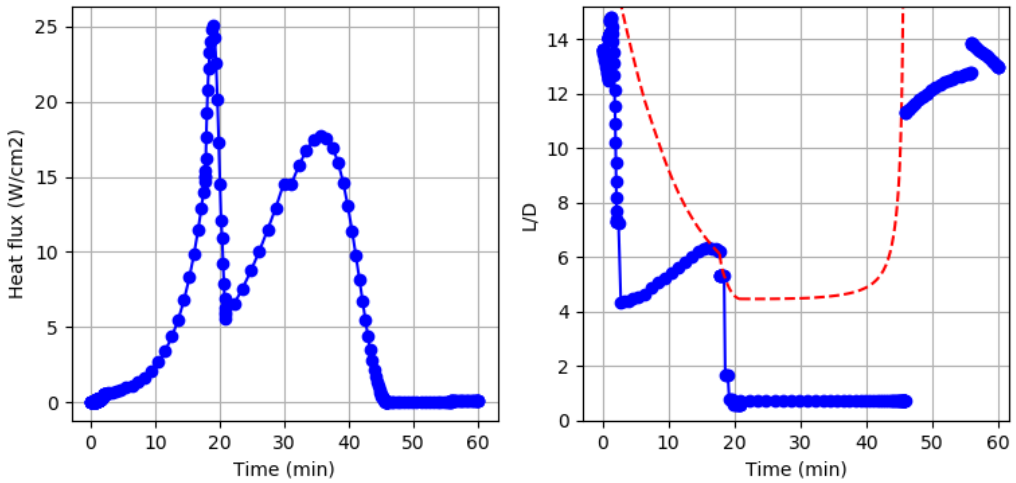


Figure 8.18: HMV-ARV optimized aerothermodynamic and aerodynamic distribution

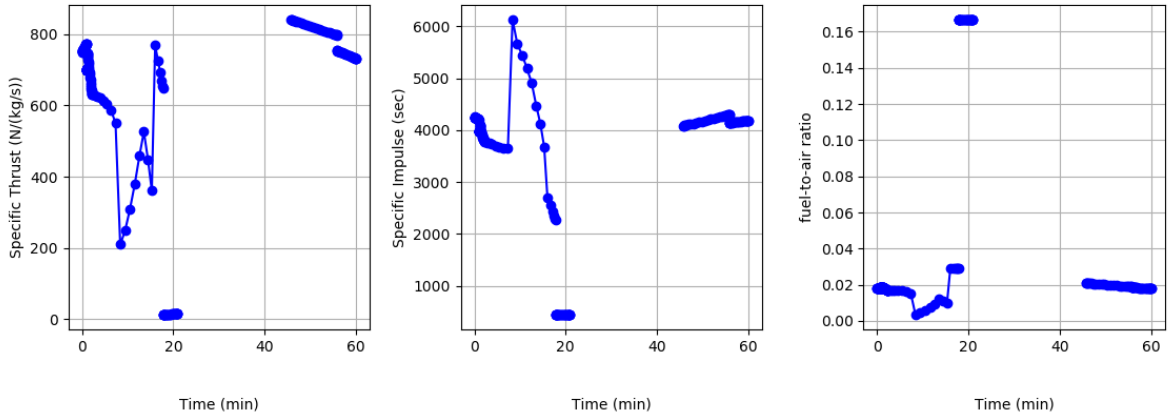


Figure 8.19: HMV-ARV optimized propulsion specific parameters

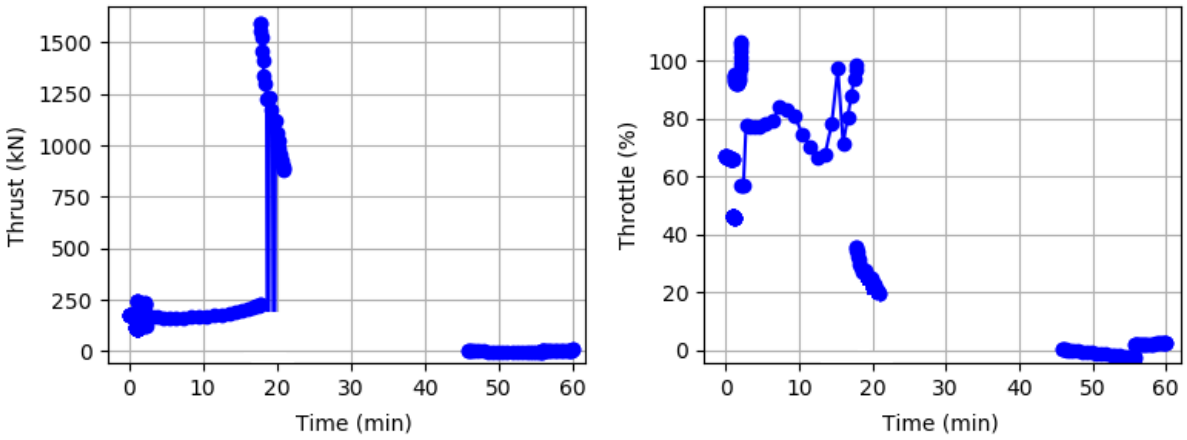


Figure 8.20: HMV-ARV optimized propulsion general parameters

## 8.4 Comparison

Relevant information from the HMV-CAV and HMV-ARV cases is compiled in Table 8.4, for both baseline and enhanced solutions.

The first thing worth mentioning is that range has increased as much as 30% for both enhanced solutions. This difference, which is only due to superior engine capabilities, demonstrates how important technology development is, particularly maintaining an efficient hypersonic combustion through a wide range of operating conditions. This ties back to the technology roadmap and highlights its relevance as a tool to track and assess technological progress.

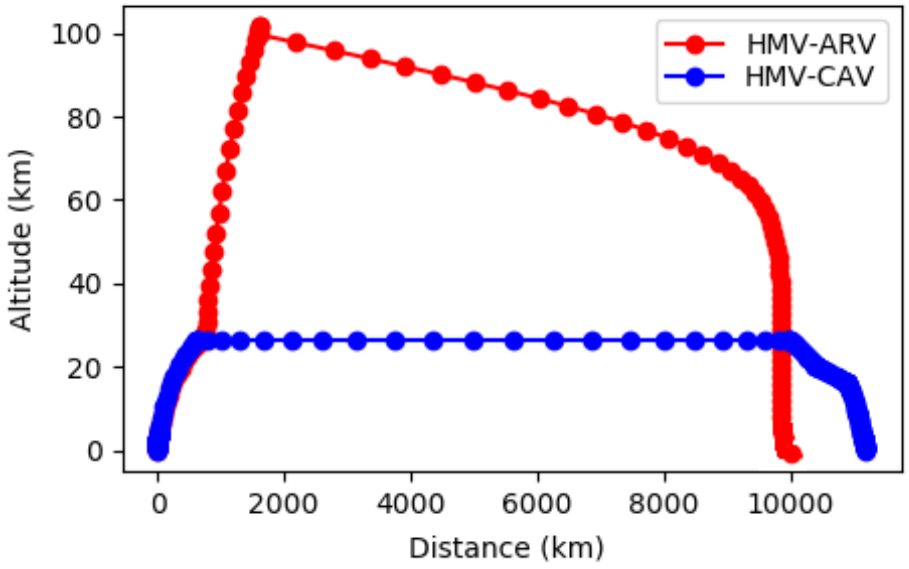


Figure 8.21: Range for enhanced solutions for HMV-CAV and HMV-ARV

The duration and range margins for both vehicles are also worth noting, particularly that of the HMV-ARV. In this case, the reentry profile demonstrates range sensitivity to any small performance gains whereas a change in flight duration is barely noticeable.

For the same fuel margin, any of the HMV-CAV simulations outclass their respective HMV-ARV counterpart when looking at range over duration; the range for the HMV-ARV is slightly shorter but time savings can go up as much as half the air-breathing cruise scenario. This is consistent with SpaceX's predictions for sub-orbital flight when applied to Earth-to-Earth transport [133], which coincidentally is one of the first applications for its future BFR rocket. However, one of the many issues of this concept is not only the safety concerns and lack of legislation for commercial activities, but also the extreme aerothermodynamic environment these vehicles endure. The heat load is considerably shorter but that is mainly because travel time has been almost cut down in half. Heat fluxes at the nose stagnation point can go as high as 173% that of the HMV-CAV, due to the extreme speeds during the final ascent. This corroborates the need for high-performance materials and TPS for the ARV scenario and justifies the current focus on UHTC and other technologies presented throughout the roadmap development.

Peak acceleration is also higher for the HMV-ARV during the final boost to sub-orbital flight, reaching up to 3.3 $g$. This is consistent with the maximum acceleration felt on the Space Shuttle, in both launch and reentry (approximately 3 $g$). The acceleration in the HMV-CAV is much more gradual and comparable to current regulatory compliances for the airline industry.

| Analysis | Range [km] | Duration [min] | Fuel margin | $a_{max}$ [$g$] | $q_{max}$ [$KPa$] | $q_{W_{max}}$ [$W/cm^2$] | $Q_W$ [$J/cm^2$] |
|---|---|---|---|---|---|---|---|
| HMV-CAV (base) | 8,839.0 | 125.4 | 2.732 | 0.28 | 61.9 | 16.01 | 104,515.6 |
| HMV-CAV (enhanced) | 11,188.3 | 158.6 | 2.678 | 0.28 | 61.9 | 16.01 | 120,433.0 |
| HMV-ARV (base) | 7,460.1 | 57.7 | 2.612 | 2.43 | 43.4 | 16.69 | 22,754.3 |
| HMV-ARV (enhanced) | 9,962.5 | 60.1 | 2.650 | 3.30 | 43.4 | 25.08 | 41,440.4 |

Table 8.4: Performance comparison

One should also notice that this is a low-fidelity analysis for a generic hypersonic vehicle and, for simplification purposes, the same vehicle design was applied to both use cases. This is an ideal scenario when in reality, there would need to be significant modifications in aircraft geometry and weight to improve its performance depending on the mission profile. This would in turn have an impact in aerodynamic and propulsion performance, a precondition that is not being considered here.

# Chapter 9

# Conclusions

## 9.1 Achievements

The main goal of this dissertation was contributing to hypersonic research. In that regard, a new hypersonic capability on a multi-fidelity analysis tool, SUAVE, was achieved and a new roadmap proposal detailing hypersonic enablers was provided. This thesis was structured to provide a funneled, linear path through hypersonics; firstly by identifying the technological barriers in hypersonic flight; secondly, by searching for a wide array of technologies to address critical requirements; thirdly by filtering plausible concepts for near-future application from the larger array and finally be demonstrating their feasibility in a preliminary design case.

The technology survey proved most useful in identifying and assessing various technological solutions in a multitude of technological areas: propulsion, aerodynamics, materials, thermal protection systems and control. To better understand if and how these new technologies could be incorporated in the future, a brief explanation for each one was presented and used to discuss their usefulness for a variety of hypersonic aircraft.

The proposed roadmap condenses the most relevant information in a single deliverable, showcasing all technologies sorted by technological area, possible future applications and expected timelines. This list is coupled with predictions and estimates for the delivery of actual hypersonic aircraft. The most valuable technologies are also highlighted based in carefully constructed arguments that try to justify their vote of confidence over others. This tool may prove its usefulness in the future as it filters through a vast number of hypersonic technologies and points towards a few deemed worth the attention. By including reference timelines associated with each one of them, the follow-up process is also facilitated.

This work also proved useful in contributing to the development of engineering tools for hypersonic applications. With a strong emphasis on propulsion, three new engine models were created, validated and uploaded to the SUAVE development team for future public access. This contribution was meaningful to the point of justifying a publication and subsequent presentation at the 2018 AIAA SciTech Conference on January 9, 2018, entitled ”Low fidelity models applied to the numerical investigation of hypersonic propulsion ”. Moreover, to complement the hypersonic analysis, a new model for weight dis-

tribution was also incorporated to better estimate aircraft weight when accounting for specific hypersonic requirements. Finally, a new reentry mission segment was created. All-in-all, SUAVE has now extended its design analysis capabilities into hypersonic flight and can provide estimates for aircraft requirements over a multitude of mission profiles.

The new numerical models were used to better understand how critical system subcomponents affect overall aircraft performance and to obtain an order of magnitude for the loads and requirements of hypersonic vehicles. Two test cases for a hypersonic air-breathing CAV-like vehicle and a ARV-like vehicle were designed to study the critical conditions each has to endure given their specific mission profiles, including thrust, fuel consumption, drag and load factors. For the HMV-CAV, the optimum design cruise point was selected based on climb dynamic pressure and cruise altitude, and the aircraft performance was displayed. However, because the engine was not sized correctly to produce the required thrust levels, combustion efficiencies were slightly modified to study their impact in the overall performance; this also establishes a connection with the technology roadmap as it highlights the importance of specific aircraft subsystems in overall performance. These test cases open the door for future studies on the impact of individual subsystems through many possible parametric studies.

## 9.2 Future Work

The roadmapping process is composed of three separate phases but only the first two (preliminary assessment and roadmap development) have been completed. The follow-up phase is responsible for tracking the technologies highlighted in this work as they mature; it is also tasked with identifying any new potential concepts that may disrupt the current roadmap. This is an iterative process that results in constant updates to the roadmap itself.

Developing tools for assessing aircraft performance is a complex, detailed process; in the case of SUAVE, this is done through individual modules which are then linked to the main system where all interdependencies are established. During the roadmap development phase, as the number of hypersonic technologies being tracked kept increasing, it became clear the shear scale of this project would make it impossible to efficiently condense a complete aircraft analysis from scratch into this dissertation. Therefore, some technological areas had to be prioritized over others and some concepts had to be purposefully kept out of the loop (propulsion and weight distribution were favored).

Considering what has been done so far, the next step is to create a set of tutorials for the SUAVE development team to publish on their forums, showcasing how the new numerical models work and how they can be incorporated in any analysis. However, since SUAVE is an open-source tool, it may be improved upon by updating the new models that have just been introduced. To provide an example, the scramjet model may be enhanced with an isolator to simulate shock trains and chemical equilibrium equations may also be added to more accurately predict the combustion temperatures. On the other hand, the rocket model can be further expanded to include other propellant combinations, using the Braeuning references. More comprehensive models can also be incorporated for the aerothermodynamic analysis, possibly providing heat distributions along the entire aircraft.

# Bibliography


[1] *Australia-UK: First non-stop flight arrives in London from Perth'*, British Broadcasting Company (BBC), 2018 (Retrieved May 10, 2018). URL http://www.bbc.com/news/world-australia-43530332.

[2] *Circus Billionaire Says Space Trip Worth Every Penny'*, Space.com, 2009 (Retrieved May 10, 2018). URL https://www.space.com/7375-circus-billionaire-space-trip-worth-penny.html.

[3] John D. Anderson. *Hypersonic and High Temperature Gas Dynamics*. American Institute of Aeronautics and Astronautics (AIAA), Reston, Virginia, US, 2006. ISBN 978-1-56347-780-5.

[4] *Records*, National Aeronautics Association (NAA), 2018 (Retrieved May 10, 2018). URL https://naa.aero/records.

[5] T. A. Barber. A Survey of Gaps, Obstacles, and Technical Challenges for Hypersonic Applications, Master's Thesis, University of Tennessee, 2012. URL http://trace.tennessee.edu/utk_gradthes/1131/.

[6] H. Besser, D. Göge, M. Huggins, and D. Zimper. Hypersonic vehicles: State-of-the-art and potential game changers for future warfare. pages 31–34, 2009.

[7] M. Silva. *Hypersonics tutorial. Class notes*.

[8] E. Hirschel. Historical Perspective on Programs, Vehicles and Technology Issues. Technical report, North Atlantic Treaty Organization (NATO), 2004.

[9] B. Perrett, B. Sweetman, and M. Fabey. U.S. Navy Sees Chinese HGV As Part Of Wider Threat. *Aviation Week Space Technology*, January 2014. URL http://aviationweek.com/awin/us-navy-sees-chinese-hgv-part-wider-threat.

[10] J. Steelant, A. Bond, A. Götz, K. Hannemann, C. Bruno, and J. Longo. LAPCAT I Publishable Final Activity Report. Technical Report April 2005, ESA-ESTEC, 2008.

[11] J. Steelant and T. Langener. The LAPCAT-MR2 hypersonic cruiser concept. *29th Congress of the International Council of the Aeronautical Sciences*, (September 2014), 2014.

[12] E. Blanvillain and G. Gallic. HIKARI : Paving the Way towards High Speed Air Transport. *20th AIAA International Space Planes and Hypersonic Systems and Technologies Conference*, (July), 2015.

[13] V. J. Bilardo, J. L. Hunt, N. T. Lovell, G. Maggio, A. W. Wilhite, L. E. McKinney, F. M. Curran, and J. L. Hunt. The benefits of hypersonic airbreathing launch systems for access to space. In *39Ih AIAA/ASMUSAE/ASEE Joint Propulsion Conference*, Huntsville, Alabama, 2003. ISBN 9781624100987. doi: doi:10.2514/6.2003-5265.

[14] D. Sziroczak and H. Smith. A review of design issues specific to hypersonic flight vehicles. *Progress in Aerospace Sciences*, 84(July), 2016. ISSN 03760421. doi: 10.1016/j.paerosci.2016.04.001.

[15] C. R. McClinton. High Speed / Hypersonic Aircraft Propulsion Technology Development. Technical report, North Atlantic Treaty Organization (NATO), 2008.

[16] E. Kulu. *Nanosatellite and Cubesat Database*, 2017 (Retrieved March 1, 2018). URL `http://www.nanosats.eu`.

[17] Commercial Market Assessment for Crew and Cargo Systems Pursuant to Section 403 of the NASA Authorization Act of 2010 ( P . L . 111-267 ) Table of Contents. 2010, 2011.

[18] G. Norris. *Skunk Works Reveals SR-71 Successor Plan*, 2013 (Retrieved February 12, 2018). URL `http://aviationweek.com/technology/skunk-works-reveals-sr-71-successor-plan`.

[19] T. Rogoway. *Boeing's Hypersonic Valkyrie will likely struggle to catch up with Lockheed's SR-72*, 2018 (Retrieved February 12, 2018). URL `http://www.thedrive.com/the-war-zone/18197/boeings-hypersonic-valkyrie-will-struggle-to-catch-up-with-lockheeds-sr-72`.

[20] E. L. H. C. Gurijanov and P. R. I. C. Harsha. AJAX - New directions in hypersonic technology. In *Space Plane and Hypersonic Systems and Technology Conference*, Norfolk, US, 1996. American Institute of Aeronautics and Astronautics (AIAA). doi: 10.2514/6.1996-4609.

[21] *NASA launches study for Skunk Works SR-72 concept'*, FlightGlobal.com . 2014 (Retrieved May 10, 2018). URL `https://www.flightglobal.com/news/articles/nasa-launches-study-for-skunk-works-sr-72-concept-407222/`.

[22] *What is the Russian Ayaks aircraft?*, North Atlantic Blog. 2015 (Retrieved May 10, 2018). URL `https://northatlanticblog.wordpress.com/2015/03/30/what-is-the-russian-ayaks-aircraft/`.

[23] M. Hempsell, R. Longstaff, and A. Bond. Skylon Users' Manual. Technical report, Reaction Engines Ltd, 2009.

[24] Falcon User's Guide. Technical report, SpaceX, 2015.

[25] *BAE invests in space engine firm Reaction Engines*, 2015 (Retrieved February 12, 2018). URL http://www.bbc.com/news/business-34694935.

[26] I. M. Blankson. NASA GRC Research in Aerospace Propulsion with Potential Collaboration Opportunities. Presentation for Great Midwestern Region Space Grant Consortia Meeting, Cleveland, Ohio, US, 2009.

[27] K. Kang. Zero Emission Hyper Sonic Transport: The Next Generation of Transportation. 2003.

[28] Reaction Engines Limited. LAPCAT A2 Facts and Figures. Technical report, Reaction Engines Limited, 2008.

[29] S. Nathan. *Your questions answered: Supersonic airliners*, 2015 (Retrieved May 10, 2018). URL https://www.theengineer.co.uk/issues/sept-2015-online/your-questions-answered-supersonic-airliners/.

[30] P. Borsky. Community reactions to sonic booms in the Oklahoma city area. Technical report, Federal Aviation Agency (FAA), 1965.

[31] Quiet Supersonic Technology X-Plane. Technical report, Lockheed Martin, 2018 (Retrieved March 5, 2018). URL https://www.lockheedmartin.com/en-us/products/quesst.html.

[32] R. S. Fry. A Century of Ramjet Propulsion Technology Evolution. *Journal of Propulsion and Power*, 20(1):27–58, 2004. ISSN 0748-4658. doi: 10.2514/1.9178.

[33] S. M. Johnson. Ultra High Temperature Ceramics Application: Issues and Prospects. In *2nd Ceramic Leadership Summit*, Baltimore, MD, US, 2011. URL http://ceramics.org/wp-content/uploads/2011/08/applicatons-uhtc-johnson.pdf.

[34] S. Kasen. *Thermal Management at Hypersonic Leading Edges*. PhD thesis, University of Virginia, May 2013.

[35] S. K. Bapanapalli. *Design of an integral thermal protection system for future space vehicless*. PhD thesis, University of Florida, 2007.

[36] David E. Glass. Hypersonic Materials and Structures. In *Society for the Advancement of Material and Process Engineering (SAMPE)*, Baltimore, MD, US, 2015.

[37] PICA heat shield. Technical report, SpaceX, 2013 (Retrieved February 12, 2018). URL http://www.spacex.com/news/2013/04/04/pica-heat-shield.

[38] D. Kwon. The Space Shuttle Thermal Protection System. - class notes, Massachusetts Institute of Technology 2005.

[39] A. P. Khokhlov and N. D. Malmuth. Low-frequency instability of hypersonic interactive boundary layers on a cooled surface. *Proceedings of the Royal Society of London A: Mathematical, Physical and Engineering Sciences*, 455(1985):1887–1921, 1999. ISSN 1364-5021. doi: 10.1098/rspa.1999.0385.

[40] W. P. Nelms and C. L. Thomas. Aerodynamic characteristics of an all-body hypersonic aircraft configuration at mach numbers from 0.65 to 10.6. Technical report, National Aeronautics and Space Administration (NASA), 1971.

[41] B. Xu and Z. Shi. An overview on flight dynamics and control approaches for hypersonic vehicles. *Science China Information Sciences*, 58(7):1–19, 2015. ISSN 1674-733X. doi: 10.1007/s11432-014-5273-7. URL http://link.springer.com/10.1007/s11432-014-5273-7.

[42] Largest spacecraft to orbit and land unmanned. Technical report, Guiness World Records, 2018 (Retrieved April 23, 2018). URL http://www.guinnessworldrecords.com/world-records/largest-spacecraft-to-orbit-and-land-unmanned.

[43] X-51A Waverider. Technical report, United States Air Force, 2011 (Retrieved February 18, 2018). URL http://www.af.mil/About-Us/Fact-Sheets/Display/Article/104467/x-51a-waverider/.

[44] *IXV (Intermediate eXperimental Vehicle)*. European Space Agency, 2018 (Retrieved February 20, 2018). URL https://directory.eoportal.org/web/eoportal/satellite-missions/i/ixv.

[45] F.-S. Gady. *China Tests New Weapon Capable of Breaching US Missile Defense Systems*, 2016 (Retrieved February 20, 2018). URL https://thediplomat.com/2016/04/china-tests-new-weapon-capable-of-breaching-u-s-missile-defense-systems/.

[46] A. Panda. *Introducing the DF-17: China's Newly Tested Ballistic Missile Armed With a Hypersonic Glide Vehicle*, 2017 (Retrieved February 20, 2018). URL https://thediplomat.com/2017/12/introducing-the-df-17-chinas-newly-tested-ballistic-missile-armed-with-\a-hypersonic-glide-vehicle/.

[47] *Russia 'test-fires hypersonic Kinzhal missile'*, British Broadcasting Company (BBC), 2018 (Retrieved March 10, 2018). URL http://www.bbc.com/news/world-europe-43362213.

[48] Technology Roadmaps - What Value for PSMC? Technical report, Defense Logistics Agency, 2013. URL http://www.dla.mil/Portals/104/Documents/LandAndMaritime/V/VA/PSMC/Nov13/LM_TechRoadmap_151030.pdf.

[49] ISO 16290:2013: Space systems — Definition of the Technology Readiness Levels (TRLs) and their criteria of assessment. Standard, International Organization for Standardization, 2013. URL https://www.iso.org/standard/56064.html.

[50] C. L. Clay. US Air Force Hypersonic Science and Technology. Technical report, United States Air Force (USAF), 2012.

[51] L. Serre. Overview of Hypersonics in Europe. In *17th AIAA International Space Planes and Hypersonic Systems and Technologies Conference*, 2012.

[52] D. Glass. Ceramic Matrix Composite (CMC) Thermal Protection Systems (TPS) and Hot Structures for Hypersonic Vehicles. In *15th AIAA International Space Planes and Hypersonic Systems and Technologies Conference*, pages 1–36, Dayton, Ohio, US, 2008. ISBN 978-1-60086-985-3. doi: 10.2514/6.2008-2682.

[53] G. Choubey, L. Suneetha, and K. M. Pandey. Composite materials used in Scramjet- A Review. *Materials Today: Proceedings*, 2018. ISSN 2214-7853. doi: 10.1016/j.matpr.2017.11.217.

[54] D. Liu and Y. Liu. Heat transfer capability simulation of high-temperature heat pipe in supersonic vehicle leading edge applications. *Advances in Mechanical Engineering*, 8(4):1–10, 2016. ISSN 16878140. doi: 10.1177/1687814016644375.

[55] *BRAHMOS Supersonic Cruise Missile*. BrahMos Aerospace, 2013 (Retrieved February 2, 2018). URL `http://www.brahmos.com/content.php?id=10&sid=10`.

[56] Y. T. Shao, M. Liu, and J. P. Wang. Numerical investigation of rotating detonation engine propulsive performance. *Combustion Science and Technology*, 182(11-12):1586–1597, 2010. ISSN 00102202. doi: 10.1080/00102202.2010.497316.

[57] F. Falempin. Continuous Detonation Wave Engine. *Advances on Propulsion Technology for High-Speed Aircraft*, 2008. ISSN 0820-3946.

[58] F. A. Bykovskii, S. A. Zhdan, and E. F. Vedernikov. Continuous Spin Detonations. *Journal of Propulsion and Power*, 22(6):1204–1216, 2006. ISSN 0748-4658. doi: 10.2514/1.17656.

[59] F. Falempin and E. Daniau. A Contribution to the Development of Actual Continuous Detonation Wave Engine. In *15th AIAA International Space Planes and Hypersonic Systems and Technologies Conference*, Dayton, Ohio, US, 2008. ISBN 978-1-60086-985-3. doi: 10.2514/6.2008-2679.

[60] F. K. Lu and E. M. Braun. Rotating Detonation Wave Propulsion: Experimental Challenges, Modeling, and Engine Concepts. *Journal of Propulsion and Power*, 30(5):1125–1142, 2014. ISSN 0748-4658. doi: 10.2514/1.B34802.

[61] M. Bulman and A. Siebenhaar. Combined Cycle Propulsion: Aerojet Innovations for Practical Hypersonic Vehicles. In *17th AIAA International Space Planes and Hypersonic Systems and Technologies Conference*, San Francisco, California, US, 2011. ISBN 978-1-60086-942-6. doi: 10.2514/6.2011-2397.

[62] L. Wenhui. *A Novel Turbo-aided Rocket-augmented Ramj et Combined Cycle Engine Concept*. Beijing Power Machinery Research Institute, Science and Technology on Scramjet Laboratory, 2015.

[63] G. Norris. *Aerojet Unveils TriJet For Reusable Hypersonic Power*. Aviation Week, 2011 (Retrieved February 7, 2018). URL `http://aviationweek.com/awin/aerojet-unveils-trijet-reusable-hypersonic-power`.

[64] R. J. Litchford, J. W. Cole, V. A. Bityurin, and J. T. Lineberry. Thermodynamic Hypersonic Cycle Analysis Engines of Airbreathing. Technical report, National Aeronautics and Space Administration (NASA), 2000.

[65] I. Blankson and S. Schneider. The MHD-controlled turbojet engine: an alternate powerplant for access to space. Workshop presentation, National Aeronautics and Space Administration (NASA), 2014.

[66] T. L. Benyo. The Effect of MHD Energy Bypass on Specific Thrust for a Supersonic Turbojet Engine. Technical report, National Aeronautics and Space Administration (NASA), 2010. URL `https://ntrs.nasa.gov/archive/nasa/casi.ntrs.nasa.gov/20110002743.pdf`.

[67] E. Gurijanov and P. Harsha. AJAX - New directions in hypersonic technology. In *International Space Planes and Hypersonic Systems and Technologies Conferences*. American Institute of Aeronautics and Astronautics (AIAA), 1996. doi: doi:10.2514/6.1996-4609.

[68] H. Kobayashi, H. Taguchi, T. Kojima, and T. Sato. Performance analysis of Mach 5 hypersonic turbojet developed in JAXA. In *18th AIAA/3AF International Space Planes and Hypersonic Systems and Technologies Conference*, Tours, France, 2012. American Institute of Aeronautics and Astronautics (AIAA). ISBN 978-1-60086-931-0. doi: 10.2514/6.2012-5839.

[69] J. L. Sloop. Liquid Hydrogen as a Propulsion Fuel, 1945-1959. In *US National Aeronautics and Space Administration History Series*. National Aeronautics and Space Administration (NASA), 1978. ISBN 1530123526.

[70] T. A. Heppenheimer. *Facing the Heat Barrier : A History of Hypersonics*. National Aeronautics and Space Administration (NASA), Washington D.C., US, 2007. ISBN 1493692569.

[71] T. Kojima, H. Taguchi, T. Aoki, T. Sato, N. Tanatsugu, J. Tomike, and H. Kobayashi. Development Study of the Air-Intake of the ATREX Engine. *12th AIAA International Space Planes and Hypersonic Systems and Technologies*, 47(11):799–808, 2003. ISSN 00945765. doi: 10.2514/6.2003-7042.

[72] H. Taguchi, H. Kobayashi, T. Kojima, M. Hongoh, D. Masaki, and S. Nishida. Performance Evaluation of Hypersonic Pre-Cooled Turbojet Engine. In *20th AIAA International Space Planes and Hypersonic Systems and Technologies Conference*, Glasgow, Scotland, United Kingdom, 2015. American Institute of Aeronautics and Astronautics (AIAA). ISBN 978-1-62410-320-9. doi: 10.2514/6.2015-3593.

[73] U. B. Mehta, M. J. Aftosmis, J. V. Bowles, and S. A. Pandya. Skylon Aerodynamics and SABRE Plumes. In *20th AIAA International Space Planes and Hypersonic Systems and Technologies Conference*, Glasgow, Scotland, United Kingdom, 2015. American Institute of Aeronautics and Astronautics (AIAA). ISBN 978-1-62410-320-9. doi: 10.2514/6.2015-3605.

[74] Z. G. Wang, Y. Wang, J. Q. Zhang, and B. C. Zhang. Overview of the key technologies of combined cycle engine precooling systems and the advanced applications of micro-channel heat transfer. *Aerospace Science and Technology*, 39:31–39, 2014. ISSN 12709638. doi: 10.1016/j.ast.2014.08.008.

[75] M. Hempsell. Progress on SKYLON and SABRE. *Proceedings of the International Astronautical Congress, IAC*, 2013. ISSN 00741795.

[76] C. Black. *Revolutionary rocket engine passes U.S. Air Force feasibility test*, 2015 (Retrieved February 5, 2018). URL http://sen.com/news/revolutionary-rocket-engine-passes-u-s-air-force-feasibility-test.

[77] G. Norris. *Reaction Begins Building U.S. Hypersonic Engine Test Site*. Aviation Week, 2017 (Retrieved February 5, 2018). URL http://aviationweek.com/space/reaction-begins-building-us-hypersonic-engine-test-site.

[78] W. G. Fahrenholtz and G. E. Hilmas. Ultra-high temperature ceramics: Materials for extreme environments. *Scripta Materialia*, 129:94–99, 2017. ISSN 13596462. doi: 10.1016/j.scriptamat.2016.10.018.

[79] R. Loehman, E. Corral, H. Dumm, P. Kotula, and R. Tandon. Ultra high temperature ceramics for hypersonic vehicle applications. Technical report, Sandia National Laboratories, Albuquerque, New Mexico, US, 2006. URL https://www.osti.gov/biblio/887260.

[80] Z. Huda and P. Edi. Materials selection in design of structures and engines of supersonic aircrafts: A review. *Materials and Design*, 46:552–560, 2013. ISSN 02641275. doi: 10.1016/j.matdes.2012.10.001.

[81] *High Temperature Materials for Hypersonic Flight Vehicles*. The Australian Defence Force Academy, 2007. URL http://seit.unsw.adfa.edu.au/ojs/index.php/hypersonics/article/viewFile/21/12.

[82] K. S. Kim, M. B. Jakubinek, Y. Martinez-Rubi, B. Ashrafi, J. Guan, K. O'Neill, M. Plunkett, A. Hrdina, S. Lin, S. Dénommée, C. Kingston, and B. Simard. Polymer nanocomposites from free-standing, macroscopic boron nitride nanotube assemblies. *RSC Advances*, 5(51):41186–41192, 2015. ISSN 2046-2069. doi: 10.1039/C5RA02988K. URL http://xlink.rsc.org/?DOI=C5RA02988K.

[83] S. M. Johnson. *Coatings and Surface Treatments for Reusable Entry Systems*. Presentation for the Interagency Coordinating Committee on Ceramics Research and Development (ICCCRD). National Aeronautics and Space Administration (NASA), 2016.

[84] *Toughened Uni-piece Fibrous Reinforced Oxidation-Resistant Composite*. National Aeronautics and Space Administration (NASA), 2015 (Retrieved February 1, 2018. URL https://www.nasa.gov/ames-partnerships/technology/toughened-uni-piece-fibrous-reinforced-oxidation-resistant-composite.

[85] *Thermacore offers first heat pipe assembly for operational prototypes after passing NASA Ames hypersonic tests*. Thermacore, 2014 (Retrieved February 1, 2018). URL https://www.thermacore.com/news/nasa-ames-arc-jet-complex.aspx.

[86] *Structurally Integrated Thermal Protection System*. National Aeronautics and Space Administration (NASA), 2017 (Retrieved February 1, 2018). URL https://www.nasa.gov/feature/hypersonics-and-space-technologies.

[87] K. M. Hanquist, K. Hara, and I. D. Boyd. Detailed modeling of electron emission for transpiration cooling of hypersonic vehicles. *Journal of Applied Physics*, 121(5), 2017. ISSN 10897550. doi: 10.1063/1.4974961.

[88] K. Daryabeigi, G. R. Cunnington, S. D. Miller, J. R. Knutson, A. Engineer, S. Mechanics, C. Branch, S. D. Miller, E. E. Technician, S. Integration, and T. Branch. Combined Heat Transfer in High-Porosity High-. In *10th AIAA/ASME Joint Thermophysics and Heat Transfer Conference*, Chicago, Illinois, US, 2010. American Institute of Aeronautics and Astronautics (AIAA). doi: 10.2514/6.2010-4660.

[89] S. Weiland and K. Daryabeigi. Thermal Testing and Analysis of an Efficient High-Temperature Multi-screen Internal Insulation. In *29th International Thermal Conductivity Conference*, Birmingham, Alabama, US, 2007. URL https://ntrs.nasa.gov/archive/nasa/casi.ntrs.nasa.gov/20070030254.pdf.

[90] K. Cui, Y. Xiao, Y. Z. Xu, and G. L. Li. Hypersonic I-shaped aerodynamic configurations. *Science China: Physics, Mechanics and Astronomy*, 61(2):2017–2019, 2018. ISSN 18691927. doi: 10.1007/s11433-017-9117-8.

[91] Y. Sun and H. Smith. Review and prospect of supersonic business jet design. *Progress in Aerospace Sciences*, 90(September 2017):12–38, 2017. ISSN 03760421. doi: 10.1016/j.paerosci.2016.12.003.

[92] M. Mirmirani, C. Wu, A. Clark, S. Choi, and B. Fidan. Airbreathing Hypersonic Flight Vehicle Modeling and Control, Review, Challenges, and a CFD-Based Example. In *Workshop on Modeling and Control of Complex Systems*, Ayia Napa, Cyprus, 2005. URL http://www.academia.edu/21312619/Airbreathing_hypersonic_flight_vehicle_modeling_and_control_review_challenges_and_a_CFD-based_example.

[93] D. R. Reddy and G. Schmidt. State of the NASA Aeropropulsion Discipline Input from the Glenn Research Center GRC Propulsion Division Main Thrust Areas. In *NESC Propulsion Technical Discipline Team (TDT) Face-to-Face Meeting*, Huntsville, Alabama, US, 2017.

[94] *Space Technology Roadmaps*. National Research Council, 2010 (Retrieved March 12, 2018). URL https://www.nap.edu/read/13354/chapter/1.

[95] P. K. McConnaughey, M. G. Femminineo, S. J. Koelfgen, R. A. Lepsch, R. M. Ryan, and S. A. Taylor. NASA'S LAUNCH PROPULSION SYSTEMS TECHNOLOGY ROADMAP. Technical report, National Aeronautics and Space Administration (NASA), 2017.

[96] G. Norris. *China Reveals Key Test Progress On Hypersonic Combined-Cycle Engine*, 2017 (Retrieved March 21, 2018). URL http://aviationweek.com/technology/china-reveals-key-test-progress-hypersonic-combined-cycle-engine.

[97] D. Thisdell. *British engineers 'crack secret of reusable spaceplane'*, 2012 (Retrieved March 21, 2018). URL https://www.flightglobal.com/news/articles/in-focus-british-engineers-crack-secret-of-reusab-379609/e.

[98] D. T. Ishikawa. *The future of environmentally friendly aviation technology: clean engines and supersonic transport*, 2003 (Retrieved May 1, 2018). URL http://global.jaxa.jp/article/special/aviation/ishikawa02_e.html.

[99] Melissa Eichner (Energetics Incorporated) and David W. Richerson (Richerson and Associates). Advanced Ceramics Technology Roadmap - charting our course. Technical report, 2000.

[100] T. Sharp. *SpaceShipOne: The First Private Spacecraft*. Space.com.

[101] L. Schweikart. The Quest for the Orbital Jet: The National Aero-Space Plane Program (1983-1995). Technical report, United States Air Force (USAF), 1998. URL http://www.dtic.mil/get-tr-doc/pdf?Location=U2{&}doc=GetTRDoc.pdf{&}AD=ADA441126.

[102] D. R. Jenkins, T. Landis, and J. Miller. *American X-Vehicles: An Inventory X-1 to X-50 Centennial of Flight Edition*. Number 31. CreateSpace Independent Publishing Platform, 2003. ISBN 1478233583.

[103] E. M. Botero, A. Wendorff, T. MacDonald, A. Variyar, J. M. Vegh, T. W. Lukaczyk, J. J. Alonso, T. H. Orra, and C. Ilario da Silva. SUAVE: An Open-Source Environment for Conceptual Vehicle Design and Optimization. *54th AIAA Aerospace Sciences Meeting*, pages 1–16, 2016. doi: 10.2514/6.2016-1275.

[104] T. MacDonald, E. Botero, J. M. Vegh, A. Variyar, J. J. Alonso, T. H. Orra, and C. R. Ilario da Silva. SUAVE: An Open-Source Environment Enabling Unconventional Vehicle Designs through Higher Fidelity. *55th AIAA Aerospace Sciences Meeting*, pages 1–14, 2017. doi: 10.2514/6.2017-0234. URL http://arc.aiaa.org/doi/10.2514/6.2017-0234.

[105] T. MacDonald, M. Clarke, E. M. Botero, J. M. Vegh, and J. J. Alonso. SUAVE: An Open-Source Environment Enabling Multi-Fidelity Vehicle Optimization. *18th AIAA/ISSMO Multidisciplinary Analysis and Optimization Conference*, pages 1–14, 2017. doi: 10.2514/6.2017-4437. URL https://arc.aiaa.org/doi/10.2514/6.2017-4437.

[106] A. J. Chaput, S. Rizo-patron, E. Mechanics, C. A. Design, F. A. Method, G. U. Interface, P. Computer, U. A. Vehicle, V. S. Pad, A. J. Chaput, S. Lecturer, E. Mechanics, S. Rizo-patron, E. Mechanics, and S. Member. Vehicle Sketch Pad Structural Analysis Module Enhancements for Wing Design. In *50th AIAA Aerospace Sciences Meeting including the New Horizons Forum and Aerospace Exposition*. American Institute of Aeronautics and Astronautics (AIAA), 2012.

[107] Embraer 190 weights. Technical report, Embraer, 2014 (Retrieved February 1, 2018). URL http://www.embraercommercialaviation.com/AircraftPDF/E190{_}Weights.pdf.

[108] G. J. Harloff and B. M. Berkowitz. Hypersonic aerospace sizing analysis for the preliminary design of aerospace vehicles. *Journal of Aircraft*, 27(2):97–98, 1990. ISSN 0021-8669. doi: 10.2514/3.45903.

[109] B. J. Cantwell. AA283: Aircraft and Rocket Propulsion. Stanford university class material, Stanford University, California, US, 2007.

[110] E. T. Currant. THE USE OF STREAM THRUST CONCEPTS FOR THE APPROXIMATE EVALUATION OF HYPERSONIC RAMJET ENGINE PERFORMANCE. Technical Report October, Air Force Aero Propulsion Laboratory, Ohio, USA, 1973.

[111] *Ideal Rocket Theory (part 1)*. Delft University, Retrieved February 19, 2018). URL https://ocw.tudelft.nl/wp-content/uploads/2.1.3-Ideal-Rocket-Theory-part-1.pdf.

[112] M. Pouliquen. Systemes propulsifs a propergols liquides. Technical report, SNECMA, 1999-200.

[113] R. A. Braeunig. *Liquid Oxygen and Liquid Hydrogen*, 2009 (Retrieved January 5, 2018). URL http://www.braeunig.us/space/index.htm.

[114] P. Hays. *How The Ramjet Engine Works*, 2017 (Retrieved October 21, 2017). URL http://www.okieboat.com/How%20the%20ramjet%20works.html.

[115] J. Seitzman. *Rayleigh Flow - Thermodynamics*. Georgia Tech College of Engineering, 2001 (Retrieved October 17, 2017). URL http://seitzman.gatech.edu/classes/ae3450/rayleighflow_two.pdf.

[116] I. K. Pate. Presentation on Scramjet Engines. Presentation, University Gurgaon, 2015.

[117] W. H. Heiser and D. T. Pratt. *Hypersonic Air-Breathing Propulsion*. American Institute of Aeronautics and Astronautics, Inc.,, 1994. ISBN 1-56347-035-7. doi: 10.2514/5.9781600867774.0051.0074.

[118] D. L. Akin. Lifting Entry. Technical report, University of Maryland, 2016 (Retrieved January 23, 2018). URL http://spacecraft.ssl.umd.edu/academics/791S16/791S16L06.lifting_entryx.pdf.

[119] R. S. Ilan Kroo. *Aircraft Design: Synthesis and Analysis*. Desktop Aeronautics, Inc., 2001.

[120] C. R. Glatt. WAATS - A computer program for weights analysis of adanced transportation systems. Technical report, National Aeronautics and Space Administration (NASA), Washington, United States, 1974. URL https://ntrs.nasa.gov/archive/nasa/casi.ntrs.nasa.gov/19740027176.pdf.

[121] C. Rothmund (SNECMA). Liquid Rocket Propulsion. Presentation, Università di Roma, 2011.

[122] *Delta IV Launch Services User's Guide*. United Launch Alliance (ULA), 2014 (Retrieved May 10, 2018). URL https://web.archive.org/web/20140710005717/http://www.ulalaunch.com/uploads/docs/Launch_Vehicles/Delta_IV_Users_Guide_June_2013.pdf.

[123] *LE-7A*. Encyclopedia Astronautica, 2002 (Retrieved May 10, 2018). URL https://web.archive.org/web/20021018023043/http://www.astronautix.com/engines/le7a.htm.

[124] *RD-0120*. Encyclopedia Astronautica, 2007 (Retrieved May 10, 2018). URL https://web.archive.org/web/20071203201403/http://www.astronautix.com/engines/rd0120.htm.

[125] J. L. Ross. A fuel data standardization study for JP-4, JP-5, JP-7 and RJ-5 combusted in air. Technical report, Air Force Aero Propulsion Laboratory, Wright-Patterson Air Force Base, Ohio, 1974.

[126] N. S. Chauhan and V. K. Singh. Fundamentals and Use of Hydrogen as a Fuel. *ISST Journal of Mechanical Engineering*, 6(1):63–68, 2015.

[127] K. Tran. *One Dimensional Analysis Program for Scramjet and Ramjet Flowpaths*. PhD thesis, Virginia Polytechnic Institute and State University, 2010. URL https://vtechworks.lib.vt.edu/bitstream/handle/10919/30857/Tran_KN_T_2010_Copyright.pdf.

[128] P. Blau. *IXV - Intermediate Experimental Vehicled*, 2015 (Retrieved April 8, 2018). URL http://www.spaceflight101.net/ixv.html.

[129] A. Ferrero. Calculation and Optimization of Aerodynamic Coefficients for Launchers and Reentry Vehicles. Master's thesis, Instituto Superior Técnico, 2014. URL https://fenix.tecnico.ulisboa.pt/downloadFile/281870113701956/Tese_MSc_AlbertoFerrero.pdf.

[130] F. Buffenoir, T. Pichon, and R. Barreteau. IXV Thermal Protection System Post-Flight Preliminary analysis. In *7th European Conference for Aeronautics and Space Sciences (EUCASS)*, pages 1–7, Milan, Italy, 2017. European Conference for Aeronautics and Space Sciences. doi: 10.13009/EUCASS2017-330.

[131] *Hypersonic Vehicle Design*. Aerospaceweb.org, 2012 (Retrieved February 10, 2018). URL http://www.aerospaceweb.org/design/waverider/design.shtml.

[132] D. F. G. Rault. Aerodynamics of the Shuttle Orbiter at High Altitudes. *Journal of Spacecraft and Rockets*, 31(6), 1994. ISSN 00224650. doi: 10.2514/3.26542.

[133] T. Malik. *Elon Musk Says SpaceX's Giant Mars Rocket Could Fly Passengers Around Earth*. Space.com, 2017 (Retrieved May 10, 2018). URL https://www.space.com/38314-elon-musk-spacex-mars-rocket-earth-travel.html.

[134] *Technology Readiness Level*. National Aeronautics and Space Administration (NASA), 2012 (Retrieved February 18, 2018). URL https://www.nasa.gov/directorates/heo/scan/engineering/technology/txt_accordion1.html.

# Appendix A

# Roadmap auxiliary documentation

## A.1 Technology Readiness Level scale

Figure A.1 describes the Technology Readiness Level scale model created by NASA, adopted by ESA and used as reference for this work.

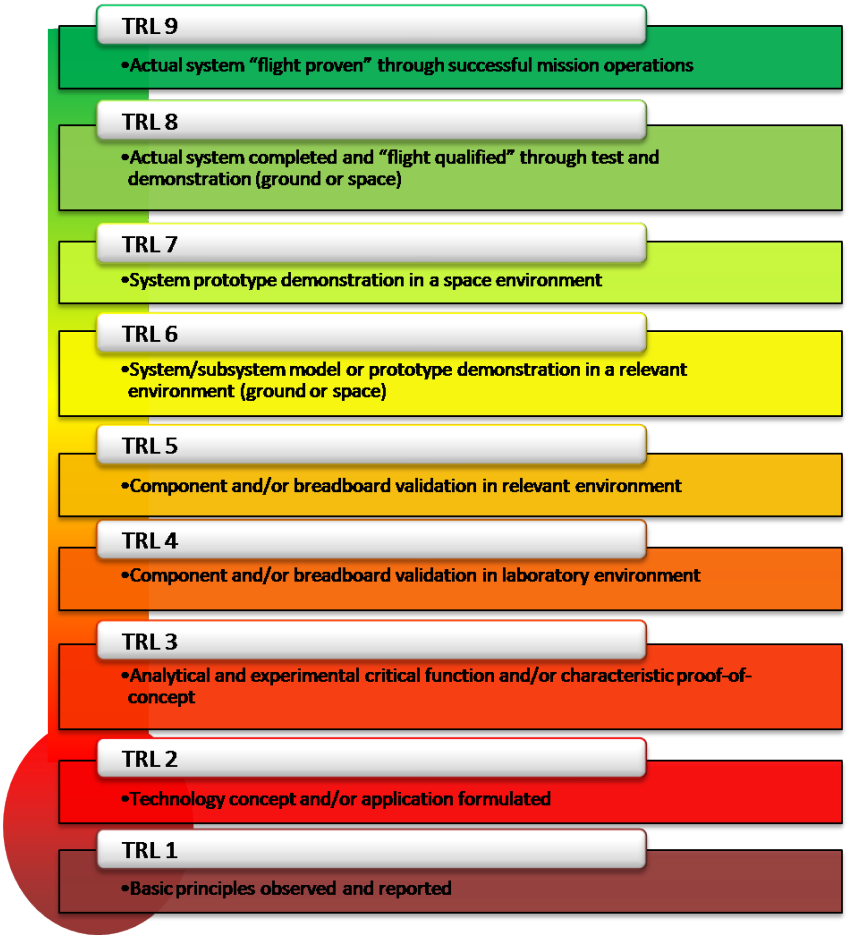


Figure A.1: Technology Readiness Level scale [134]

## A.2 World distribution of major R&D activities

Figure A.2 displays major R&D centers in the world. The list is obviously incomplete but it gathers all the R&D activities mentioned in this work. The marker color code is used to distinguish the nature of the research: red for government/state facilities, blue for military facilities, green for private companies and yellow for universities. This information is stored in Google Fusion Tables, a web service provided by Google for data management. As such, it is instantly accessible and can be easily updated (`https://fusiontables.google.com/DataSource?docid=1Ladk5iN1jcLuMqbY_Gjvc3Txb7q_ta94luaitV00`)

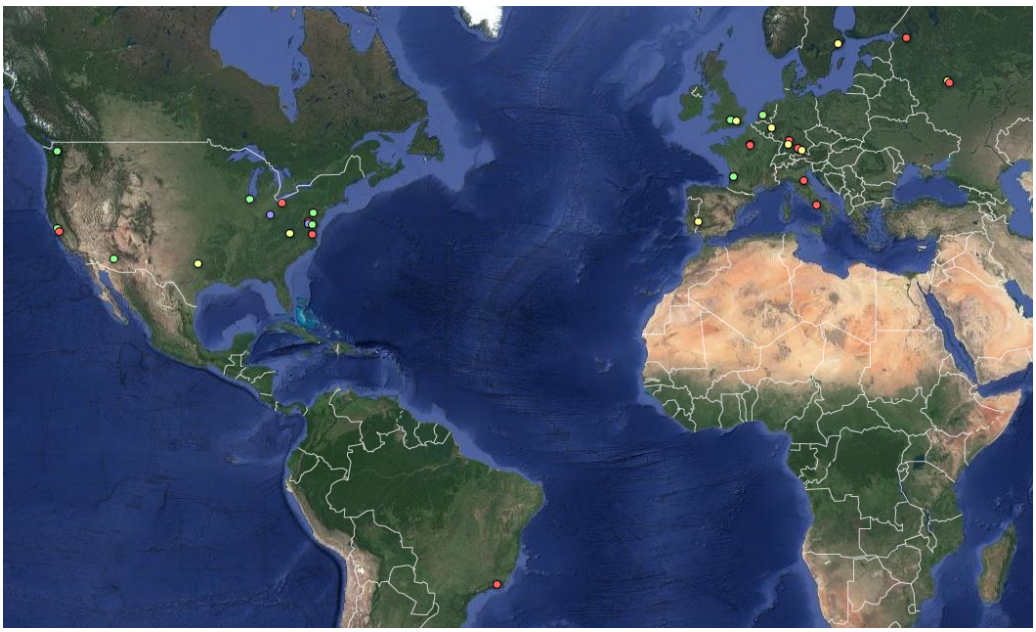

(a) America and Europe

(b) Asia

Figure A.2: Major R&D focus centers

# Appendix B

# Numerical models auxiliary notes

## B.1 HASA equations

**Body weight estimate**

$$W_b = 0.341 \cdot mf \cdot \left(\frac{L_b \cdot n_{ult}}{D_{be}}\right)^{0.15} \cdot {q_{max}}^{0.16} \cdot {S_{btot}}^{1.05} \tag{B.1}$$

**Wing weight estimate**

$$W_b = 0.2958 \cdot mf \cdot \left[\left(\frac{EW \cdot n_{ult}}{1000}\right)^{0.52} \cdot {S_{ref}}^{0.7} \cdot AR^{0.47} \cdot \left(\frac{1+\lambda}{t/c}\right)^{0.4} \cdot \left(3 + \frac{0.7}{\cos(\lambda_{1/2})}\right)\right]^{1.017} \tag{B.2}$$

**Tail weight estimate**

$$W_{vt} = 5.0 \cdot {S_{w_{vt}}}^{1.09} \tag{B.3}$$

**TPS weight estimate**

$$W_{tps} = W_{ins} \cdot (S_{tb} + S_{ref}) \tag{B.4}$$

**Landing gear weight estimate**

$$W_{gear} = 0.00916 \cdot GTOW^{1.124} \tag{B.5}$$

**Thrust structure weight estimate**

$$W_{thrust_{rk}} 0.0025 F_{rk_{total}} \tag{B.6}$$

**Scramjet weight estimate**

$$W_sj = N_{eng}(87.5 \cdot H_{sj} - 850.0) \tag{B.7}$$

## B.2 Isentropic relations

$$\frac{T_t}{T} = 1 + \frac{\gamma - 1}{2} M^2 \tag{B.8}$$

$$\frac{p_t}{p} = \left(1 + \frac{\gamma - 1}{2} M^2\right)^{\gamma/(\gamma-1)} \tag{B.9}$$

$$\frac{\rho_t}{\rho} = \left(1 + \frac{\gamma - 1}{2} M^2\right)^{1/(\gamma-1)} \tag{B.10}$$

$$\frac{A_t}{A} = \left(\frac{\gamma + 1}{2}\right)^{\frac{\gamma+1}{2(\gamma-1)}} \cdot \left[\left(1 + \frac{\gamma + 1}{2} M^2\right)^{-\frac{\gamma+1}{2(\gamma-1)}}\right] \cdot \frac{1}{M} \tag{B.11}$$

## B.3 LOX/LH2 rocket model polynomials

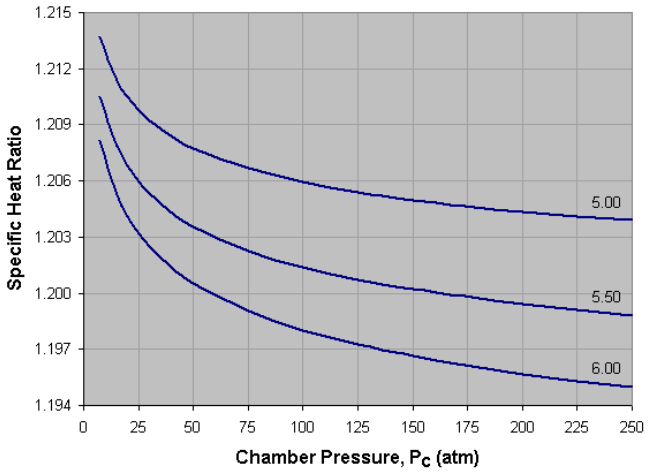


Figure B.1: Specific heat ratio vs. chamber pressure [113]

| | Basic equation form $Az^6 + Bz^5 + Cz^4 + Dz^3 + Ez^2 + Fz + G$ | | | | | | |
|---|---|---|---|---|---|---|---|
| | A | B | C | D | E | F | G |
| $O/F$ = 5.00 | 9.666E-16 | -8.598E-13 | 3.068E-10 | -5.641E-08 | 5.772E-06 | -3.448E-04 | 1.216E+00 |
| $O/F$ = 5.50 | 1.733E-15 | -1.478E-12 | 5.012E-10 | -8.649E-06 | 8.144E-06 | -4.360E-04 | 1.213E+00 |
| $O/F$ = 6.00 | 2.142E-15 | -1.787E-12 | 5.928E-10 | -1.000E-07 | 9.197E-06 | -4.835E-04 | 1.211E+00 |

Table B.1: 6th order polynomials obtained for specific heat ratio as a function of chamber pressure

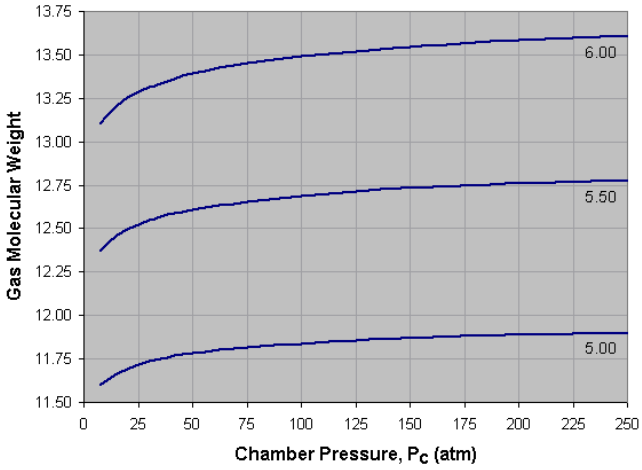


Figure B.2: Gas molecular weight vs. chamber pressure [113]

| | Basic equation form $Az^6 + Bz^5 + Cz^4 + Dz^3 + Ez^2 + Fz + G$ | | | | | | |
|---|---|---|---|---|---|---|---|
| | A | B | C | D | E | F | G |
| $O/F$ = 5.00 | -1.923E-14 | 1.808E-11 | -6.941E-09 | 1.396E-06 | -1.590E-04 | 1.105E-02 | 1.313E+01 |
| $O/F$ = 5.50 | -4.133E-14 | 3.502E-11 | -1.175E-08 | 1.996E-06 | -1.858E-04 | 1.044E-02 | 1.238E+01 |
| $O/F$ = 6.00 | 2.142E-15 | -1.787E-12 | 5.928E-10 | -1.000E-07 | 9.197E-06 | -4.835E-04 | 1.211E+00 |

Table B.2: 6th order polynomials obtained for gas molecular weight as a function of chamber pressure

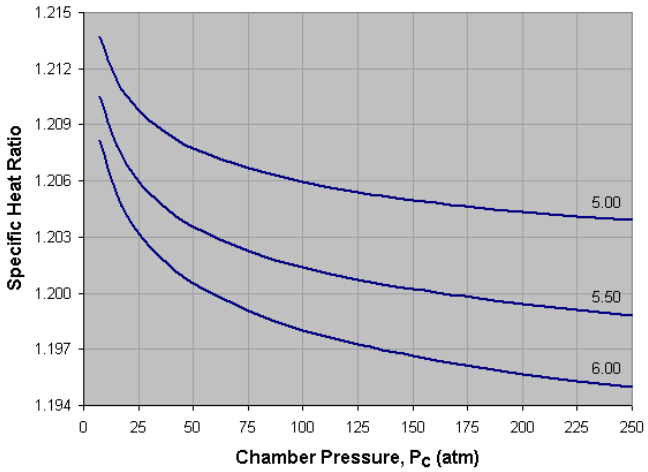


Figure B.3: Adiabatic flame temperature vs. chamber pressure [113]

| | Basic equation form $A \cdot ln(z) + B$ | |
|---|---|---|
| | A | B |
| $O/F$ = 5.00 | 81.171 | 2957.179 |
| $O/F$ = 5.50 | 100.220 | 2991.662 |
| $O/F$ = 6.00 | 117.310 | 3004.516 |

Table B.3: Logarithmic expression obtained for adiabatic flame temperature as a function of chamber pressure

# Appendix C

# Verification and Validation

## C.1 Rocket model validation results

| | | | | $I_{sp}$ (SL) [s] | | | $I_{sp}$ (vac) [s] | | |
|---|---|---|---|---|---|---|---|---|---|
| Engine | $p_c$ [$bar$] | $\kappa$ | $O/F$ | Experimental | SUAVE | Error (%) | Experimental | SUAVE | Error (%) |
| SSME | 206.4 | 69.0 | 6.0 | 366.0 | 356.25 | 2.66 | 452.0 | 444.34 | 1.69 |
| Vulcain 2 | 100.0 | 45.1 | 6.2 | — | — | — | 431.0 | 429.19 | 0.42 |
| RD-0120 | 219.0 | 85.7 | 6.0 | 353.0 | 345.10 | 2.24 | 455 | 44.337 | 1.46 |
| VINCI | 60.0 | 240.0 | 5.8 | — | — | — | 465.0 | 458.01 | 1.50 |
| J-2 | 30.0 | 28.0 | 5.5 | 200.0 | 180.88 | 9.56 | 421.0 | 426.01 | 1.19 |
| LE-7A | 127.0 | 51.9 | 5.9 | 349.0 | 331.14 | 5.12 | 446.0 | 438.81 | 1.66 |
| YF-77 | 102.0 | 49.0 | 5.5 | 310.2 | 316.11 | 1.91 | 430.0 | 444.08 | 3.28 |
| RS-68 | 97.21 | 21.5 | 6.0 | — | — | — | 412.0 | 417.63 | 1.37 |

Table C.1: LOX/LH2 rocket validation